ISSN: 0376–7388

MEMBRANE SCIENCE AND DESALINATION

journal of MEMBRANE SCIENCE

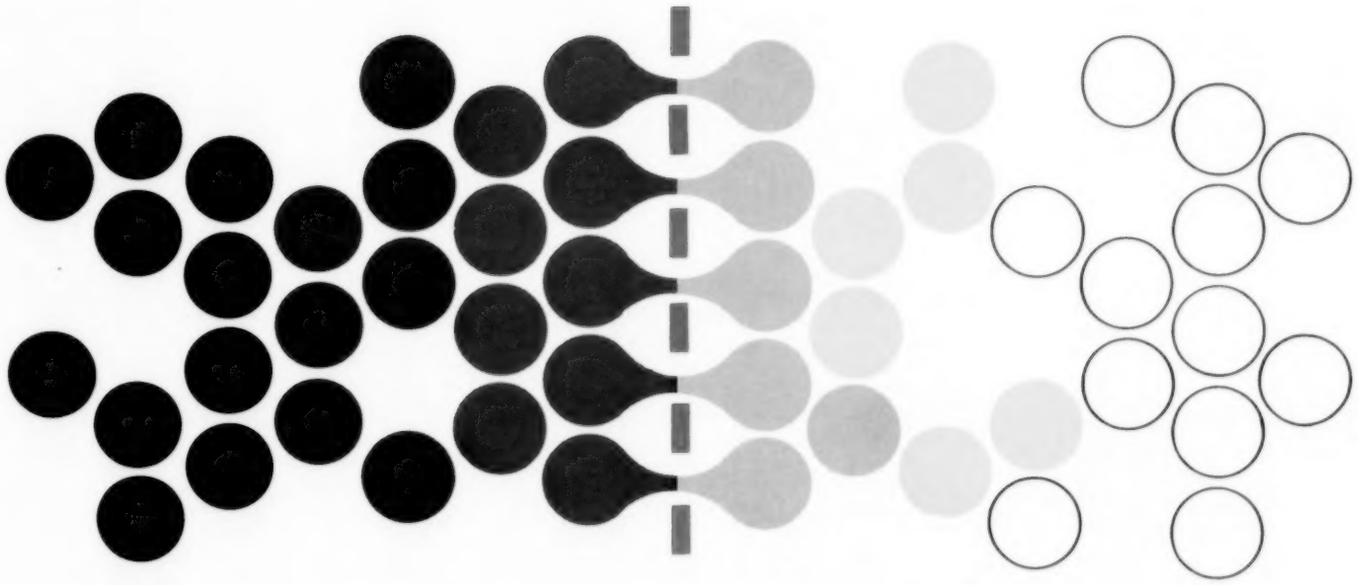

VOLUME 57 – NO. 1
APRIL 1, 1991

ELSEVIER

MONTHLY

journal of MEMBRANE SCIENCE

The journal provides a focal point for "membranologists" and a vehicle for the dissemination of information dealing with the science and technology of membrane processes and phenomena. The primary emphasis is on the structure and function of non-biological membranes, but papers bridging the gap between non-biological and biological membranes are sought. A broad spectrum of papers is encouraged:

- theory of membrane transport
- experimental data on membrane permeation
- membrane structure
- applications: separations (excluding water desalination and purification), biomedical, packaging, membrane electrodes, membrane-bound enzymes, and biomembrane analogs.

This is a practical journal. Economic studies of separation processes, for example, are encouraged. Regular papers and short communications are published. An important feature of the journal is periodic reviews of important subject areas. Other features include announcements of forthcoming meetings of interest to membranologists, a meetings calendar, and book reviews.

Editor: H.K. LONSDALE

Acting Editor: Scott McCray

Assistants to the Editor: Sharon K. Maier and Rebecca M. French

Advisory Board:

R.M. Barrer
Ora Kedem
Pat Meares
Alan Michaels
Sam Spiegler
Vivian Stannett

Editorial Board:

P. Aptel (Toulouse, France)
G. Belfort (Troy, NY, USA)
K.W. Böddeker (Geesthacht, Germany)
D.A. Butterfield (Lexington, KY, USA)
T.M.S. Chang (Montreal, Quebec, Canada)
E.L. Cussler (Minneapolis, MN, USA)
E. Drioli (Naples, Italy)
A.G. Fane (Kensington, N.S.W., Australia)
H.B. Hopfenberg (Raleigh, NC, USA)
R.Y.M. Huang (Waterloo, Ont., Canada)
S.-T. Hwang (Cincinnati, OH, USA)
G. Jonsson (Lyngby, Denmark)
E. Klein (Louisville, KY, USA)
W.J. Koros (Austin, TX, USA)
S. Loeb (Beer-Sheva, Israel)
E.A. Mason (Providence, RI, USA)
S.L. Matson (Marlborough, MA, USA)
M.H. Mehta (Baroda, India)
U. Merten (San Diego, CA, USA)
J. Néel (Nancy, France)
D.R. Paul (Austin, TX, USA)
J. Petropoulos (Athens, Greece)
J.A. Quinn (Philadelphia, PA, USA)
R.P. Rastogi (Varanasi, India)
R. Rautenbach (Aachen, Germany)
R.L. Riley (La Jolla, CA, USA)
C.E. Rogers (Cleveland, OH, USA)
J.S. Schultz (Pittsburgh, PA, USA)
T. Shimidzu (Kyoto, Japan)
K.K. Sirkar (Hoboken, NJ, USA)
J.A.M. Smit (Leiden, The Netherlands)
C.A. Smolders (Enschede, The Netherlands)
S.A. Stern (Syracuse, NY, USA)
H. Strathmann (Stuttgart, Germany)
W.J. Ward III (Schenectady, NY, USA)

JOURNAL OF MEMBRANE SCIENCE

VOL. 57 (1991)

journal of MEMBRANE SCIENCE

Editor:
H.K. LONSDALE

Assistants to the Editor:
Sharon K. Maier
Rebecca M. French

Acting Editor: Scott McCray

Advisory Board:

R.M. Barrer
Ora Kedem
Pat Meares
Alan Michaels
Sam Spiegler
Vivian Stannett

Editorial Board:

P. Aptel (Toulouse, France)
G. Belfort (Troy, NY, USA)
K.W. Böddeker (Geesthacht, Germany)
D.A. Butterfield (Lexington, KY, USA)
T.M.S. Chang (Montreal, Quebec, Canada)
E.L. Cussler (Minneapolis, MN, USA)
E. Drioli (Naples, Italy)
A.G. Fane (Kensington, N.S.W., Australia)
H.B. Hopfenberg (Raleigh, NC, USA)
R.Y.M. Huang (Waterloo, Ont., Canada)
S.-T. Hwang (Cincinnati, OH, USA)
G. Jonsson (Lyngby, Denmark)
E. Klein (Louisville, KY, USA)
W.J. Koros (Austin, TX, USA)
S. Loeb (Beer-Sheva, Israel)
E.A. Mason (Providence, RI, USA)
S.L. Matson (Marlborough, MA, USA)
M.H. Mehta (Baroda, India)
U. Merten (San Diego, CA, USA)
J. Néel (Nancy, France)
D.R. Paul (Austin, TX, USA)
J. Petropoulos (Athens, Greece)
J.A. Quinn (Philadelphia, PA, USA)
R.P. Rastogi (Varanasi, India)
R. Rautenbach (Aachen, Germany)
R.L. Riley (La Jolla, CA, USA)
C.E. Rogers (Cleveland, OH, USA)
J.S. Schultz (Pittsburgh, PA, USA)
T. Shimidzu (Kyoto, Japan)
K.K. Sirkar (Hoboken, NJ, USA)
J.A.M. Smit (Leiden, The Netherlands)
C.A. Smolders (Enschede, The Netherlands)
S.A. Stern (Syracuse, NY, USA)
H. Strathmann (Stuttgart, Germany)
W.J. Ward III (Schenectady, NY, USA)

VOLUME 57 (1991)

ELSEVIER, Amsterdam – Oxford – New York – Tokyo

Abstracted/indexed in:

Applied Mechanics Reviews
Biological Abstracts
Centre de Documentation Scientifique et Technique – PASCAL Database
Chemical Abstracts
Current Contents (Engineering, Technology & Applied Sciences)
(Physical, Chemical & Earth Sciences)
Engineering Index
Excerpta Medica: Physiology, Biophysics, and Pharmacology Sections
ISMEC Bulletin
Membrane Quarterly
Physics Abstracts (INSPEC)
Polymer Contents
Science Citation Index
Science Research Abstracts Journal
Solid State Abstracts Journal

© 1991, ELSEVIER SCIENCE PUBLISHERS B.V.

0376-7388/91/$03.50

All rights reserved. No part of this publication may be reproduced, stored in a retrieval system or transmitted in any form or by any means, electronic, mechanical, photocopying, recording or otherwise, without the prior written permission of the publisher, Elsevier Science Publishers B.V., P.O. Box 330, 1000 AH Amsterdam, The Netherlands.
Upon acceptance of an article by the journal, the author(s) will be asked to transfer copyright of the article to the publisher. The transfer will ensure the widest possible dissemination of information.
Submission of an article for publication entails the author(s) irrevocable and exclusive authorization of the publisher to collect any sums or considerations for copying or reproduction payable by third parties (as mentioned in article 17 paragraph 2 of the Dutch Copyright Act of 1912 and in the Royal Decree of June 20, 1974 (S. 351) pursuant to article 16b of the Dutch Copyright Act of 1912) and/or to act in or out of Court in connection therewith.
Special regulations for readers in the USA. – This journal has been registered with the Copyright Clearance Center, Inc. Consent is given for copying of articles for personal or internal use, or for the personal use of specific clients. This consent is given on the condition that the copier pay through the Center the per-copy fee for copying beyond that permitted by Sections 107 or 108 of the U.S. Copyright Law. The per-copy fee is stated in the code-line at the bottom of the first page of each article. The appropriate fee, together with a copy of the first page of the article, should be forwarded to the Copyright Clearance Center, Inc., 27 Congress Street, Salem, MA 01970, USA. If no code-line appears, broad consent to copy has not been given and permission to copy must be obtained directly from the author(s). All articles published prior to 1980 may be copied for a per-copy fee of US $2.25, also payable through the Center. This consent does not extend to other kinds of copying, such as for general distribution, resale, advertising and promotion purposes, or for creating new collective works. Special written permission must be obtained from the publisher for such copying.
No responsibility is assumed by the Publisher for any injury and/or damage to persons or property as a matter of products liability, negligence or otherwise, or from any use or operation of any methods, products, instructions or ideas contained in the material herein.
Although all advertising material is expected to conform to ethical standards, inclusion in this publication does not constitute a guarantee or endorsement of the quality or value of such product or of the claims made of it by its manufacturer.

This issue is printed on acid-free paper.

PRINTED IN THE NETHERLANDS

Journal of Membrane Science, 57 (1991) 1–20
Elsevier Science Publishers B.V., Amsterdam

The formation of microporous polyvinylidene difluoride membranes by phase separation

A. Bottino[a], G. Camera-Roda[b], G. Capannelli[c] and S. Munari[a]

[a]*Centro di Studi Chimico-Fisici di Macromolecole Sintetiche e Naturali, Corso Europa 30, 16132 Genova (Italy)*
[b]*Istituto di Chimica Industriale, Corso Europa 30, 16132 Genova (Italy)*
[c]*Dipartimento di Chimica Industriale, Università di Messina, Salita Sperone 31, Sant'Agata, 98100 Messina (Italy)*

(Received August 11, 1989; accepted in revised form July 30, 1990)

Abstract

Microporous polyvinylidene fluoride (PVDF) membranes were prepared by casting and coagulating solutions of the polymer in eight different solvents. The membranes were characterized by scanning electron microscope observations, water content measurements and water permeability tests. The possible correlations between the resulting membrane characteristics and the properties of both the polymer–solvent solutions and the solvent–nonsolvent systems are extensively discussed. The analysis indicates that most of the correlations suggested or adopted in the literature do not hold for PVDF membranes, whereas the transport properties of the solvent–nonsolvent system seem to affect significantly the final membrane structure and the resulting performances in separation processes.

Keywords: membrane preparation and structure; microporous membrane; polyvinylidene fluoride membrane; scanning electro microscopy; water content

Introduction

Phase separation is a widely used method for making microporous polymer membranes. In this process a viscous solution is first cast on a suitable support, then immersed in a nonsolvent bath. The membrane is formed by polymer precipitation, which occurs as a consequence of concentration variations following diffusive interchange between the solvent and the nonsolvent. The rate of polymer precipitation is determined at each point by the progress of the concentration, which is in turn governed by the interchange rate.

Depending on the rate of polymer precipitation, the following three types of membranes can be obtained:

(a) symmetric, with an almost even porosity across the membrane cross-section;
(b) asymmetric, with a selective thin microporous upper layer (skin) on a thicker macroporous globular or spongy sub-layer;

0376-7388/91/$03.50 © 1991 — Elsevier Science Publishers B.V.

(c) asymmetric, with large voids and/or finger-like cavities beneath the microporous upper layer.

There is evidence that a low precipitation rate leads to type (a) membranes, whereas a high precipitation rate gives type (c) membranes. Nonetheless membrane formation is complex to describe, as it occurs in very short times and involves a great number of elementary processes. In consequence, the modelling of membrane formation is very difficult for three main reasons: (i) the number of the intervening elementary processes is very high; (ii) many involved mechanisms and phenomena (such as convective contributions, thermal effects, demixing kinetics, dependence of the chemical potential on the system composition and the stress distribution) are still poorly described or understood; (iii) the independent evaluation of many relevant parameters (including ternary diffusivities, interaction parameters, and boundary and initial conditions) is difficult or highly approximate. However, it is likely that in some systems a few or just one mechanism could control the process. In such cases only some or one parameter could be important, so that it could be worthwhile to look for some consistent correlation between a single parameter and the obtainable membrane structure. This alternative approach can furnish both practical guidance in membrane preparation and an insight into the process. Of course this approach is not intended to substitute the modelling of the process; preferably, the holding correlation should be related back to a possible model and justified by it.

In this sense, several experimental observations and qualitative comments on the effect of polymer–solvent and/or solvent–nonsolvent interactions on the structure and properties of the resulting membrane are reported in the literature [1–17]. A large amount of work has been carried out on a limited class of polymers, essentially cellulose acetate and its derivatives [1–5,7,9–11,14–16], polyamides [4,13,15,17] and polysulphones [10,12,14,15], but very little information is available on polyvinylidene fluoride (PVDF), which nowadays is widely used as a membrane material since it exhibits excellent chemical resistance and good physical and thermal stability [18].

The purpose of this work is to investigate for the PVDF system the existence of correlations between the properties of both PVDF–solvent solutions and solvent–nonsolvent systems and the structure and properties (water content, water flux, thickness and void volume) of the membranes. An attempt is also made to draw general conclusions and inferences, so that the obtained indications should furnish valuable help in the analysis of other systems and in the development and improvement of models of the process.

Experimental

Materials

The PVDF was a commercial product (Foraflon 1000 HD, Ugine Kuhlmann) with an average molecular mass $M = 4.5 \times 10^5$. The total polymer sol-

TABLE 1

Density, viscosity, solubility parameters and mutual water diffusivity of PVDF solvents

Solvent	ρ_S[a] (kg/m^3)	η_S[a] (mPa-sec)	$\delta_{d,S}$ (MPa$^{1/2}$)	$\delta_{p,S}$ (MPa$^{1/2}$)	$\delta_{h,S}$ (MPa$^{1/2}$)	$\delta_{t,S}$[b] (MPa$^{1/2}$)	$D_{S\text{-}W}\times10^6$ (cm^2/sec)	$D_{W\text{-}S}\times10^6$ (cm^2/sec)	$D_m\times10^6$ (cm^2/sec)
DMA	941.2	0.9472	16.8	11.5	10.2	22.7	9.1	16.8	11.8
DMF	949.1	0.8499	17.4	13.7	11.3	24.8	10.2	17.1	12.8
DMSO	1100.4	2.1878	18.4	16.4	10.2	26.7	10.7	6.9	8.4
HMPA	1025.8	3.5570	18.4	8.6	11.3	23.2	6.2	6.4	6.3
NMP	1032.4	1.8179	18.0	12.3	7.2	22.9	8.9	9.3	9.1
TEP	1069.4	1.6753	16.8	11.5	9.2	22.3	6.3	13.7	8.7
TMP	1213.4	2.1937	16.8	16.0	10.2	22.3	8.0	9.2	8.6
TMU	968.1	1.5330	16.8	8.2	11.1	21.7	7.8	12.0	9.5

[a]Temperature 20°C; Ref. [20].

[b]Temperature 25°C; Ref. [21], pp. 153–158.

ubility parameter was $\delta_{t,P}=23.2$ MPa$^{1/2}$ and the dispersion ($\delta_{d,P}$), polar ($\delta_{p,P}$) and hydrogen bonding ($\delta_{h,P}$) parameters were $\delta_{d,P}=17.2$, $\delta_{p,P}=12.5$ and $\delta_{h,P}=9.2$ MPa$^{1/2}$, respectively [19].

The polymer solvents were of reagent grade: *N,N*-dimethylacetamide (DMA), *N,N*-dimethylformamide (DMF), dimethylsulphoxide (DMSO), hexamethylphosphoramide (HMPA), *N*-methyl-2-pyrrolidone (NMP), tetramethylurea (TMU), triethyl phosphate (TEP) and trimethyl phosphate (TMP). Some physical constants such as density (ρ_S), absolute viscosity (η_S) and solubility parameters for these solvents are listed in Table 1.

Properties of PVDF–solvent solutions

Limiting viscosity numbers at 20°C of PVDF in each solvent were taken from Ref. [19]. The kinematic viscosity (ν_{CS}) of 15 wt.% casting solutions was measured at 20°C by using a Cannon Fenske capillary viscometer. Absolute viscosity (η_{CS}) is defined as:

$$\eta_{CS}=\rho_{CS}\nu_{CS} \tag{1}$$

where the solution density ρ_{CS} was measured with a pycnometer. Specific viscosity (η^{sp}_{CS}) was determined by the ratio:

$$\eta^{sp}_{CS}=\frac{\eta_{CS}-\eta_S}{\eta_S} \tag{2}$$

Properties of water–solvent systems

Excess enthalpies of mixing at 37°C of the water–solvent systems were taken from Ref. [20].

Mutual diffusivities $D_{S\text{-}W}$ of solvent at very low concentrations in water and

$D_{W\text{-}S}$ of water at very low concentrations in solvent were evaluated from the Wilke–Chang equation [22]:

$$D_{a\text{-}b} = 7.4 \times 10^{-11} \frac{(\varphi_b M_b)^{1/2} T}{\eta_b V_a^{0.6}} \tag{3}$$

where $D_{a\text{-}b}$ (cm^2/sec) is the liquid mutual diffusivity of a in essentially pure b; T (K) is the absolute temperature; M is the molecular mass; V (cm^3/mol) is the molar volume; η (Pa-sec) is the absolute viscosity; and φ is the association factor.

The following assumptions are made for computations:
(i) the molar volume of water is taken as 4 times greater than the actual value as suggested in [23];
(ii) association factors are 2.26 and 1.1 for $D_{S\text{-}W}$ and $D_{W\text{-}S}$, respectively.

Cloud points

A set of ternary system samples with increasing water concentration was prepared by adding known amounts of water–solvent mixtures of fixed composition to weighed PVDF solutions. The samples were continuously stirred at 50°C for 2 hr, then at 20°C for 8 hr. The cloud point was assumed to be at the concentration of the first sample of the set showing constant turbidity at visual inspection. The solubility diagram was obtained by repeating this procedure on several sets with different solvent contents.

Membrane preparation

Solutions of different PVDF concentration were cast at 20°C on a glass plate as films of $\simeq 350$ μm thickness, and after 30 sec, immersed in water at 4°C. Membranes were leached for 48 hr under running water before characterization.

Membrane characterization

Membrane cross-sections were prepared according to the procedure reported in Ref. [24] and observed by a Cambridge Stereoscan 250 MK2 scanning electron microscope (SEM).

Membrane water content was determined as follows:

$$H_2O\ (\%) = 100 \left(\frac{W - W_0}{W} \right) \tag{4}$$

where W and W_0 are the weights of the wet and dried membrane, respectively.

The degree of crystallinity of the polymer in the membrane was measured by a calorimetric method in order successively to evaluate the polymer density in the membrane, as the densities of amorphous and crystalline PVDF are 1680 and 1920 kg/m^3, respectively [19]. A differential scanning calorimeter (Perkin-Elmer DSC IIB) was used, and the enthalpy of fusion of PVDF crystals

was assumed to be 6.7 kJ/mol, according to Ref. [25]. The degree of crystallinity ranged from 55–60% according to the type of solvent used, and consequently the polymer density obtained in the membrane was approximately 1820 kg/cm^3.

The knowledge of the polymer density in the membrane and of the value of the water content allowed assessment of the void fraction via the hypothesis that in the wet membrane all the voids are filled with water.

The thickness of the wet membrane was measured with a micrometer. The product of the thickness of the wet membrane and the void fraction gives a measure of the volume of voids or cavities per unit surface area.

Transmembrane water flux was evaluated with a 2 hr permeation run at 20°C for a pressure difference of 200 kPa and a 5 m/sec recirculation rate. Details of the permeation unit are reported elsewhere [26].

Results and discussion

Membrane structure and properties

Figure 1 shows SEM micrographs of cross-sections of membranes cast from 15 wt.% PVDF solutions. Most of the membranes exhibit highly inhomogeneous structures owing to the presence of large voids and cavities of different size and shape beneath the upper layer. SEM micrographs reported in Figs. 2–9 supply more detailed information on the structure of the membrane through magnified views of the upper and the lower parts of the membrane cross-section. By using TEP as solvent a membrane forms with a honeycomb structure without cavities (Fig. 2). The size of the alveoli progressively increases from the top to the bottom of the membrane. The DMF cast membrane (Fig. 3) exhibits a large number of short finger-like cavities beneath the upper layer. The cavities are separated by walls composed of discrete polymer globules. The structure of the porous sublayer is globular and the size of globules appears to be fairly uniform over the entire membrane cross-section. In the membranes cast from DMA (Fig. 4), TMU (Fig. 5) and TMP (Fig. 6) the cavities progressively extend through a considerable fraction of the membrane thickness. In addition, it is apparent that the globules near the upper layer are more compacted and larger than those near the bottom. By using NMP (Fig. 7) or DMSO (Fig. 8) as solvent, cavities are seen to grow in breadth and length towards the bottom of the membrane without a well defined shape. In the membrane cast from HMPA (Fig. 9) short cavities and isolated voids appear in the porous globular sublayer.

An increase of the polymer concentration in the casting solution leads to a reduction of both the number and the size of cavities, but the structure always remains of the globular type. This effect is apparent in Figs. 10 and 11, where SEM micrographs of cross-sections of membranes cast from NMP and TMP solutions, respectively, of different PVDF concentrations are reported.

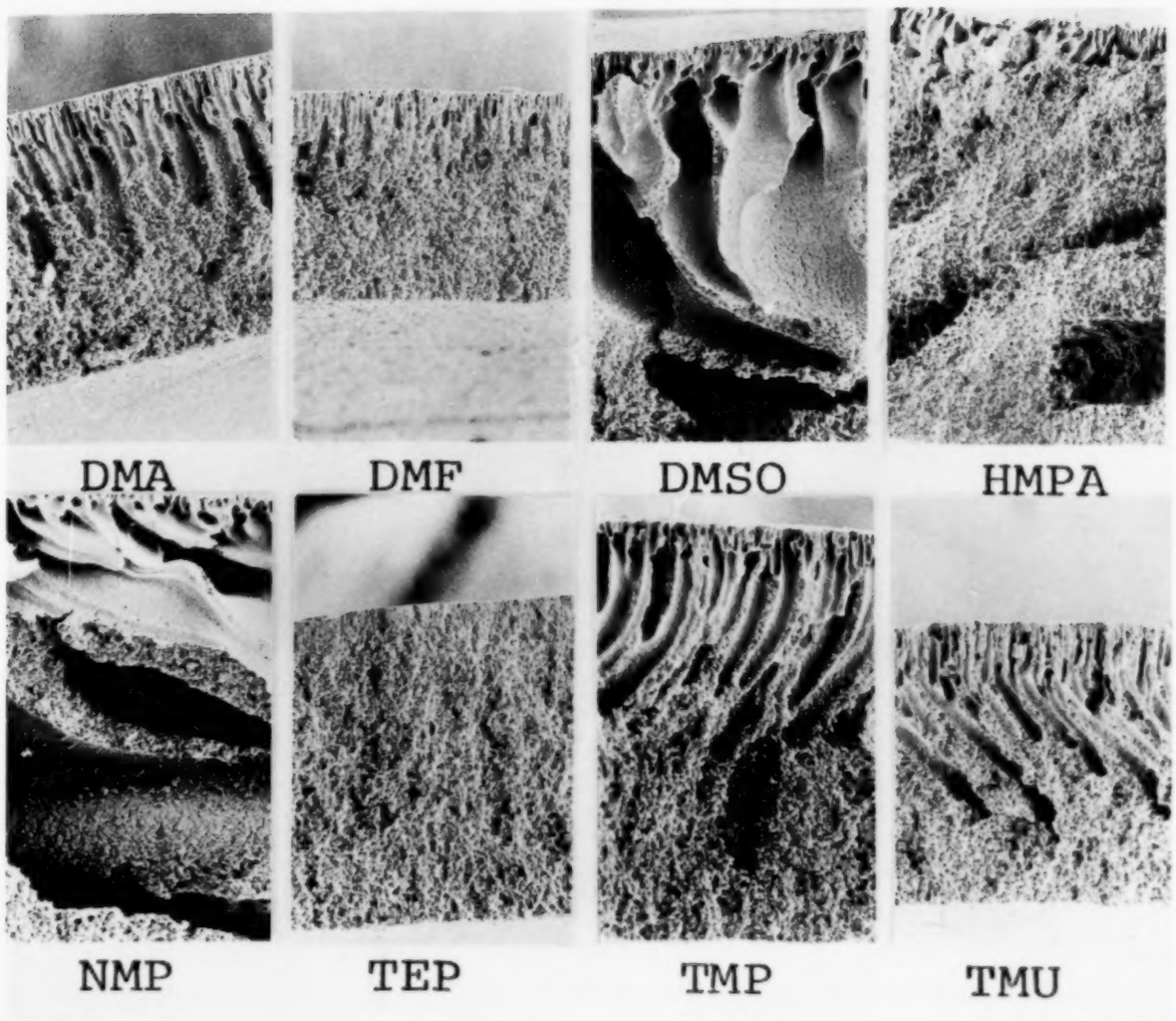

Fig. 1. Scanning electron micrographs of cross-sections of membranes cast from 15 wt.% PVDF solutions in different solvents.

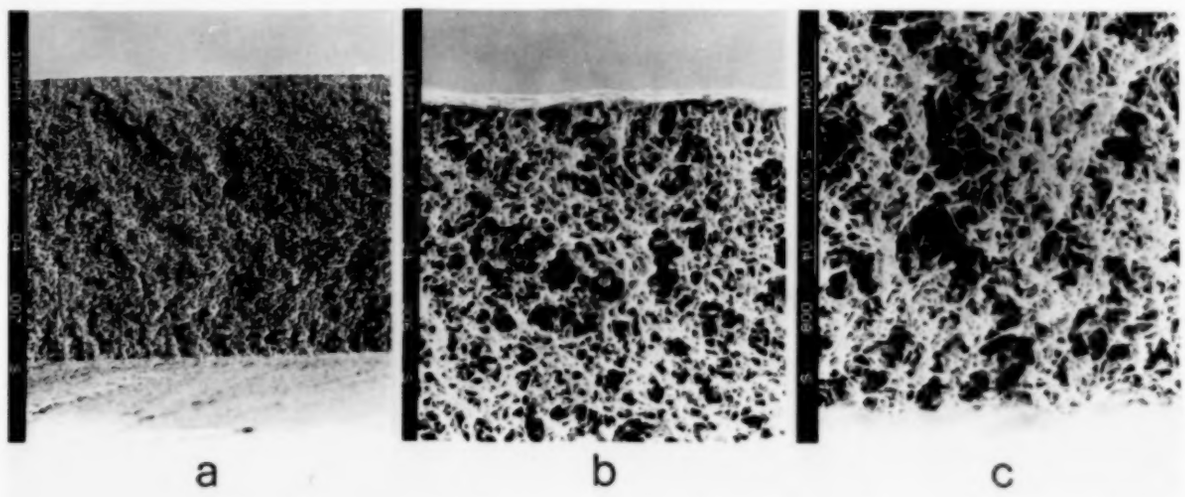

Fig. 2. Scanning electron micrographs of cross-sections of the membrane cast from 15 wt.% PVDF solution in TEP: (a) overall cross-section; (b) upper part of (a); (c) bottom part of (a).

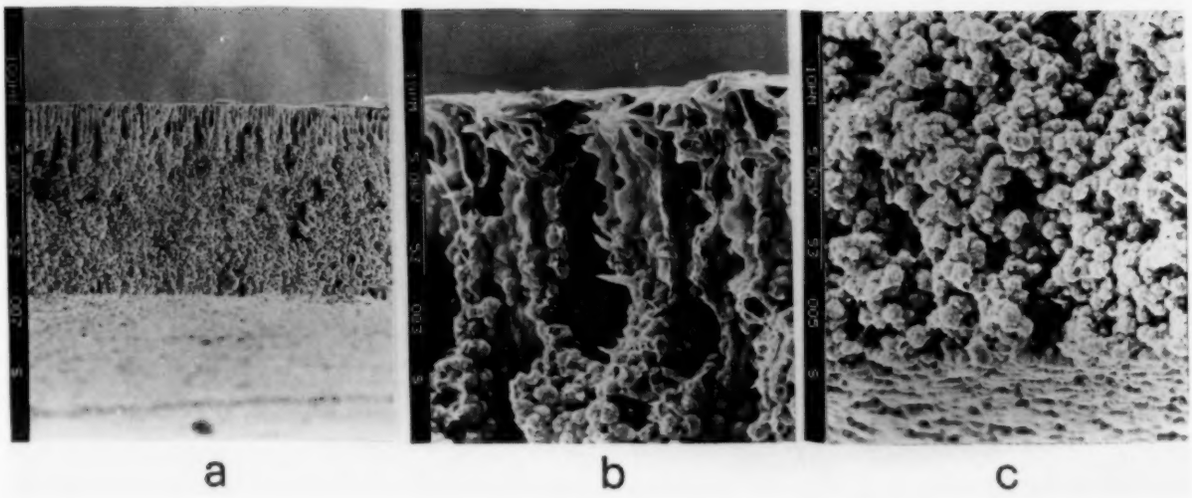

Fig. 3. Scanning electron micrographs of cross-sections of the membrane cast from 15 wt.% PVDF solution in DMF: (a) overall cross-section; (b) upper part of (a); (c) bottom part of (a).

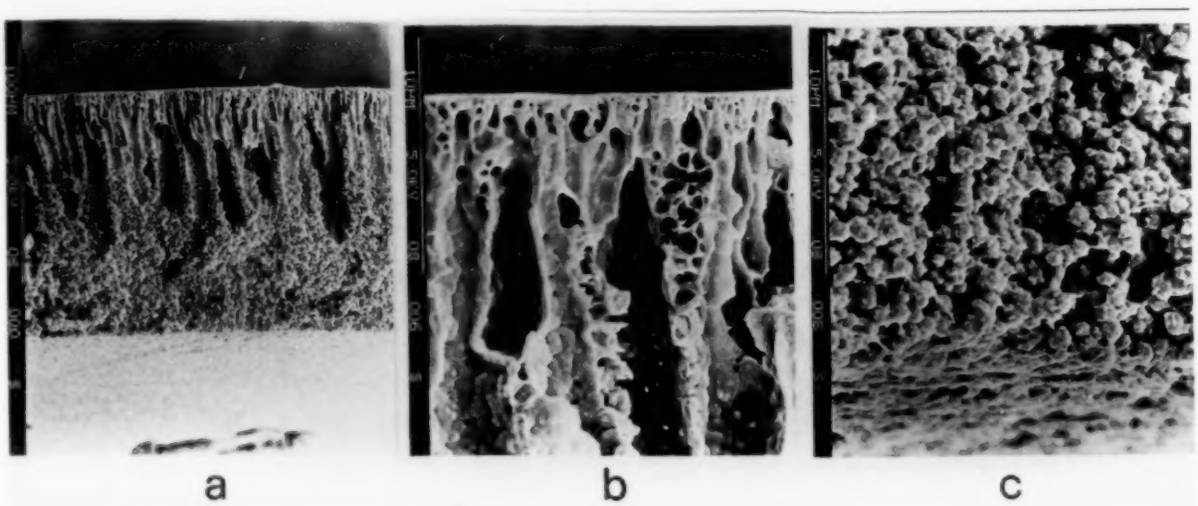

Fig. 4. Scanning electron micrographs of cross-sections of the membrane cast from 15 wt.% PVDF solution in DMA: (a) overall cross-section; (b) upper part of (a); (c) bottom part of (a).

Membrane properties are listed in Table 2.

Of all the investigated solvents HMPA yields membranes with the highest water content and water flux. It is worthwhile to observe that an increase in both the number and the size of the cavities in the sublayer does not necessarily cause an increase in the water flux. This is because the water flux is mainly controlled by the porosity of the upper layer. Indeed, preliminary results obtained from porosity measurements and ultrafiltration tests with aqueous solutions of dextran (nominal average molecular mass $M \simeq 10{,}000$; Fluka Chemie AG) indicate that the membrane cast from HMPA (the structure of which appears more homogeneous than that of the membranes cast from NMP or

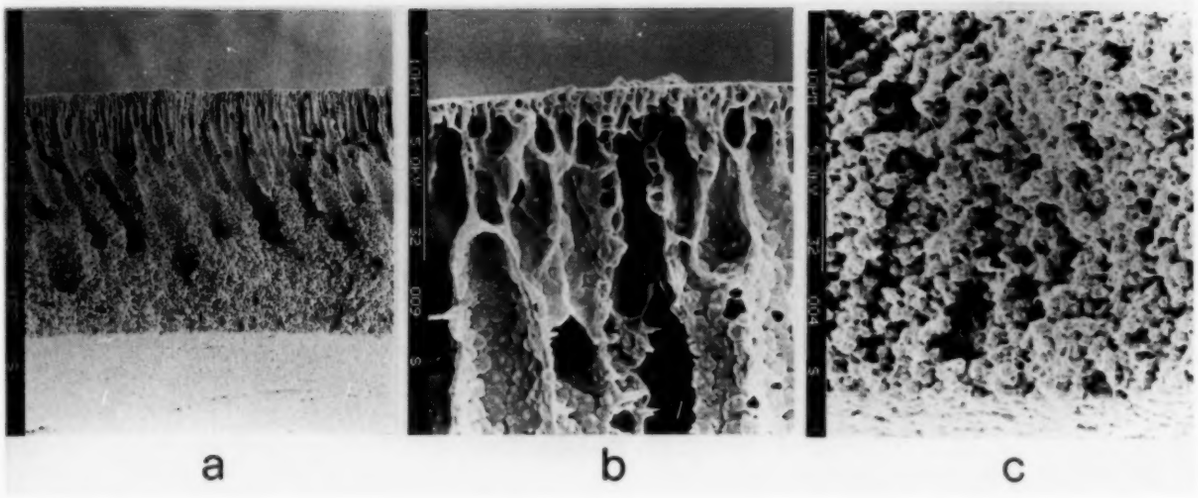

Fig. 5. Scanning electron micrographs of cross-sections of the membrane cast from 15 wt.% PVDF solution in TMU: (a) overall cross-section; (b) upper part of (a); (c) bottom part of (a).

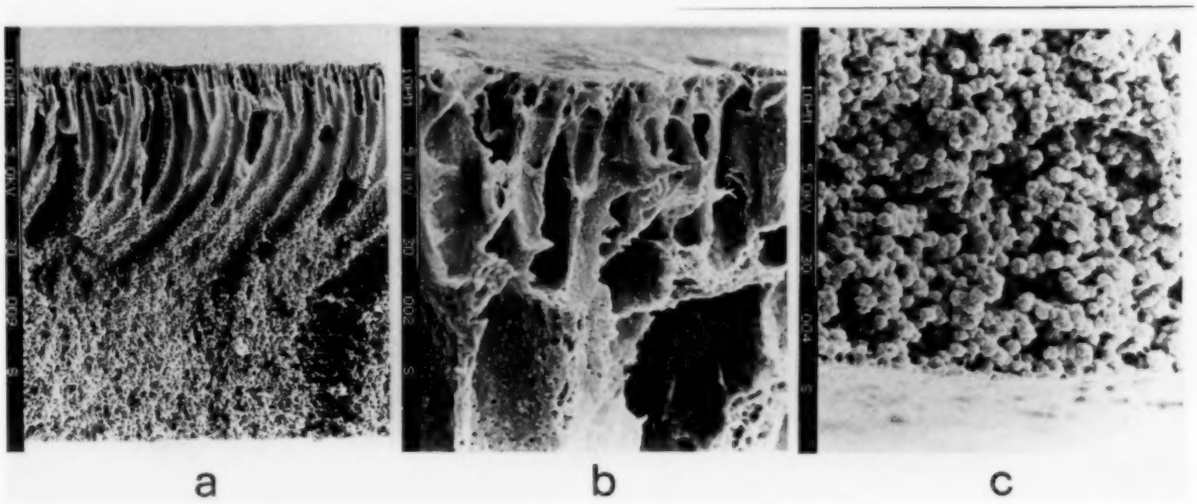

Fig. 6. Scanning electron micrographs of cross-sections of the membrane cast from 15 wt.% PVDF solution in TMP: (a) overall cross-section; (b) upper part of (a); (c) bottom part of (a).

DMSO) shows a higher number of larger pores in the upper layer. In consequence it exhibits a greater permeate flux and a much lower dextran retention.

When the different membranes are sorted according to any property, the resulting sequence is always the same. This is shown in Fig. 12, where normalized values of the properties are plotted for the different membranes. This fact agrees with the consideration that the morphology of the sublayer in an asymmetric membrane (which is somehow described by the values for the water content, membrane thickness and cavity volume) should be mainly determined by the structure of the skin [3,13], which the value of the water depends on directly. Actually, the skin should be formed in very short times (very small fractions of a second) and consequently acts as a barrier against subsequent

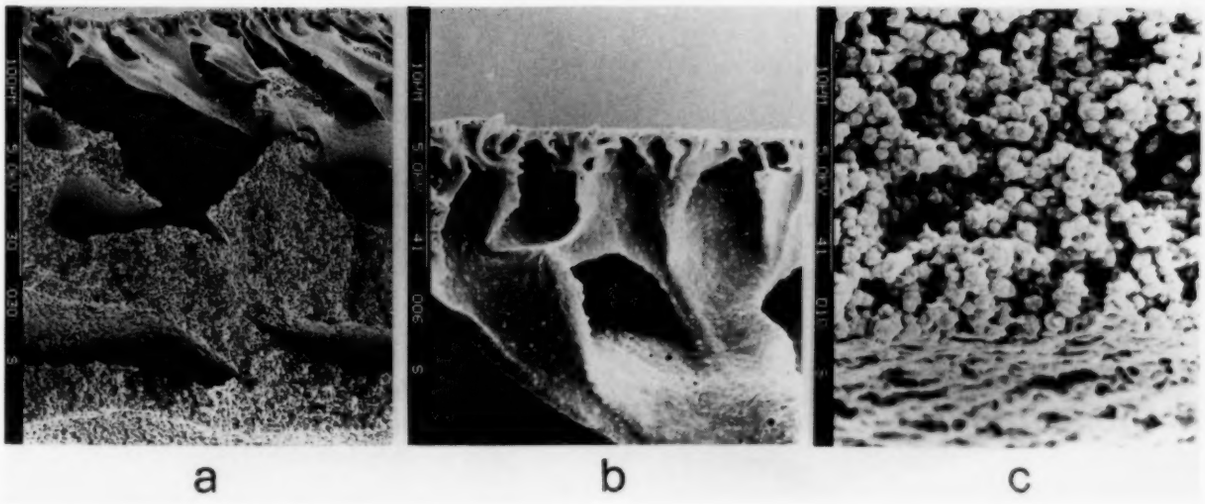

Fig. 7. Scanning electron micrographs of cross-sections of the membrane cast from 15 wt.% PVDF solution in NMP: (a) overall cross-section; (b) upper part of (a); (c) bottom part of (a).

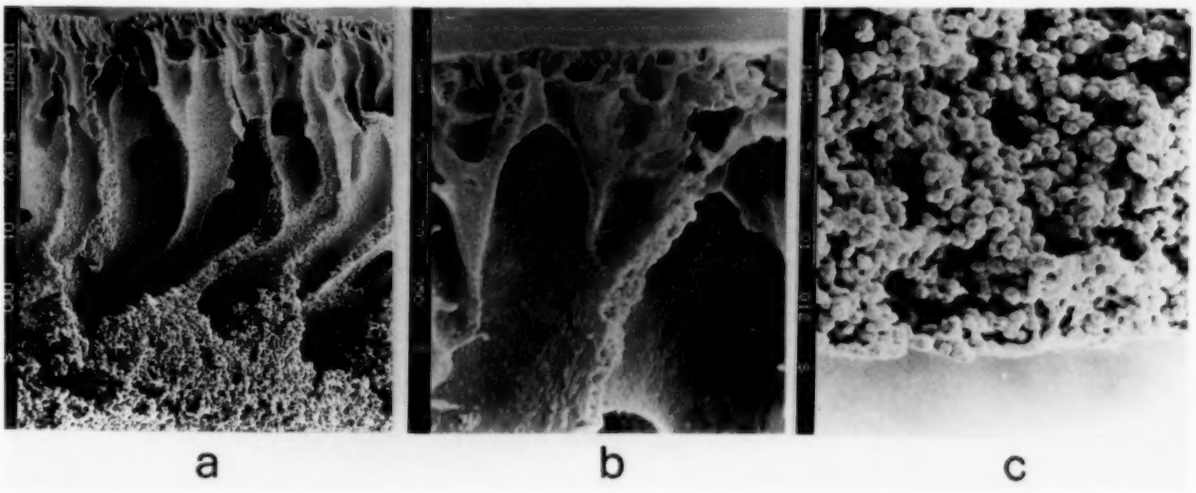

Fig. 8. Scanning electron micrographs of cross-sections of the membrane cast from 15 wt.% PVDF solution in DMSO: (a) overall cross-section; (b) upper part of (a); (c) bottom part of (a).

interdiffusion of solvent and nonsolvent in the bulk of the forming membrane. Thus the structures of the skin and the underlying zone are correlated to some extent for the investigated asymmetric membranes. As a consequence, for PVDF membranes the water flux should not be considered merely as a measure of the membrane permeability, which is directly determined by the skin porosity, but can be used also as an indirect indication of sublayer morphology.

Factors affecting membrane structure and properties

Many authors have searched for correlations between membrane structure and one or some properties of the system used to form the membrane. For this reason, the properties of the current eight water–solvent–PVDF systems have

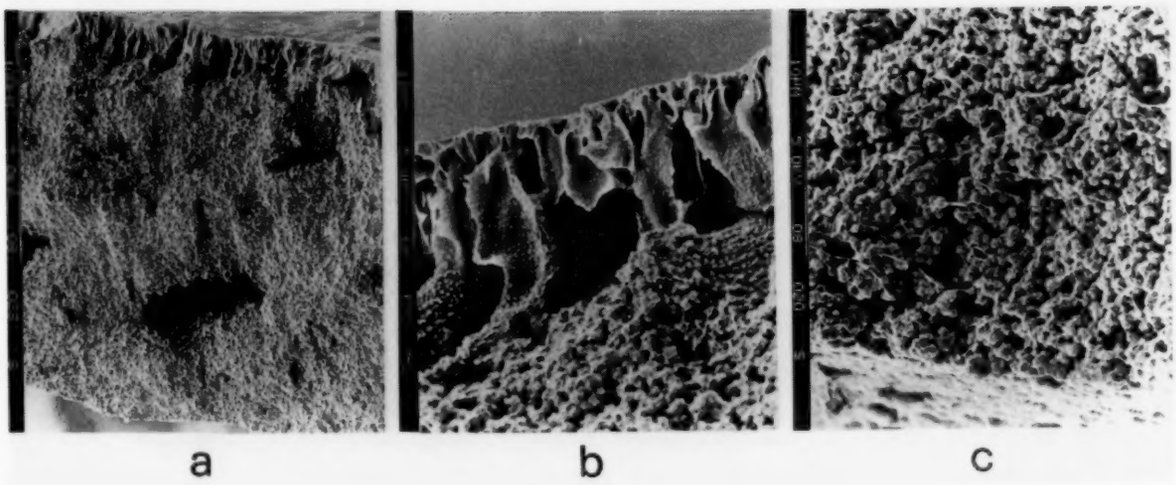

Fig. 9. Scanning electron micrographs of cross-sections of the membrane cast from 15 wt.% PVDF solution in HMPA: (a) overall cross-section; (b) upper part of (a); (c) bottom part of (a).

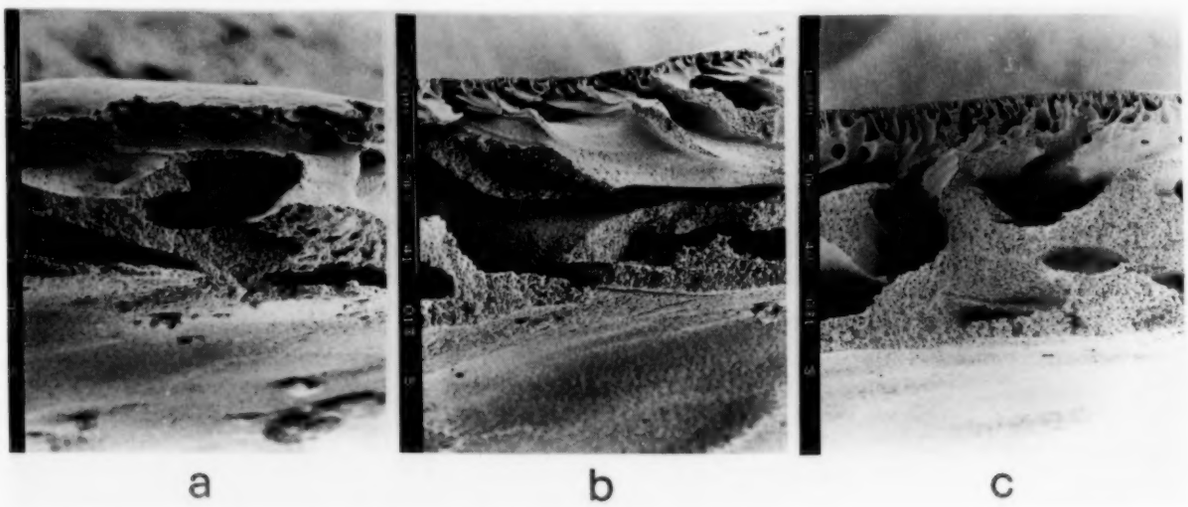

Fig. 10. Scanning electron micrographs of cross-sections of membranes cast from 10 wt.% (a), 15 wt.% (b) and 20 wt.% (c) PVDF solutions in NMP.

been investigated in order to determine the existence of correlations, to check the correlations suggested in the literature, and simultaneously to give some insight into or knowledge of the mechanism of membrane formation.

(i) Polymer–solvent interactions

The effect of polymer–solvent interactions on the structure and properties of the membrane has been studied by various authors [2,7,8,10,11,14]. It is generally observed that the lower are these interactions, the higher is the rate of polymer precipitation, with consequent formation of finger-like structures. Strathmann [8,13,14] assumes as a measure of the compatibility of polymer and solvent the difference of their solubility parameters:

$$\delta_{t,P\text{-}S} = \delta_{t,P} - \delta_{t,S} \tag{5}$$

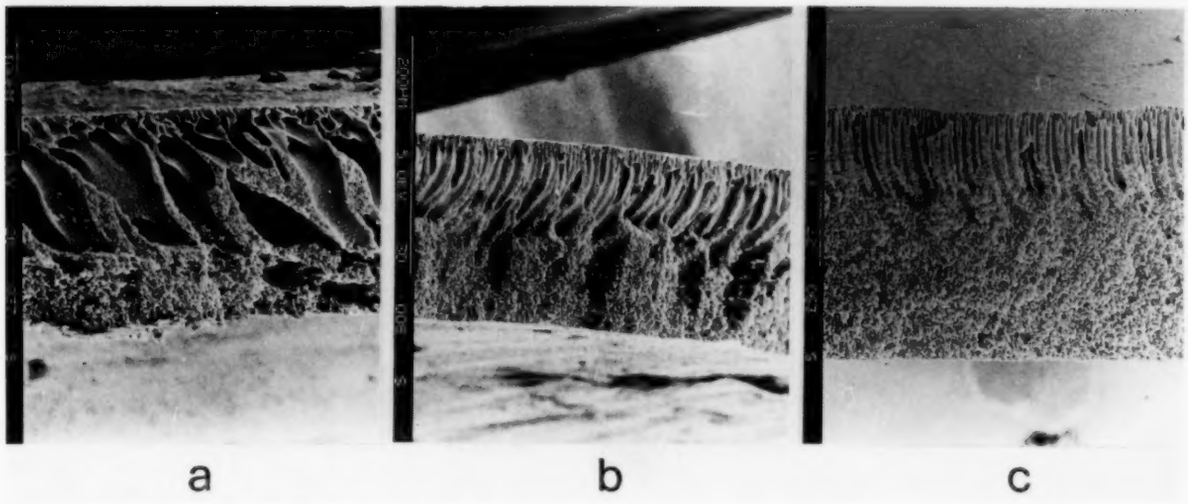

Fig. 11. Scanning electron micrographs of cross-sections of membranes cast from 10 wt.% (a), 15 wt.% (b) and 20 wt.% (c) PVDF solutions in TMP.

TABLE 2

Properties of membranes cast from 15 wt.% PVDF solutions in different solvents

Solvent	Water flux (μm/sec)	Water content (%)	Thickness of wet membrane (μm)	Void volume per unit area (μm)
DMF	0.7	52	135	88
DMA	1.7	57	150	104
TMU	0.5	60	150	108
TEP	2.7	60	140	101
NMP	11.6	67	200	155
TMP	11.6	67	220	171
DMSO	24.3	67	240	186
HMPA	38.2	81	270	237

and concludes that the larger this difference is, the higher is the tendency to form finger-like structures. By comparing the values of $\delta_{t,P-S}$ for the PVDF–solvent systems reported in column 2 of Table 3 with the SEM micrographs shown in Figs. 1–9, it is possible to conclude that the membrane structure does not depend on $\delta_{t,P-S}$. Due to the particular chemical nature of PVDF and the solvents, it is preferable to consider a more sophisticated formulation where the three components δ_d, δ_p, and δ_h of δ_t appear. According to Hansen [27]:

$$\delta_t^2 = \delta_d^2 + \delta_p^2 + \delta_h^2 \tag{6}$$

and hence

$$\delta_{t,P-S} = [(\delta_{d,p} - \delta_{d,S})^2 + (\delta_{p,P} - \delta_{p,S})^2 + (\delta_{h,P} - \delta_{h,S})^2]^{1/2} \tag{7}$$

Here $\delta_{t,P-S}$ represents the distance between the polymer and the solvent coor-

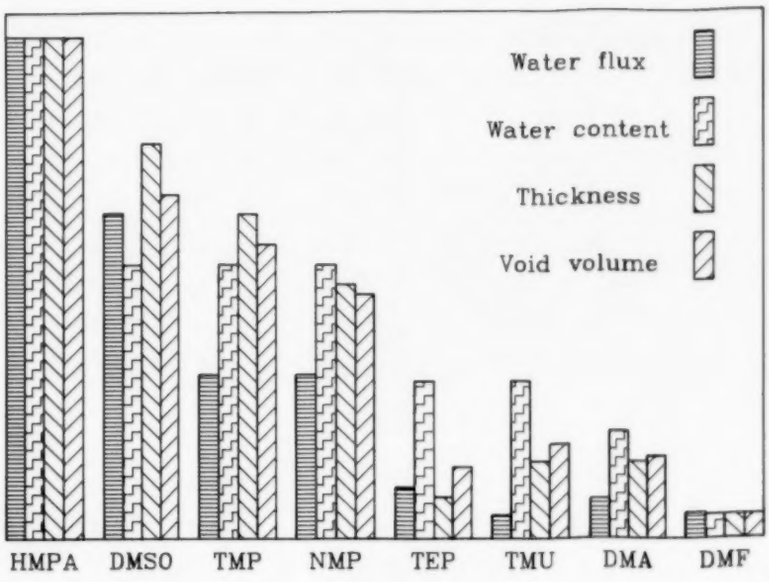

Fig. 12. Bar graph of four normalized membrane properties as a function of the solvent used.

TABLE 3

Solubility parameter disparity of PVDF and solvents and limiting viscosity numbers of the polymer

Solvent	$\delta_{t,P-S}$[a] ($mPa^{1/2}$)	$\delta_{t,P-S}$[b] ($mPa^{1/2}$)	$[\eta]$ (ml/g)
DMA	−0.5	1.5	129
DMF	1.6	2.4	117
DMSO	3.5	4.2	105
HMPA	0	4.6	158
NMP	−0.3	2.2	128
TEP	−0.9	1.1	130
TMP	−0.9	3.7	115
TMU	−1.5	4.7	142

[a]From eqn. (5).
[b]From eqn. (7).

dinates in a three-dimensional δ_d, δ_p, δ_h Hansen space. The lower this distance, the better the solvent. The $\delta_{t,P-S}$ values calculated from eqn. (7) are reported in column 3 of Table 3. But even this approach yields no significant correlation between the values of the solubility parameters of the casting solution components and the structure of the membrane.

Strictly speaking, the quality of the solvent is determined by the value of the osmotic second virial coefficient, A_2 [28], since the higher the value of this coefficient the better the solvent. For solutions of flexible-chain polymers, such as PVDF [29], a correlation holds between A_2 and $[\eta]$. By comparing the values of $[\eta]$ for the PVDF–solvent systems reported in the last column of Table

3 with the SEM micrographs in Figs. 1–9, one can conclude that no correlation exists between polymer–solvent compatibility and the membrane structure.

For concentrated solutions, Frommer et al. [2] indicate that the concentration of nonsolvent (water) at which the polymer precipitates is somehow a measure of the solvation power, which can be correlated with the membrane structure. Furthermore, this quantity can furnish an appraisal of solvent–nonsolvent interactions. Cloud point data for PVDF–solvent–water systems are reported in the ternary phase diagram shown in Fig. 13. The amount of water required for precipitating PVDF increases, at a fixed PVDF concentration, with the following order for the different solvents:

HMPA > TMU > NMP > DMA > DMF > TEP > TMP > DMSO

However, even in this way the order does not correspond to that found for the membrane structures obtained from the different solvents.

(ii) Solvent–nonsolvent interactions

It has been shown by various authors [3,5,8–13] that a high tendency of a solvent to mix with the nonsolvent plays an important role in membrane porosity and the formation of finger-like cavities. So et al. [4] report on the preparation of asymmetric membranes cast from several polymer–solvent solutions immersed in water, and find, in most cases, that the higher the difference of the solubility parameter of water ($\delta_{t,W}=47.8$ MPa$^{1/2}$ from Ref. [21]) and solvent

$$\delta_{t,W\text{-}S}=\delta_{t,W}-\delta_{t,S} \tag{8}$$

and hence the lower the tendency of mixing [6], the higher the membrane water content. Values of $\delta_{t,W\text{-}S}$ for the present systems can easily be obtained

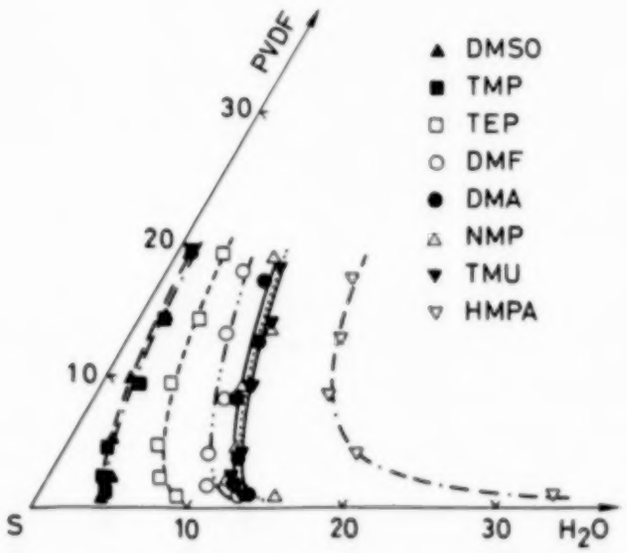

Fig. 13. Ternary phase diagram at 20 °C for PVDF–solvent–water systems.

once $\delta_{t,S}$ is read from Table 1. However, the calculated values appear to be random with respect to the water content of the PVDF membranes in Table 2.

Frommer and Lancet [3] assume the enthalpy of mixing to be an indicative parameter of the tendency of water and of the solvent to dissolve mutually in one another, and show that high values of this parameter correspond to high rates of polymer precipitation, which favour the formation of finger-like membrane structures. Similar trends are reported in Refs. [5], [8] and [13]. The values of the excess enthalpy of mixing for the investigated water–solvent systems [20] are plotted as a function of composition in Fig. 14. Again, by comparing this figure with Figs. 1–9, it can be concluded that on the basis of the thermal effect alone it is not possible unequivocally to predict the final structure of the PVDF membranes. Actually, the tendency of mixing is more precisely described by the free energy of mixing. However, the influence of this quantity has already been investigated by Altena [30], who did not find any correlation between membrane properties and the free energy of mixing. For this reason the free energy of mixing is not examined in the present work.

(iii) Viscosity of the casting solutions

As is generally found [5–8,10,11,13,15,31], an increase in solution viscosity due to an increase of polymer concentration hinders the penetration of the nonsolvent during the immersion step, and hence the formation of cavities in the membrane. Friedrich et al. (10] investigated the effect of the viscosity of

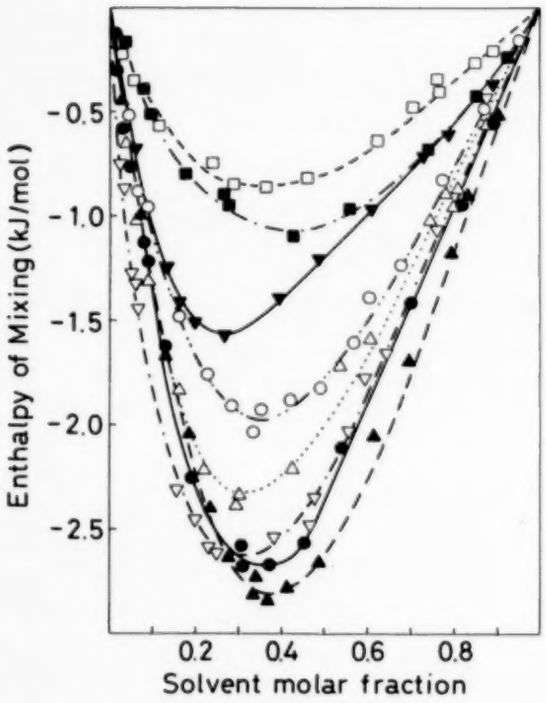

Fig. 14. Excess enthalpy of mixing at 37 °C of water–solvent systems as a function of solvent molar fraction [20]. (See Fig. 13 for symbols.)

equally concentrated polymer solutions in different solvents on membrane structure. They showed that the lower is the solution viscosity, the higher is the occurrence of cavities in the membrane. For the current system, by comparing the values of the viscosity for the PVDF solutions, listed in columns 4 and 5 of Table 4, with SEM micrographs of the membranes shown in Figs. 1–11, it is possible to check the validity of the conclusions drawn in Ref. [9]. When the viscosity value is determined by the polymer concentration, a correlation holds between viscosity and membrane structure. In fact, with increasing polymer concentration a trend towards a disappearance of cavities is observed (Figs. 10 and 11). However, if different viscosities follow merely from the type of casting solvent, membrane structure (Figs. 1–9) appears to be largely independent of the viscosity and the results of Friedrich et al. are not confirmed.

(iv) Diffusivities

It is likely that in some cases mass transfer could become the controlling mechanism of the formation of asymmetric membranes. Unfortunately it is not easy to quantify the importance of mass transfer or to model it, since in the configurations and systems under investigation mass transfer is a very complex process, mainly because of the simultaneous presence of multiple diffusion, convective transport, thermal effects, nonlinear diffusivities, and phase separation.

Nonetheless it is plausible that, during the very first moments following the immersion of the casting solution in the precipitation bath, solvent and nonsolvent interdiffuse to some extent before polymer diffusion becomes important and/or the skin is formed. The characteristic time for mutual diffusion, t_d, of solvent and nonsolvent in a typical thickness of the skin ($\simeq 0.1$ μm, or

TABLE 4

Density and viscosity of PVDF casting solutions

Solvent	PVDF concentration (%)	ρ_{CS} (kg/m^3)	η_{CS} (mPa-sec)	η_{CS}^{SP}
DMA	15	1008.7	889.1	937.7
DMF	15	1014.3	639.5	751.4
DMSO	15	1156.1	3053.1	1394.5
HMPA	15	1085.0	9074.3	2550.1
NMP	10	1074.8	447.6	245.2
NMP	15	1096.2	2239.8	1231.1
NMP	20	1119.4	8943.4	4918.6
TEP	15	1129.4	3021.2	1802.4
TMP	10	1247.6	886.9	403.3
TMP	15	1265.1	5324.3	2426.1
TMU	15	1032.0	1687.9	1100.1

10^{-7} m) can be evaluated from the order of magnitude of the solvent–nonsolvent diffusivity $D \simeq 10^{-5}$ cm^2/sec, or 10^{-9} m^2/sec [32–34]. It follows that $t_d = (10^{-7})^2/10^{-9} = 10^{-5}$ sec. The diffusivity for the polymer is at least one order of magnitude smaller than 10^{-5} cm^2/sec [25]. This implies a diffusion time for the polymer in the typical thickness of the skin of much longer than t_d. The inference is that for many systems, in the very first steps before skin formation, the polymer can be considered practically stable, whereas solvent and nonsolvent interdiffuse. Similar arguments are the basis of some recently developed models [36] where a pseudobinary (solvent and nonsolvent) diffusion is adopted to describe the early stages of asymmetric membrane formation, and are also consistent with the observation that the net macroscopic polymer movement in such systems can be safely neglected, as the final polymer distribution suggests [37]. It must be pointed out that such models reproduce with good agreement the experimental data and observations.

The rate of phase separation is determined by the kinetics and depends on the degree of penetration in the demixing gap. In any case, macromolecules must rearrange before forming a solid phase. This process cannot be considered instantaneous, and the delay between attaining the suitable precipitation concentration and the actual growth of a solid skin can be evaluated as being some orders of magnitude longer than t_d [9].

In such a scheme it makes sense to assume that the local concentration at formation of the skin, and consequently the skin structure, depends essentially on solvent–nonsolvent diffusion. So even if, strictly speaking, diffusion takes place in a ternary system, the binary diffusivity of solvent and nonsolvent can give some significant insight into the rate of the process. Experimental evaluation of the binary concentration dependent diffusivities for the different solvent–nonsolvent systems is difficult and time consuming, but a simple prediction of an average value should be sufficient for the present purpose and qualitative reasoning. As previously illustrated, this prediction was made using the Wilke–Chang technique [22]. The computed values at 25°C are reported in Table 1 for the different solvents, together with the harmonic mean value $D_m = 2D_{S\text{-}W}D_{W\text{-}S}/(D_{S\text{-}W} + D_{W\text{-}S})$ between $D_{S\text{-}W}$ and $D_{W\text{-}D}$.

The values of D_m can be sorted to identify an order of solvents with increasing mean diffusivity. The resulting order nicely reproduces the same sequence as previously detected for decreasing water flux, water content, thickness, or cavity volume per unit membrane area.

A significant dependence of the water flux on the mean diffusivity seems to exist, as can be appreciated from Fig. 15, where this quantity is plotted vs. D_m. In contrast, plots in Fig. 16 of water flux vs. solubility parameter of solvent, $[\eta]$, mean cloud point, or enthalpy of mixing do not show any firm and precise correlation, or look to be largely random.

Some explanations can be given of the dependence of the resulting structure on the solvent–nonsolvent diffusivity. This influence should not be surprising,

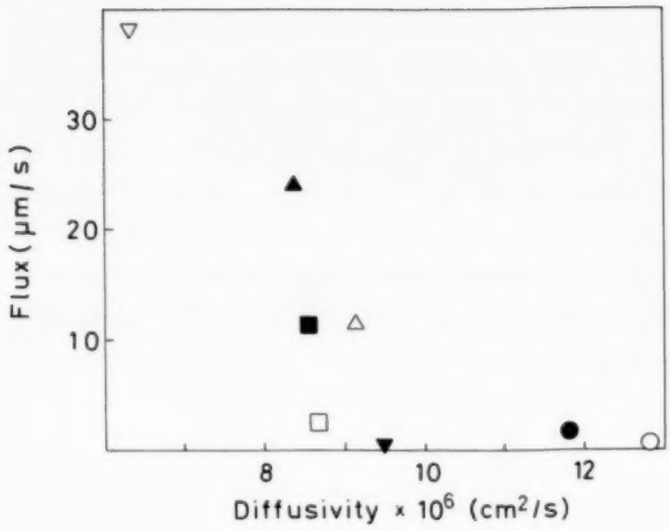

Fig. 15. Water flux vs. mean mutual diffusivity of the system solvent–nonsolvent. (See Fig. 13 for symbols.)

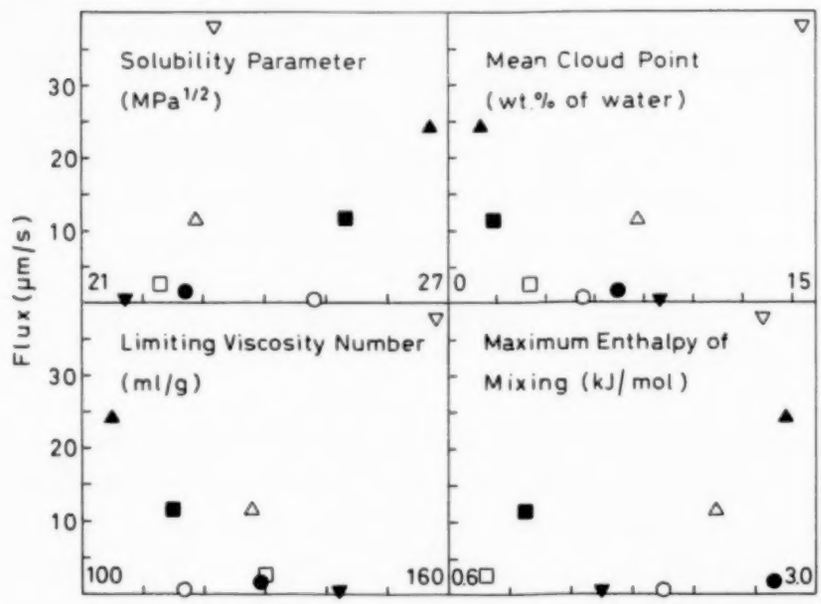

Fig. 16. Water flux vs. solubility parameter of solvent, limiting viscosity number, mean cloud point and maximum enthalpy of mixing. (See Fig. 13 for symbols.)

as in many models a parameter related to the solvent–nonsolvent diffusivity appears. In particular, some models, such as those in Refs. [9] and [36], predict that, when the value of the solvent–nonsolvent diffusivity increases, the concentration path in the ternary diagram during membrane formation should lead to entry into the demixing gap at higher polymer concentration. On the other hand, some experimental observations suggest that the occurrence of phase separation at high polymer concentration determines the formation of

denser and less porous structures than those obtained at lower polymer concentration. By these arguments, the present postulated effects of the solvent–nonsolvent diffusivity on the final membrane structure are justified. Nonetheless, as many existing models do not focus particularly on simultaneous mass transfer both in the "nonsolvent" bath and in the "casting" solution in the very first moments of membrane formation, it might be advisable to check further on the influence of the solvent–nonsolvent diffusivity parameter through a model that takes special account of these aspects. It is the intention of the authors to accomplish this task in future work.

Conclusions

The properties and performances of a membrane produced by the phase separation technique depend very much on the type of solvent utilized for the casting solution. The consequence is that the selection of the proper solvent is essential in the design and engineering of a membrane suitable for a certain given ultrafiltration process. However, difficulties and uncertainties arise in the prediction of membrane characteristics on the basis of the properties of the system used to form the membrane. The prediction implies the capability of quantifying the relative importance of the mechanisms participating in the formation of the membrane, which are mainly phase separation and diffusion in the ternary system of polymer–solvent–nonsolvent. Since these two mechanisms are affected to different extents by thermodynamic and transport properties, the influence of some of these properties on the membrane structure was investigated. To this end the solubility parameters of both polymer–solvent and solvent–nonsolvent, polymer–solvent compatibility, cloud points, solvent–nonsolvent excess enthalpy of mixing, casting solution viscosity, and solvent–nonsolvent diffusivity were measured or evaluated. Results indicate that, contrary to some other systems investigated in the literature, thermodynamic properties, examined one by one, do not influence the performance of the final PVDF membrane, whereas a good correlation was found between solvent–nonsolvent mutual diffusivity and the membrane structure. This seems to indicate that, in the present system, diffusion is the controlling mechanism of membrane formation, in accordance with the conclusions and hypotheses of other researchers (see, e.g. Ref. [8]).

It must finally be noted that, for PVDF membranes obtained from different solvents, many membrane characteristics, such as water flux, water content, membrane thickness and void volume per unit area, are correlated one to another as a consequence of the processes involved in the formation of the membrane. So any of the previous characteristics, besides quantifying the measured property, may furnish information on the resulting membrane structure.

Acknowledgement

This work was financially supported by Consiglio Nazionale delle Ricerche, Progetto Finalizzato Chimica Fine II, Rome, Italy.

References

1 R. Bloch and M.A. Frommer, The mechanism for formation of 'skinned' membranes. I. Structure and properties of membranes cast from binary solutions, Desalination, 7 (1970) 259.

2 M.A. Frommer, I. Feiner, O. Kedem and R. Bloch, The mechanism for formation of 'skinned' membranes. II. Equilibrium properties and osmotic flows determining membrane structure, Desalination, 7 (1970) 393.

3 M.A. Frommer and D. Lancet, The mechanism of membrane formation: membrane structures and their relation to preparation conditions, in: H.K. Lonsdale and H.E. Podall (Eds.), Reverse Osmosis Membrane Research, Plenum, New York, NY, 1972, p. 85.

4 M.T. So, F.R. Eirich, H. Strathmann and R.W. Baker, Preparation of asymmetric Loeb-Sourirajan membranes, J. Polym. Sci., Polym. Lett. Ed., 11 (1973) 201.

5 M.A. Frommer and R.M. Messalem, Mechanism of membrane formation. VI. Convective flows and large void formation during membrane precipitation, Ind. Eng. Chem., Prod. Res. Dev., 12 (1973) 328.

6 H. Strathmann, K. Kock, P. Amar and R.W. Baker, The formation mechanism of asymmetric membranes, Desalination, 16 (1975) 179.

7 M. Guillotin, C. Lemoyne, C. Noel and L. Monnerie, Physicochemical processes occurring during the formation of cellulose diacetate membranes. Research of criteria for optimizing membrane performance. IV. Cellulose diacetate–acetone–additive casting solutions, Desalination, 21 (1977) 165.

8 H. Strathmann and K. Kock, The formation mechanism of phase inversion membranes, Desalination, 21 (1977) 241.

9 C. Cohen, G.B. Tanny and S. Prager, Diffusion-controlled formation of porous structure in ternary polymer systems, J. Polym. Sci., Polym. Phys. Ed., 17 (1979) 477.

10 G. Friedrich, A. Driancourt, C. Noel and L. Monnerie, Asymmetric reverse osmosis and ultrafiltration membranes prepared from sulfonated polysulfone, Desalination, 36 (1981) 39.

11 T.C. Shen and I. Cabasso, Ethyl cellulose anisotropic membranes, in: R.B. Seymour and G.A. Stahl (Eds.), Macromolecular Solutions, Pergamon, New York, NY, 1982, p. 108.

12 J.G. Wijmans, J. Kant, M.H.V. Mulder and C.A. Smolders, Phase separation phenomena in solutions of polysulfone mixtures of a solvent and a nonsolvent: relationship with membrane formation, Polymer, 26 (1985) 1539.

13 H. Strathmann, Production of microporous media by phase inversion processes, in: D.R. Lloyd (Ed.), Material Science and Synthetic Membranes, ACS Symp. Ser., No. 269 American Chemical Society, Washington, DC, 1985, p. 165.

14 H. Strathmann, Synthetic membranes and their preparation, in: P.M. Bungay et al. (Eds.), Synthetic Membranes: Science, Engineering and Applications, D. Reidel, Dordrecht, 1986, p. 1.

15 H. Strathmann, Preparation of microporous membranes by phase inversion processes, in: E. Drioli and M. Nakagaki (Eds.), Membranes and Membrane Processes, Plenum, New York, NY, 1986, p. 115.

16 A.J. Reuvers, F.W. Altena and C.A. Smolders, Demixing and gelation behavior of ternary cellulose acetate solutions, J. Polym. Sci., Polym. Phys. Ed., 24 (1986) 793.

17 C.W. Yao, R.P. Burford, A.G. Fane and C.J.D. Fell, Effect of coagulation conditions on structure and properties of membranes from aliphatic polyamides, J. Membrane Sci., 38 (1988) 113.

18 A.J. Lovinger, Poly(vinylidene fluoride), in: D.C. Bassett (Ed.), Development in Crystalline Polymers, Vol. 1, Applied Science, London, 1982, p. 195.

19 A. Bottino, G. Capannelli, S. Munari and A. Turturro, Solubility parameters of poly(vinylidene fluoride), J. Polym. Sci., Polym. Phys. Ed., 26 (1988) 785.

20 A. Bottino, G. Capannelli, E. Franceschi and A. Turturro, in preparation.

21 A.F.M. Barton, Handbook of Solubility Parameters and Other Cohesion Parameters, CRC Press, Boca Raton, FL, 1983, p. 153.
22 C.R. Wilke and P. Chang, Correlation of diffusion coefficients in dilute solutions, AIChE J., 1 (1955) 264.
23 D.R. Olander, The diffusivity of water in organic solvents, AIChE J., 7 (1961) 175.
24 A. Bottino, G. Capannelli and S. Munari, Effect of coagulation medium on properties of sulfonated polyvinylidene fluoride membranes, J. Appl. Polym. Sci., 30 (1985) 3009.
25 K. Hakagawa and Y. Ishida, Annealing effect in poly(vinylidene fluoride) as revealed from specific volume measurements, differential scanning calorimetry and electron microscopy, J. Polym. Sci., Polym. Phys. Ed., 11 (1973) 2153.
26 A. Bottino, G. Capannelli, A. Imperato and S. Munari, Ultrafiltration of hydrosoluble polymers. Effect of operating condition on the performance of the membranes, J. Membrane Sci., 21 (1984) 247.
27 C.M. Hansen, The universality of the solubility parameters, Ind. Eng. Chem. Prod. Res. Dev., 8 (1969) 2.
28 P.S. Flory, Principles of Polymer Chemistry, Cornell University Press, Ithaca, NY, 1953.
29 G.J. Welch, Solution properties and unperturbated dimensions of poly(vinylidene fluoride), Polymer, 15 (1974) 429.
30 F.W. Altena, Phase separation phenomena in cellulose acetate solutions in relation to asymmetric membrane formation, Ph.D. Thesis, Twente University of Technology, 1982, Chap. 7.
31 I. Cabasso, E. Klein and J.K. Smith, Polysulphone hollow fibers. II. Morphology, J. Appl. Polym. Sci., 21 (1977) 165.
32 G. Guarino, O. Ortona, R. Sartorio and V. Vitagliano, Diffusion, viscosity, and refractivity data on the systems dimethylformamide–water and *N*-methylpyrrolidone–water at 5°C, J. Chem. Eng. Data, 30 (1985) 366.
33 C. Della Volpe, G. Guarino, R. Sartorio and V. Vitagliano, Diffusion, viscosity, and refractivity data on the system dimethylformamide–water at 20 and 40°C, J. Chem. Eng. Data, 31 (1986) 37.
34 H.G. Herzt and H. Leiter, Hydrophobic interactions in aqueous mixtures of methanol, ethanol, acetonitrile, and dimethylformamide, Z. Phys. Chem. (Wiesbaden), 133 (1982) 45.
35 L. Abrosone, G. Guarino, R. Sartorio and V. Vitagliano, Diffusion data on the system PVDF–H_2O–DMA at 20°C. Implication on the membrane casting process, presented at US–Europe Symposium on Advanced Membrane Science and Technology, Ravello, Italy, October 2–7, 1988.
36 L. Yilmaz and A.J. McHugh, Modelling of asymmetric membrane formation. I. Critique of evaporation models and development of diffusion equation formalism for the quench period, J. Membrane Sci., 28 (1986) 287.
37 D.R. Paul, Diffusion during the coagulation step of wet-spinning, J. Appl. Polym. Sci., 12 (1968) 383.

Journal of Membrane Science, 57 (1991) 21–42
Elsevier Science Publishers B.V., Amsterdam

Continuous membrane fermentor separator for ethanol fermentation

Chung-Won Cho and Sun-Tak Hwang*

Department of Chemical Engineering, University of Cincinnati, Cincinnati, OH 45221-0171 (USA)

(Received October 2, 1987; accepted in revised form September 24, 1990)

Abstract

The integration of continuous fermentation and membrane separation in the same unit to enhance the performance of a bioreactor has been studied. Pervaporation with ethanol selective silicone rubber hollow fibers was considered. This is called the "Continuous Membrane Fermentor Separator (CMFS)". In order to observe the membrane effects, the continuous fermentation experiments were conducted through the cyclic operations of dead membrane phase (conventional continuous fermentation) and live membrane phase (CMFS) under the same geometrical and physicochemical conditions. Relative to conventional continuous fermentation, the performance of CMFS results in high yeast cell densities, reduction of ethanol inhibition, longer residence time of substrate, more glucose consumption, and recovery of clean and concentrated ethanol; these are called "membrane effects." A 10–20% increase in ethanol productivity was achieved and pervaporated ethanol concentration was over 7 times higher than that in the fermentor. A mathematical model was developed and used to determine the effects of design and operation parameters of the CMFS. Computer simulation results predict significant improvement in ethanol productivity as well as in glucose utilization when the dimensionless membrane volume was increased.

Keywords: biotechnology; membrane reactor; pervaporation; ethanol fermentation; silicone rubber membrane; hollow fiber membrane

Introduction

Membrane technology may be divided into three categories: membrane preparation, separation of various mixtures, and membrane reactor development. The membrane preparation is an essential element of membrane technology. In a separation process, the role of the membrane is to act as a selective barrier. Once we have the membrane and know its separation performance characteristics [1], the next step would be to apply the membrane to a chemical reaction. This is called the membrane reactor. Membrane application to a biochemical reaction is one of the most attractive research areas since the membrane reactor using synthetic semipermeable membranes of the appropriate chemical nature and physical configuration can provide numerous ad-

*To whom correspondence should be addressed.

0376-7388/91/$03.50 © 1991 — Elsevier Science Publishers B.V.

vantages to the development of a bioreactor; the biocatalysts (whether microbial cells or enzymes) are physically trapped on one side of a suitable membrane, the resulting product is recovered by selective permeation through the membrane, heat sensitive materials in the biosystem can be treated without denaturing, etc.

The limitation and unstable supply of petroleum resources will direct interest to the production of fermenting ethanol from renewable agricultural products or cellulosic wastes in the near future. The fermentation ethanol may be used as a liquid fuel or as a feedstock for the production of organic chemicals currently manufactured from petroleum [2]. Development in enzymatic or acid hydrolysis of cellulosic materials to glucose may supply fermentable carbohydrates at a lower cost [3,4].

Ethanol fermentation is a product-inhibited reaction with a maximum tolerable ethanol concentration from 6 to 10%, depending on the microorganisms. Traditionally, fermentation ethanol has been produced in batches. Batch fermentations are inherently inefficient because they remain "down" for a long period of time between batches and are quite unproductive during the startup period [5]. Moreover, the ethanol productivity is very low (2–2.5 g ethanol/l-hr) due to low concentration of yeast cells, end product inhibition, and substrate depletion. Conducting fermentation in a continuous mode rather than in a batch process is advantageous because of higher productivity, better process control, improved yield, etc. However, conventional continuous fermentors have one major disadvantage. The dilution rate cannot exceed the growth rate of the yeast cells, or there will be cell "washout." Cell density and dilution rate in the conventional continuous fermentations were low, thus limiting productivity. Ethanol inhibition is also an important limiting factor because a high tolerance of ethanol permits concentrated glucose substrates to be fermented with higher utilization of glucose. Therefore, improvement in the productivity of end product-inhibited fermentation requires the removal of the product as it is formed. And the beer which is produced with an ethanol content of 6–10% is conventionally distilled to at least 95% ethanol in order to be suitable as a fuel. In commercial ethanol production, high concentration of clean ethanol is desired for economy in the downstream processing.

There have been several attempts to achieve a simultaneous separation of ethanol as it is formed, along with fermentation. Various product removal methods have been coupled with fermentation, including vacuum evaporation [6,7], flash vaporization [8], solvent extraction [9,10], and membrane permeation. Systems based upon membrane permeation have been suggested in a variety of processes, including dialysis [11], ultrafiltration or microfiltration [12–14], and pervaporation [15]. Pervaporation has been considered for the ethanol-to-water separation with various membranes [16]. The performance of silicone rubber has been reported to have a high ethanol-to-water selectivity, while most of the other membrane materials exhibit high water-to-ethanol

selectivity. Hoover and Hwang [17] have studied the continuous membrane column with pervaporation of alcohols and described a mathematical model for capillary membrane pervaporation. Permeability data and separation factors as a function of alcohol concentration were also obtained and fitted to a polynomial equation. The separation factor of ethanol-to-water was 7 to 8 when the concentration of ethanol was below 5%.

When the conventional continuous fermentation is coupled with pervaporation by a capillary permeator, it is called the CMFS. The objectives of this study were to investigate the effects of membrane pervaporation on the continuous fermentation process and to demonstrate that the CMFS fermentation system would be superior to the conventional continuous fermentation in terms of ethanol productivity, utilization of substrate, and downstream processing by comparing both processes under the same geometrical and physicochemical environment. In addition, a mathematical analysis has been developed which adequately describes the CMFS and predicts the performance of the CMFS when the system parameters change.

Theory

1. CMFS concepts

The CMFS, illustrated in Fig. 1, has a shell and tube configuration; in other words, a bunch of hollow fiber membranes are retained in a cylindrical shell container.

The proposed CMFS consists of two basic segments: (1) a well-mixed fermenting region in the shell side termed as the "fermentor" and (2) a product pervaporating region through the lumen of the hollow fibers, termed as the "separator." Fresh substrate is fed to the fermentor. In the fermentor, glucose is converted to ethanol. Pervaporation takes place across the interposed membrane between the fermentor and the separator. The pervaporated permeate contains highly concentrated ethanol solution. Ethanol inhibition may be diminished, which can cause faster rates of ethanol production and yeast cell growth. When the appropriate amount of residue is taken from the fermentor to keep the continuous fermentation operation, there is a mismatch in flow rates between fresh substrate and residue; that is, the amount of residue stream becomes less than that in conventional continuous fermentation. Comparing the same case in conventional continuous fermentation, yeast cells in the fermentor will be accumulated and the residence time of the substrate in the fermenting region will get longer. The degree of flow mismatch depends on the design and operation of the CMFS, such as dilution rate, membrane module, permselectivity of the membrane, etc. As a consequence, more ethanol can be produced by better utilization of glucose because of the reduction of ethanol inhibition and higher yeast cell densities. Hence, the CMFS is expected to

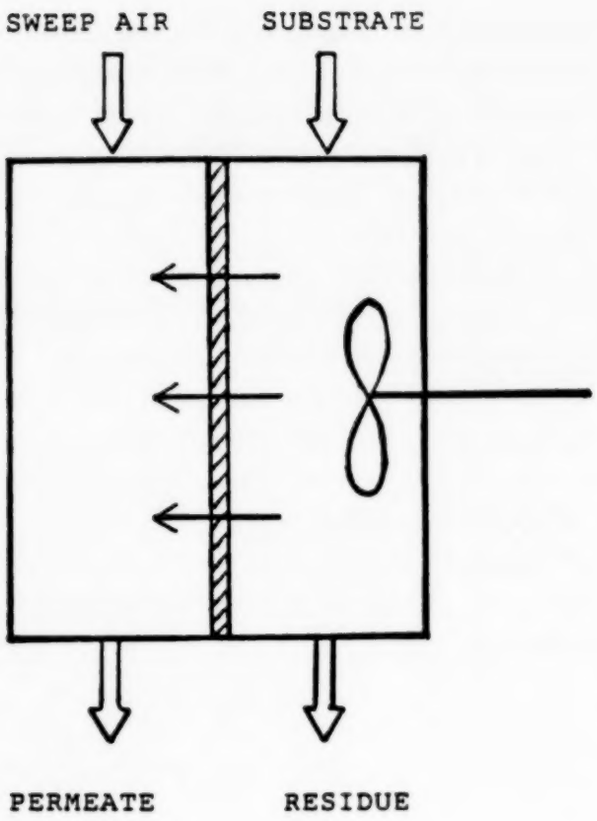

TUBE SIDE	SHELL SIDE
SEPARATOR	FERMENTOR
PERVAPORATION	FERMENTATION
SILICONE RUBBER	YEAST
PLUG FLOW	WELL-MIXED

Fig. 1. Concept of the continuous membrane fermentor separator.

result in higher yeast cell densities and higher ethanol productivities along with the simultaneous recovery of highly concentrated clean ethanol.

2. CMFS modeling

The CMFS is the integration of the fermentor and the separator. The fermentor considered is the continuous fermentor from which the ethanol is removed by membrane pervaporation. The separator is the capillary permeator in which fermentation occurs in the shell side. Combining the information of the conventional continuous fermentation and that of capillary permeator provides the appropriate expression for the CMFS model.

Analysis of a single stage chemostat [18], shown in Fig. 2, will serve as a basis for the conventional continuous fermentation. A set of equations relating concentrations of yeast cells X, product ethanol E, and limiting substrate glucose S to the primary independent operating variable, the flow rate of the fresh medium, can be derived through the use of material balances as follows:

$$\frac{dX_o}{dt}=\left(\mu-\frac{v_i}{V}\right)X_o \tag{1}$$

$$\frac{dE_o}{dt}=\frac{v_i}{V}(E_i-E_o)+\nu X_o \tag{2}$$

$$\frac{dS_o}{dt}=\frac{v_i}{V}(S_i-S_o)-\frac{1}{Y_{X/S}}\mu X_o \tag{3}$$

Here, subscripts i and o represent inlet and outlet conditions, respectively.

At steady state conditions, the left hand sides of eqns. (1)–(3) are zero. Then,

$$\mu=\frac{v_i}{V}=D \tag{4}$$

$$\nu=\frac{D\,E_o}{X_o} \tag{5}$$

$$Y_{X/S}=\frac{X_o}{S_i-S_o} \tag{6}$$

Now we can get the values of μ, ν, and $Y_{X/S}$ using eqns. (4)–(6) since the

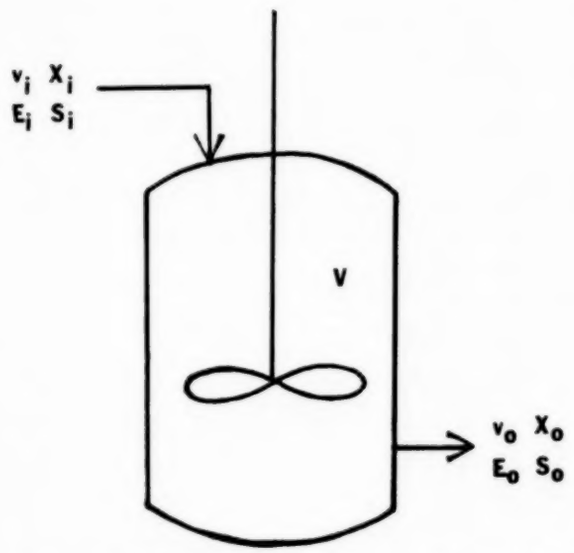

Fig. 2. Schematic diagram of conventional continuous fermentor.

values of D, X_o, S_i, S_o, and E_o can be obtained by the conventional continuous fermentation experiment.

Hoover and Hwang [17] have described the pervaporation process with the overall phenomenological equation, and the capillary permeator has been modeled in terms of the liquid pervaporation process. Referring to Fig. 3, which shows all the different elements at external connections to the CMFS, the model will treat the fermentor as the well-mixed region of fermentation broth and the separator as the plug flow region of sweep air stream. The flow rates and mole fractions of the ethanol E, water W, and sweep air S in the separator side are as follows:

$$G_T = G_S + G_E + G_W \tag{7}$$

$$Y_E = G_E / G_T \tag{8}$$

$$Y_W = G_W / G_T \tag{9}$$

The differential forms of the pervaporation equation for ethanol and water were written for a cylindrical geometry for n hollow fibers with radial dimension of r_o and r_i over a differential length dZ [17].

$$\frac{d\,G_E}{d\,Z} = \frac{Q_E\, 2\pi\, n\, (P_E^o X_E - P_S Y_E/\gamma_E)}{\ln\,(r_o/r_i)} \tag{10}$$

$$\frac{d\,G_W}{d\,z} = \frac{Q_W\, 2\pi\, n\, (P_W^o X_W - P_S Y_W/\gamma_W)}{\ln\,(r_o/r_i)} \tag{11}$$

Since membrane permeation is a slow process, the pervaporation process can be considered as a pseudo steady state process during the short time period, which means the amount of pervaporation remains constant. The amounts of

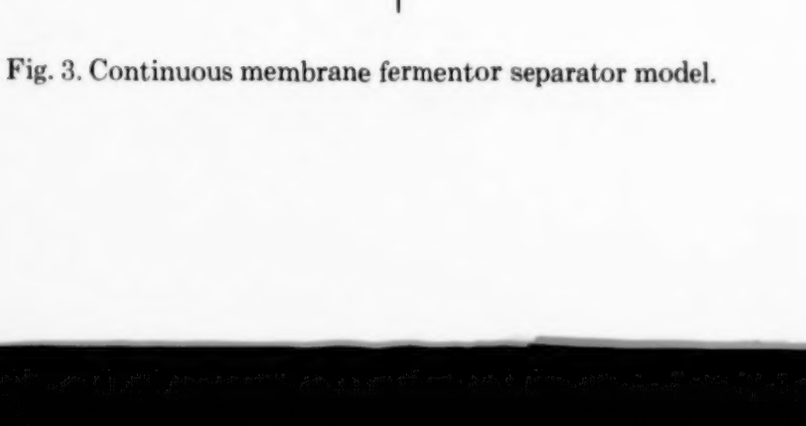

Fig. 3. Continuous membrane fermentor separator model.

ethanol and water pervaporated in a short time interval were obtained by integrating eqns. (10) and (11) along the length of the separator l. Then,

$$G_{Eo} - G_{Ei} = \int_0^l \frac{Q_E\, 2\pi\, n\, (P_E^o X_E - P_S\, Y_E/\gamma_E)}{\ln\,(r_o/r_i)}\, dZ \tag{12}$$

$$G_{Wo} - G_{Wi} = \int_0^l \frac{Q_W\, 2\pi\, n\, (P_W^o X_W - P_S\, Y_W/\gamma_W)}{\ln\,(r_o/r_i)}\, dZ \tag{13}$$

If the model of the separator is coupled with that of the conventional continuous fermentor, the component mass balances of ethanol E, glucose S, and yeast cell X in the fermentor side can be modified from eqns. (1)–(3) taking into account eqns. (12) and (13) as follows:

$$\frac{d\,E_o}{d\,t} = -\frac{1}{v}\,(G_{Eo} - G_{Ei} + v_o E_o) + \nu X_o \tag{14}$$

$$\frac{d\,S_o}{d\,t} = \frac{1}{v}\,(v_i S_i - v_o S_o) - \frac{1}{Y_{X/S}}\,\mu X_o \tag{15}$$

$$\frac{d\,X_o}{d\,t} = \left(\mu - \frac{v_o}{V}\right) X_o \tag{16}$$

Initially inlet and outlet conditions from the steady state of the conventional continuous fermentation and inlet conditions of the separator are given. Then solving eqns. (14)–(16) after first computing eqns. (12) and (13) gives the dynamic behavior of the CMFS along the given time intervals. These computations are repeated until the concentrations of yeast cells, ethanol and glucose reach the steady state. At each time increment, the values of component permeabilities and any other variables must be reevaluated as necessary. Vapor–liquid equilibrium behavior was recovered from the Antoine vapor pressure equation and activity coefficients from the Wilson equation to the extent that these equations approximate the actual data. The program was solved on a Wilbur computer using the differential equation solver DGEAR developed by IMSL.

Experiments

After the membrane module was constructed, a series of permeation tests were conducted to verify the permeability values of ethanol and water through silicone rubber membrane. They were very close to the reported values by the previous investigators [15,17].

1. Yeast strain and culture

The yeast organism used in the ethanol fermentation studies was *Saccharomyces cerevisiae* NRRL-Y-2034 obtained from the U.S. Department of Agriculture's Northern Regional Research Laboratory (Peoria, IL). For the preparation of YM broth to cultivate yeasts, the medium was composed of 3 g yeast extract, 3 g malt extract, 5 g pepton, 10 g glucose, 20 g agar and 1 l of distilled water without adjusting the pH. Every month new slants of the yeast were cultured to insure high viability and to lower the changes of strain degradation. The composition of the substrate medium was adapted from Cysewski and Wilke [7] and is given in Table 1. Ergosterol was supplemented to eliminate the oxygen need to retain the yeast cell viability during the anaerobic conditions [19]. Citric acid and sodium were added as a buffer to maintain the pH of 4.0–4.5 for minimizing the chances of contamination. The medium components were mixed and sterilized together at 121 °C for 20 min in an autoclave.

2. Design and operation of the CMFS fermentation system

Figure 4 illustrates the design of a laboratory-scale CMFS that was fabricated in such a manner that it could be readily assembled and disassembled between experiments in order to clean and sterilize the various components and to change its configuration. The CMFS has a shell and tube configuration which consists of an outer shell made of 1 in. glass pipe, 100 cm in height. The glass shell is joined at the top to a stainless steel Swagelok cross. One side of this cross acted as the access to the fermentor. The other side of the cross allowed for venting gases from the top of the CMFS. The bottom of the glass shell was joined to a stainless steel Swagelok T connector. The side port of the T was the exit from the fermentor. The hollow fiber bundle was made of 103 fibers with an active length of 98 cm and total surface area, based on log mean radius, of 1430 cm^2. Both end portions of the hollow fibers were potted within the 3/4 in. O.D., 1/25 in. thick wall, and the 10 cm long glass tubing end pieces,

TABLE 1

Base fermentation media

Component*	g/l
Glucose	100.0
Yeast extract	8.50
NH_4Cl	1.32
$MgSO_4 \cdot 7H_2O$	0.11
$CaCl_2$	0.06
Anti-foam	0.2 ml
Ergosterol	10.0 mg
Tap water	Make up to 1 l

*All salts and glucose are reagent grade.

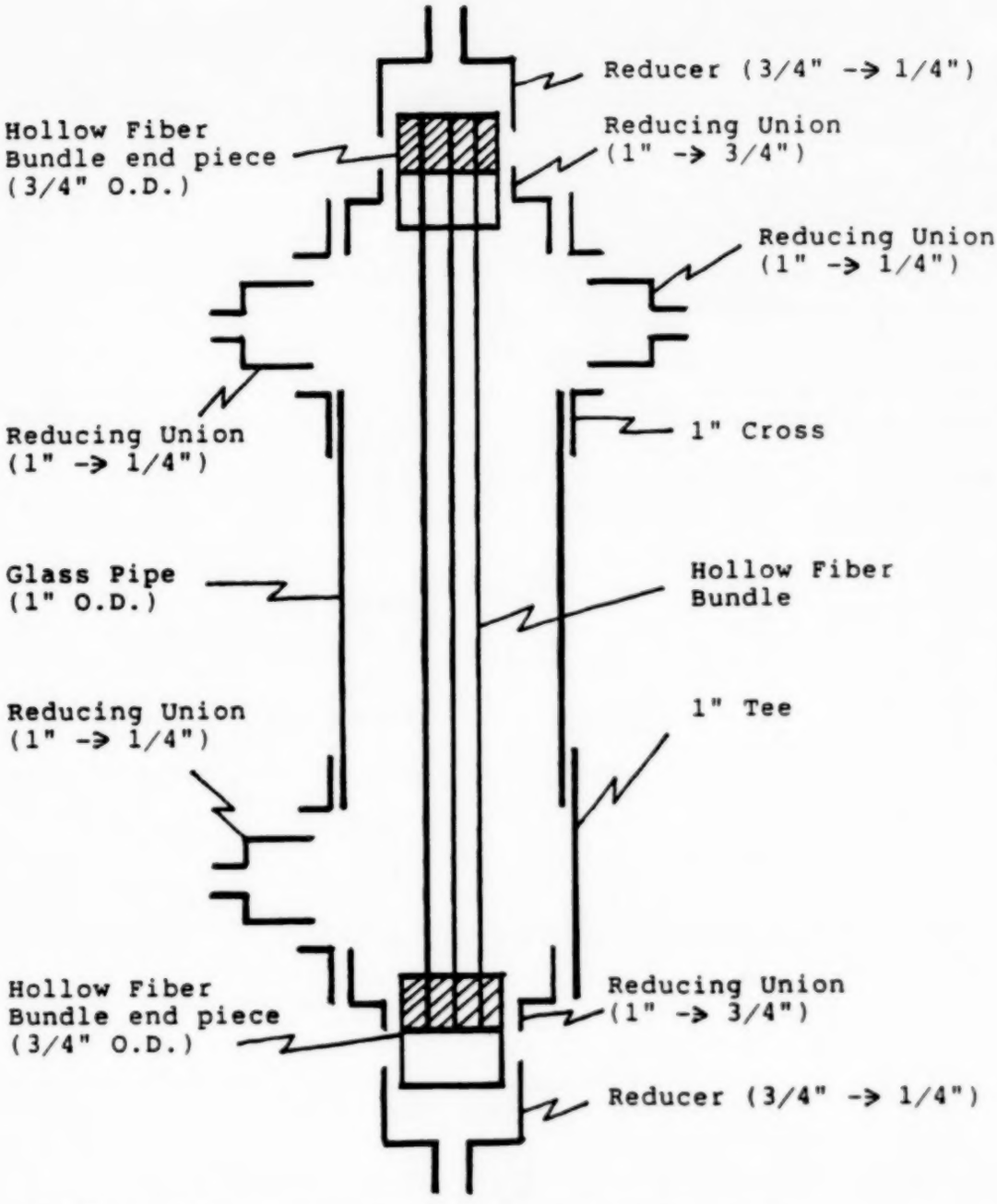

Fig. 4. Details of the continuous membrane fermentor separator unit.

respectively. The membrane used in this study was Silastic Medical Grade silicone rubber capillary tubing obtained from Dow Corning Corporation, Midland, MI. Table 2 lists some information about the tubing dimensions. Dow Corning 730 RTV fluorosilicone sealant was used as a potting material for the membranes, because of its strong fuel and solvent resistance. Two bore-through stainless steel Swagelok reducing unions (from 1 in. to 3/4 in.) for the entrance of a 3/4 in. glass tube were connected to the top of the cross and to the bottom of the T respectively. The top and bottom of the CMFS were ended with stainless steel Swagelok reducers. The hollow fiber bundle connected with two 3/4

TABLE 2

Silastic tubing dimensions (cm)

Inside radius	0.015
Outside radius	0.032
Wall thickness	0.017
Log mean radius	0.0224

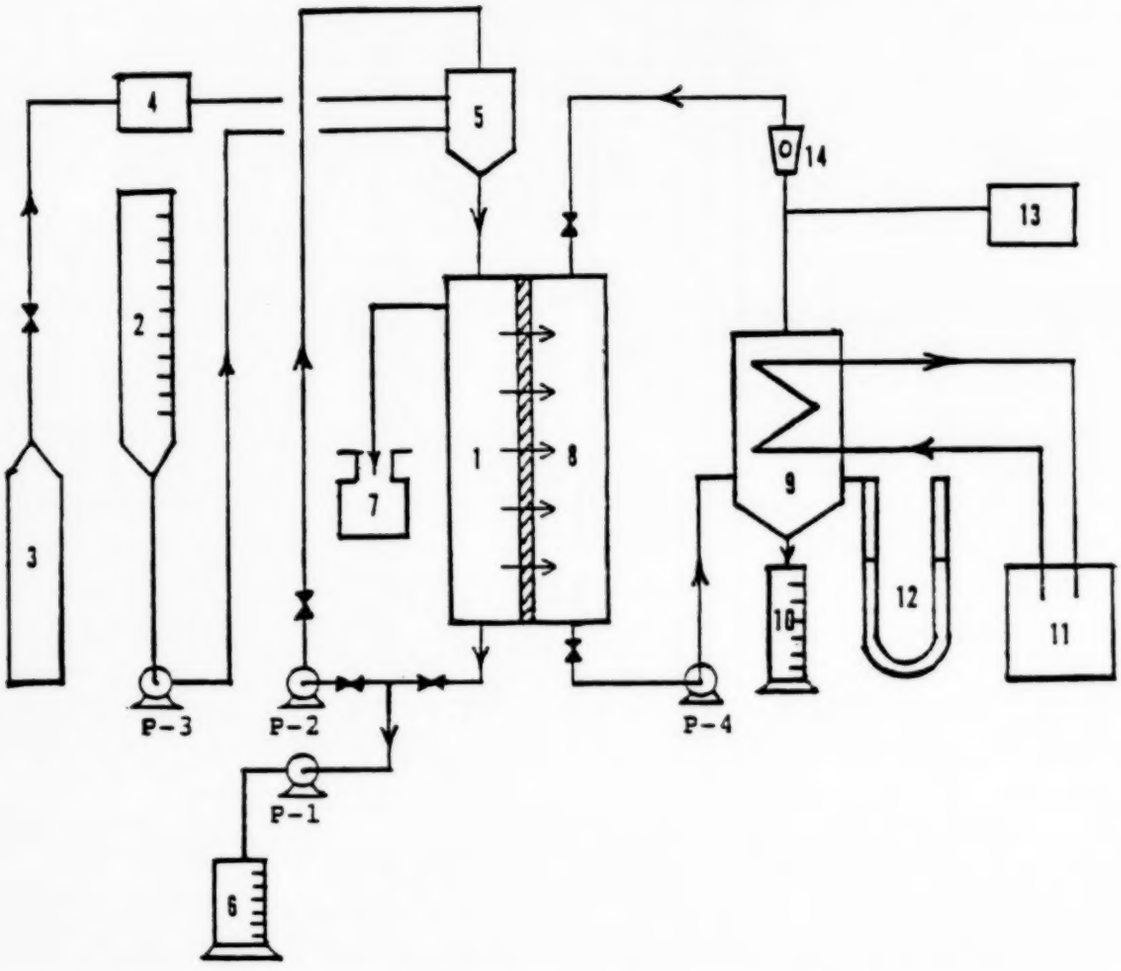

Fig. 5. Continuous membrane fermentor separator fermentation system.

1. Fermentor
2. Feed reservoir
3. Nitrogen cylinder
4. Nitrogen purifier
5. Intermediate tank
6. Residue receiver
7. Gas discharging bottle
8. Separator
9. Condenser
10. Product receiver
11. Refrigerated bath
12. Manometer
13. Digital thermometer
14. Rotameter

P-1. Residue pump
P-2. Recirculating pump
P-3. Feed pump
P-4. Air circulating pump

in. glass tubes can be easily charged inside the 1 in. glass shell. All the ferrules were made of Teflon.

The laboratory-scale CMFS fermentation system was constructed to demonstrate the feasibility of the CMFS concept and to investigate the effects of operating conditions on the performance of the CMFS. A schematic diagram of the apparatus used in this study is shown in Fig. 5. The continuous fermentation experiments were conducted through the cyclic operations of dead and live membrane phases at various dilution rates by changing the flow rates of fresh feed stream.

In order to start the dead membrane phase, the valves connecting into and out of the separator were closed. Setting the fresh feed flow rate, the residue stream was controlled to maintain the liquid level in the fermentor. The system was allowed to come to a steady state. Samplings of residue were made every 4 hr to confirm whether or not steady state had been achieved. When the concentrations of yeast cells, glucose and ethanol remained constant over a 12-hr period, steady state operation was assumed. At the end of a certain steady state of the dead membrane phase, the live membrane phase was started by opening the valves into and out of the separator. Then the air circulating pump in the separation part was started. As the fermentor level dropped due to the pervaporation of ethanol, the residue stream was adjusted to maintain the fermentor level for keeping the working volume constant. If the amount of permeated ethanol and residual ethanol was matched to the amount of ethanol produced in the fermentor, a new steady state was established. This was the completion of one cyclic operation of dead and live membrane phases. The dilution rates of 0.071 to 0.262 based upon the total fermentor working volume were covered by changing the feed flow rate from 30 to 110 ml/hr. The fermenting broth was circulated with a reflux ratio $\geqslant 200$. Cyclic operation was repeated for every dilution rate.

3. Analysis

The yeast cell concentration was determined from the optical density measurement, using a Bausch & Rohm Spectronic 20 Spectrophotometer at a wavelength of 520 nm. The calibration curve was prepared by measuring absorbance of samples of varying yeast cell concentrations. The yeast cell concentration of the unknown samples was then obtained by measuring the optical density and reading the yeast cell concentration directly from the calibration curve. Yeast cell viability was determined periodically, using the methylene blue staining technique [20]. Concentrations of glucose and ethanol were determined by liquid chromatography. The instrument was a Hewlett-Packard model 1812A liquid chromatograph equipped with a refractive index detector and fitted with 700-CH beer analysis carbohydrate column (300 mm $\times$ 6.5 mm), purchased from Alltech Inc. The column consisted of a sulfonated polystyrene resin as the calcium form. HPLC grade water was used as the mobile phase.

The column temperature was 90°C, the column pressure was 40 bar, and the eluent flow rate was 0.5 ml/min. Calibration curves for glucose and ethanol were prepared, using standard solutions.

Results and discussion

1. Fermentation kinetics

The ethanol fermentation kinetics is discussed based upon the results of conventional continuous fermentation (dead membrane phase). Specific rates of yeast cell growth μ, and ethanol production ν were obtained using eqns. (4) and (5). They are plotted against ethanol concentration in Figs. 6 and 7. Two scattered points in Figs. 6 and 7 were obtained at very low dilution rates at which the concentration of glucose was less than 1 g/l. Specific rates of yeast cell growth and ethanol production show strong dependence upon the concentration of glucose in these situations. Experimental data were fitted to the generalized nonlinear fermentation kinetic model described by Luong [21]. This model describes the kinetic pattern of ethanol inhibition in terms of the following eight parameters. These values were computed by the nonlinear regression procedure using ZXSSQ developed by IMSL as follows.

$\mu_o = 0.284$ $\quad E_M = 69$ $\quad \alpha = 1.48$ $\quad K_S = 0.18$
$\nu_o = 1.23$ $\quad E_{M'} = 70$ $\quad \beta = 2.69$ $\quad K_{S'} = 0.26$

In general, as the ethanol concentration is increased, the specific rates of yeast cell growth and ethanol production decrease. At the fermentation tem-

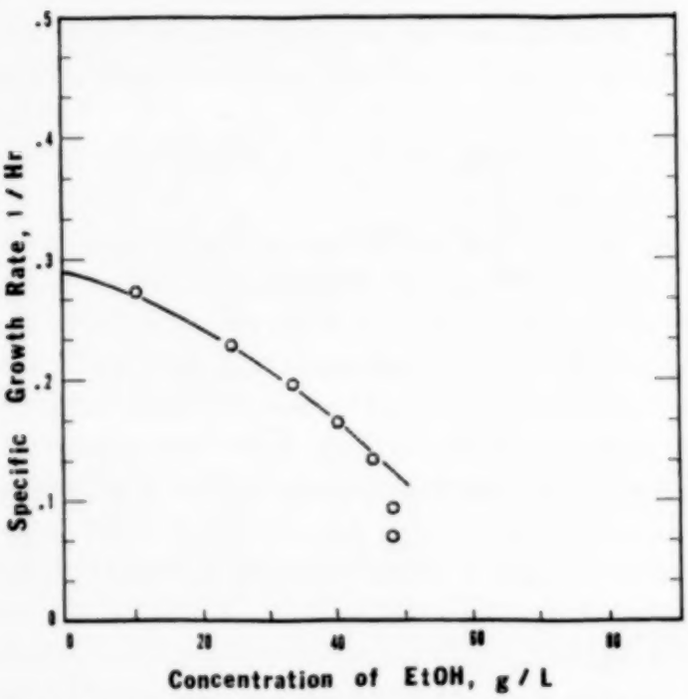

Fig. 6. Specific yeast cell growth rate vs. concentration of ethanol obtained from continuous fermentation experiments at 25°C.

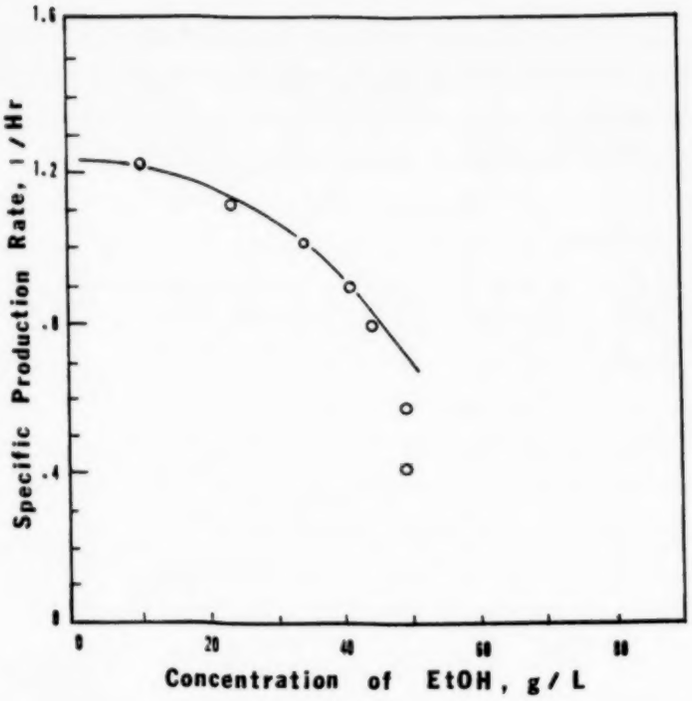

Fig. 7. Specific ethanol production rate vs. concentration of ethanol obtained from continuous fermentation experiments at 25 °C.

perature of 25 °C, ethanol had a noticeable effect on the growth rate at concentrations even above 5 g/l, and the maximum ethanol concentration at which the cells did grow was ca. 69 g/l. Ethanol-producing capability did not change much below 20 g/l and was considered to reach complete inhibition at 70 g/l of ethanol concentration if the curves are extrapolated. Substrate inhibition was not considered in this study since it was not encountered, and because the glucose concentration was not high and fermentation took place in a well-mixed state. However, if much greater concentrations of glucose (greater than 150 g/l) appeared in the fermentor, the kinetic model may need to treat substrate inhibition by adding an additional term [22,23].

2. Performance of the CMFS

The CMFS unit was operated not only at the dead membrane phase but also at the live membrane phase with pervaporation. The improvement of the CMFS fermentation system can be clearly observed since both cases were compared under the same geometrical and physical conditions. The goal of this work was to find out the membrane effects of the CMFS compared with the conventional continuous fermentation.

Cyclic operations between the dead membrane phase and the live membrane phase experienced the stepwise changes of steady state along with the dilution rate increase. One steady state shifted very slowly to another steady state. Approximately 3 to 4 fermentor volumes of fresh feed supply were needed to get to the steady state. During the live membrane phase, flow mismatch be-

tween the fresh feed and residue stream was encountered in the range of 1.3–1.9 ml/hr, which equals the amount of pervaporation through the membrane. Pervaporated ethanol in the live membrane phase is glucose-free, clear, and highly concentrated up to 30%, so this stream should be considered as more than a product of the conventional fermentor alone. Silicone rubber membranes have been found to be very durable. There was no tendency for the yeast cells to form a layer on the membrane. A low pH of 4.0–4.5 was maintained. Yeast viability remained over 95% for the duration of the 19-day experiment.

Figure 8 shows the results of continuous fermentations with a 10% synthetic glucose medium. The glucose, ethanol, and yeast cell mass concentrations are plotted against the dilution rate. The solid line shows the result of conventional continuous fermentation and the broken line represents the CMFS fermentation system. As would be expected, ethanol and yeast cell concentrations decrease with the increasing dilution rates, and glucose concentration increases accordingly in both cases. However, the CMFS results relative to the conventional continuous fermentation show that the yeast cell mass concentration in the fermentor was increased, highly concentrated ethanol was pervaporated through the membrane, ethanol concentration was kept at almost the same level, and more glucose was consumed. Table 3 contains experimental data from the continuous fermentation experiments.

The yeast cell concentration became higher since the cells were accumulated

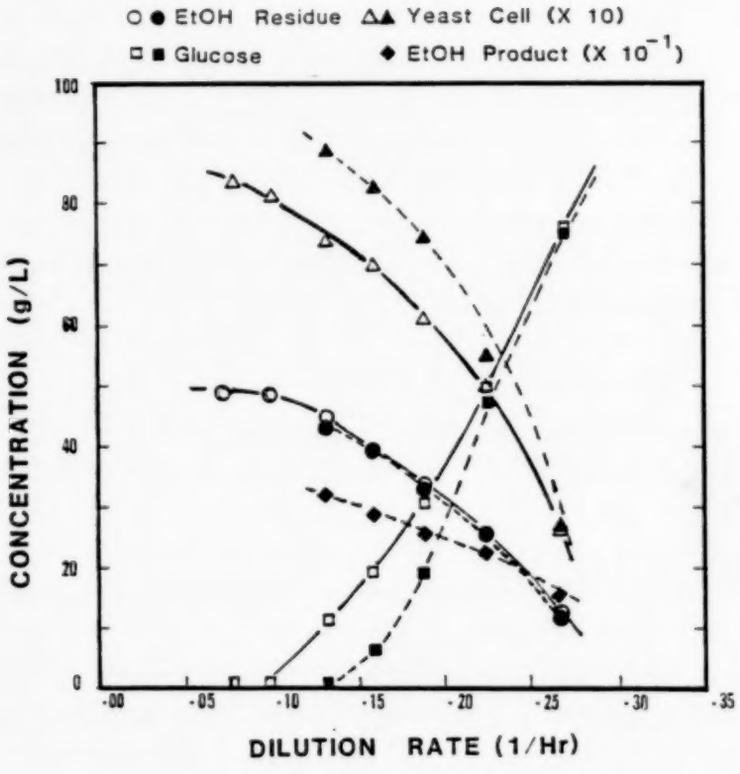

Fig. 8. Continuous fermentation experiments. (——) conventional continuous fermentation; (– – –) continuous membrane fermentor separator.

TABLE 3

Experimental results of continuous fermentation

Operating mode[a]	Flow rate feed	Dilution rate	Concentration in residue			Permeate		EtOH produced
			EtOH	Glu.	Cell	EtOH conc.	Flow rate	
	v	D	E	S	X	P	v	E
D	30	0.0714	48.0	0.3	8.32			3.43
D	41	0.0976	48.0	0.7	8.13			4.69
D	56	0.1333	45.1	11.2	7.30			6.00
L	56	0.1333	42.0	0.3	8.80	300	1.87	6.75
D	65	0.1548	40.2	19.3	6.90			6.19
L	65	0.1548	40.1	4.1	8.10	294	1.80	7.28
D	77	0.1833	34.2	30.4	6.02			6.23
L	77	0.1833	33.3	19.3	7.20	2.59	1.69	7.00
D	93	0.2214	25.0	49.2	4.90			5.54
L	93	0.2214	25.0	47.4	5.25	218	1.58	6.26
D	110	0.2619	12.0	74.2	2.60			3.14
L	110	0.2619	11.1	73.5	2.70	144	1.30	3.29

Feed Conditions: $E_i = 0$ g/l, $S_i = 100$ g/l, $X_i = 0$ g/l.
Fermentor working volume: 420 ml.
All data are reported at steady state.
[a]D: Dead membrane phase.
L: Live membrane phase.

in the fermentor due to the flow mismatch; that is, the amount of residue (outlet stream) was less than that of fresh feed. It should also be noted that the residence time of the substrate became longer as a result of flow mismatch. When higher cell density in the fermentor is obtained, the ethanol production rate increases. Then, if the ethanol is not removed, accumulation of ethanol takes place and its concentration will be increased. Therefore, the fact that the ethanol concentration is kept at almost the same level in the CMFS implies that the reduction of potential ethanol inhibition is achieved. It should be mentioned that the ethanol permselective property of the silicone rubber membrane facilitates the reduction of ethanol inhibition (otherwise ethanol accumulation might occur) and gives highly concentrated, clean ethanol by the pervaporation. With an increase of yeast cell densities and the reduction of the ethanol inhibition level, along with longer residence time, more consumption of glucose can be accomplished. All of these phenomena are called "membrane effects," which are graphically shown as the gap between the solid line and the broken line in Fig. 8.

At the dilution rate of 0.15 hr^{-1}, for example, only 82% of the initial glucose

was fermented. In other words, it was not possible to ferment a 10% glucose feed completely in the conventional continuous culture. In the case of the CMFS, glucose consumption was increased to 97% along with higher yeast cell density and almost the same ethanol level as compared with the conventional continuous fermentation. Permeate ethanol concentration was 290 g/l, which was 7 times higher than that in the fermentor. One of the important factors to consider is the final product concentration leaving the fermentor and entering the recovery system, since the cost of recovery is proportional to the amount of liquid to be handled and is inversely proportional to product concentration.

It can be seen that lowering the dilution rate allows the complete consumption of glucose where glucose concentration in the fermentor was held near zero. The dilution rate for the complete utilization of glucose in the feed was shifted from 0.09 in the conventional continuous fermentation to 0.13 in the CMFS. The percentage utilization of glucose may be counted in the productivity consideration, if necessary.

The ethanol productivity is shown in Fig. 9 as a function of the dilution rate. The ethanol productivity was the sum of the net weights of ethanol in the permeate and in the residue divided by the fermentor volume per unit time. The solid line is the result of the conventional continuous fermentation and the broken line represents that of the CMFS. Although the ethanol concentration in the residue stream shown in Fig. 8 decreases with increasing dilution rate, ethanol productivity actually increases up to the dilution rate of 0.17 since

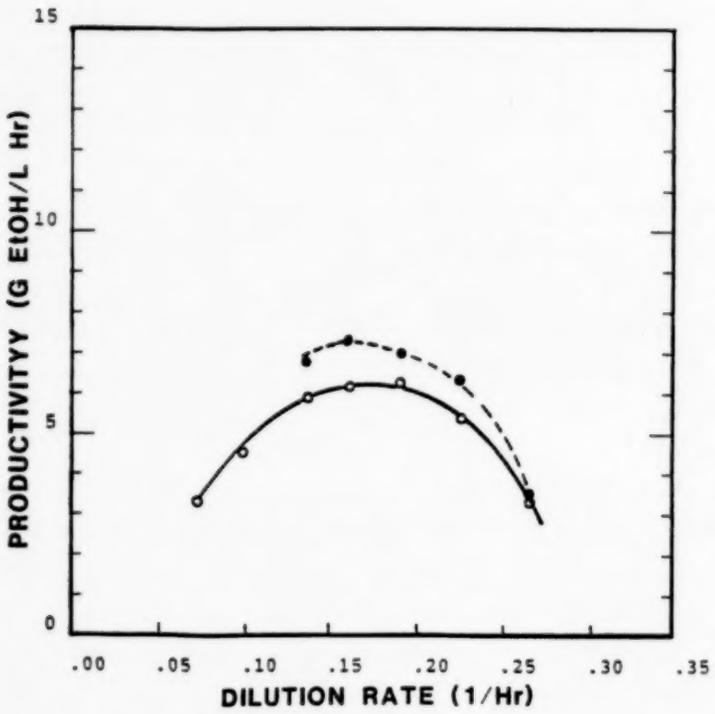

Fig. 9. EtOH productivity in continuous fermentation. (——) conventional continuous fermentation; (– – –) continuous membrane fermentor separator.

the productivity is generally the product of ethanol concentration and the dilution rate. After that maximum point, it begins to decrease because, due to yeast cell washout, the increase of the dilution rate cannot catch up with the decrease of the product concentration. The maximum ethanol productivity of the CMFS was 7.3 g ethanol/l-hr, which was a 18% increase over the maximum productivity of 6.2 g ethanol/l-hr in conventional continuous fermentation. Interestingly, maximum productivity does not necessarily occur at a dilution rate corresponding to the maximum conversion of substrate or the maximum permeate ethanol concentration. Therefore, optimization compromises may be made, taking into account productivity, permeate ethanol concentration, residual substrate, etc.

Potential advantages of the CMFS include increased ethanol productivity and the ability to obtain a highly concentrated clean product. The former allows a more efficient use of fermentor volume and reduces the size of auxiliary equipment, such as media sterilizers, pumps, etc. In addition, the removal and isolation of the product in the separator could lead to savings in the downstream processing steps since the pervaporated product is a highly concentrated clean ethanol. Furthermore, the hollow fiber module may permit more compact and simpler process equipment than any other membrane modules.

3. Simulation analysis

The data obtained from the laboratory-scale CMFS fermentation system were used to refine and demonstrate the validity of the CMFS model described earlier. The points on Fig. 10 are concentrations of ethanol, glucose and yeast cells against dilution rates from the CMFS fermentation experiments for which the simulation was performed. Computed results of the CMFS model are plotted with the solid lines. The simulations show that the quantity and composition are in good agreement with the experimental results.

The model of the CMFS could predict the performance of the CMFS fermentation system when the system parameters change. Volume ratio of separator fermentor (dimensionless membrane volume) and glucose concentration of the fresh feed were chosen for the demonstration, taking into account possible membrane effects on productivity improvement and glucose utilization, etc. Here, the dimensionless membrane volume was introduced to indicate the relative membrane area per fermentor volume. As this quantity becomes larger the membrane area grows proportionally for a given fermentor.

The CMFS performances shown in Fig. 11 were evaluated at four different dilution rates by varying the dimensionless membrane volume in the range 0–1.0, while the other operating conditions remained the same as those in the CMFS experiments. At a certain dilution rate, e.g. following line Number 2, ethanol productivity increases as the dimensionless membrane volume increases due to membrane effects. However, there exists a maximum ethanol productivity at which the complete utilization of glucose occurs. In order to

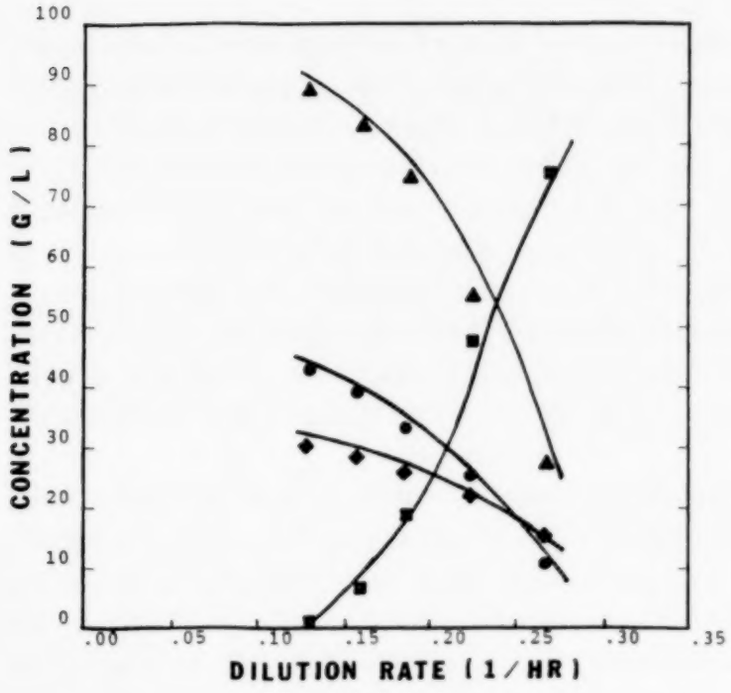

Fig. 10. Comparison of the continuous membrane fermentor separator performance between experimental data and model computations. (●) ethanol residue; (■) glucose; (▲) yeast cell ($\times 10$); (◆) ethanol product ($\times 10^{-1}$).

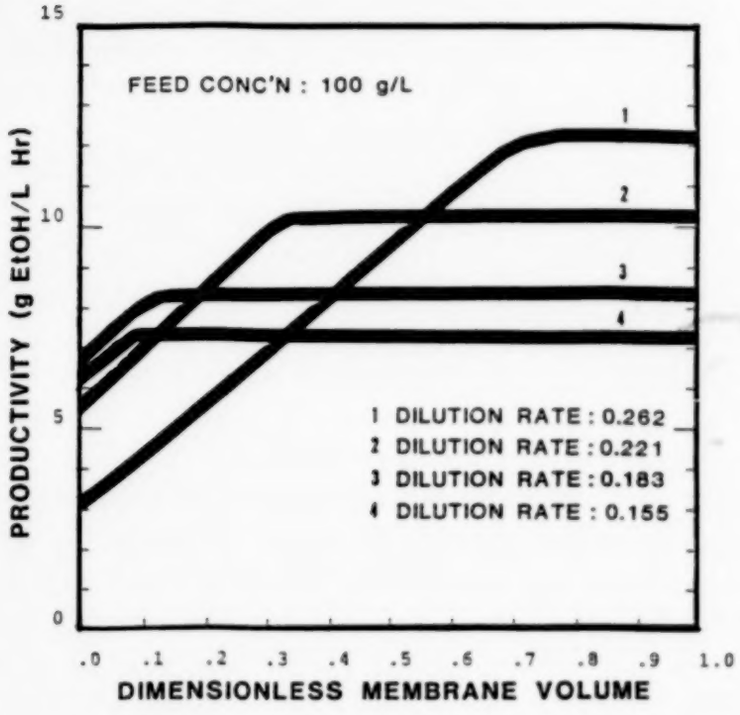

Fig. 11. Influence of membrane capacity on EtOH productivity at various dilution rates.

attain this maximum ethanol productivity, a minimum dimensionless membrane volume is required. This may be a design criterion, since ethanol productivity cannot be improved even though the dimensionless membrane volume is increased. In any case, it is indicated that complete utilization of the glucose can be achieved by increasing the dimensionless membrane volume. If the dimensionless membrane volume is limited at a certain level for some reason, e.g. 0.1, the dilution rate necessary to reach the highest ethanol productivity is 0.18, whereas this value is 0.22 for a dimensionless membrane volume of 0.3. This may also be another design criterion. At the limit of the dimensionless membrane volume tending to zero, we obtain the conventional continuous fermentation result.

Figure 12 shows the CMFS performance for 20% glucose feed at the dilution rate of 0.15. The dimensionless membrane volume was varied in the range 0–1.0 while the other operating conditions remained the same as those in the CMFS experiments. A dimensionless membrane volume of 0.6 will be needed for the total consumption of substrate. There also exists the maximum ethanol productivity, along with the minimum dimensionless membrane volume required, which may again be a design criterion. The higher the glucose concentration in the feed, the greater the improvement of the ethanol productivity as the dimensionless membrane volume increases. This is because ethanol inhibition becomes a major limiting factor as the glucose concentration in the feed is increased.

The demonstration of significant improvement in ethanol productivity, as

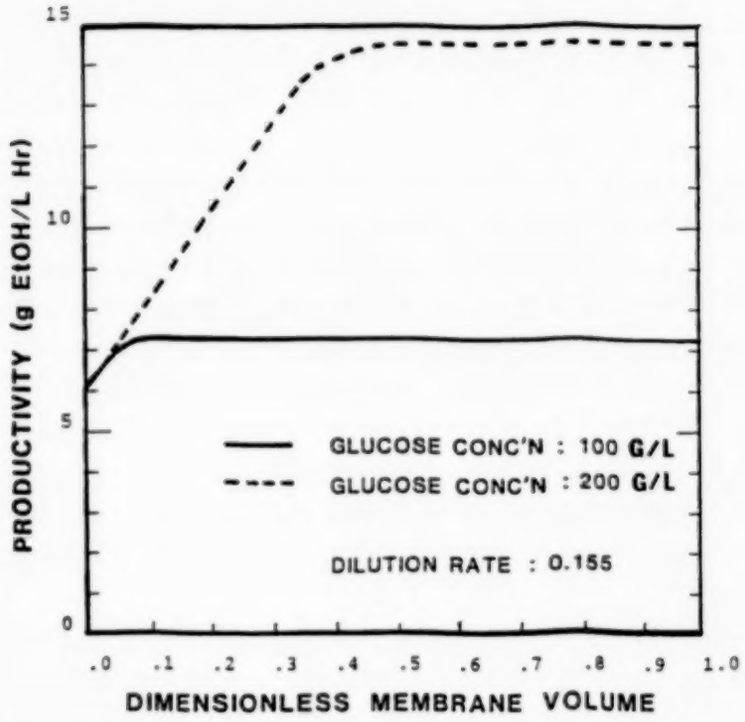

Fig. 12. Influence of membrane capacity on EtOH productivity at high glucose concentration.

well as the minimum dimensionless membrane volume for the complete utilization of glucose will be of major importance. The CMFS concept may allow complete fermentation of high substrate concentration even by severely inhibited microorganisms, assuming that there is a suitable membrane which can be fabricated into a well-engineered membrane module. In summary, the membrane effects strongly depend on the design of the membrane module and the CMFS can be optimized to maintain high ethanol productivity and/or good glucose utilization, etc., depending upon the desired situation.

Conclusions

The effect of ethanol inhibition on yeast cell growth and ethanol production by *Saccharomyces cerevisiae* NRRL Y-2034 was studied by conventional continuous fermentation experiments. Both the yeast cell growth rate and ethanol production rate decrease as the concentration of ethanol increases. The parameters of the generalized nonlinear kinetic relationship model were determined, using the nonlinear regression method. At 25°C, maximum specific rates of yeast cell growth and ethanol production were 0.4 hr^{-1} and 1.2 hr^{-1}, respectively, with complete ethanol inhibition around 70 g/l.

A laboratory-scale continuous membrane fermentor separator unit was designed so that it could be assembled and disassembled easily. A silicone rubber hollow fiber bundle was used for the pervaporation of ethanol. A medium of 10% synthetic glucose was fermented in the dilution rate range of 0.071–0.262 hr^{-1}. Comparing the CMFS fermentation system relative to the conventional continuous fermentation, it was observed that ethanol inhibition was reduced, yeast cell concentration was increased, residence time of substrate was longer, and a highly concentrated clean product was recovered. These are called "membrane effects."

In the CMFS fermentation system, ethanol productivity is increased by 18% over the conventional continuous fermentation. The dilution rate at which the complete utilization of glucose occurs is shifted from 0.9 to 0.13. The permeate stream was free from microbial cells and any other substrate, and was a highly concentrated ethanol solution, with a concentration up to 300 g/l. The experiments proved that the CMFS can provide stable performance up to 19 days.

A mathematical model was developed to determine the kinetics of ethanol fermentation and to simulate the CMFS performances satisfactorily. Model computations indicate that the improvement in ethanol productivity and/or complete utilization of highly concentrated sugar substrate could be achieved by a greater membrane capacity.

This study will give a basis for the rationale for the design and scale up of the CMFS for ethanol production and provide a framework for the evaluation of the CMFS for application other than ethanol production. Attention needs to be focused on the CMFS-based fermentation as a means of improving the

productivity of product-inhibited fermentations, such as acetone–butanol–ethanol by *Clostridium acetobutylicum* [25], acetic acid [25], etc.

For the industrial-scale CMFS fermentation system, it is expected that standard size modules would be fabricated and these would be connected in parallel to obtain the required capacity for a given design.

List of symbols

D	dilution rate (1/hr)
E	ethanol concentration (g/l)
E_M, $E_{M'}$	max. EtOH concentration for growth, production (g/l)
E_p	ethanol productivity (g ethanol/l-hr)
G	molar flow rate (mole/sec)
K_s, $K_{s'}$	Monod constants for growth, production (g/l)
P^o	vapor pressure of pure component (kPa)
P_s	total pressure of the sweep air stream (kPa)
Q	permeability coefficient (mol-m/sec-m^2-kPa)
r	radius (cm)
S	glucose concentration (g/l)
t	membrane thickness (m)
v	flow rate (l/hr)
V	fermentor volume (l)
X	mole fraction in the liquid side
y	mole fraction in the vapor side
$Y_{x/s}$	yeast cell yield factor
Z	fermentor length (cm)

Greek letters

γ	activity coefficient
μ	specific yeast cell growth rate [1/hr]
ν	specific ethanol production rate [1/hr]
α,β	toxic powers for growth, production

Subscripts

E	ethanol
i	inlet
o	outlet
S	sweep air
T	total
W	water

References

1 S.T. Hwang and K. Kammermeyer, Membranes in Separations, Wiley-Interscience, New York, NY, 1975.

2 S.F. Afshar and D.F. Rudd, Biomass ethanol as a chemical feedstock in the United States, Biotechnol. Bioeng., 22 (1980) 677.
3 S.K. Tangnu, Process development for ethanol production based on enzymatic hydrolysis of cellulosic biomass, Process Biochem., May/June (1982) 36.
4 F. Alfani, M. Cantarella and V. Scardi, Use of a membrane reactor for studying enzymatic hydrolysis of cellulose, J. Membrane Sci., 16 (1983) 407.
5 M. Cheryan and M.A. Mehaia, Membrane bioreactors, Chemtech., Nov. (1986) 676.
6 A. Ramalingham and R.K. Finn, The vacuferm process: a new approach to fermentation alcohol, Biotechnol. Bioeng., 19 (1977) 583.
7 C.R. Cysewski and C.R. Wilke, Rapid ethanol fermentations using vacuum and cell recycle, Biotechnol. Bioeng., 19 (1977) 1125.
8 M.S. Dale, M.R. Okos and P.C. Wankat, An immobilized cell reactor with simultaneous product separation, Biotechnol. Bioeng., 27 (1985) 932.
9 M. Miner and G. Goma, Ethanol production by extractive fermentation, Biotechnol. Bioeng., 24 (1982) 1565.
10 T. Cho and M.L. Schuler, Multimembrane bioreactor for extractive fermentation, Biotechnol. Progress, March (1986) 53.
11 K.H. Kyung and P. Gerhardt, Continuous production of ethanol by yeast immobilized in a membrane contained fermentor, Biotechnol. Bioeng., 26 (1984) 252.
12 H. Hoffmann, W. Kuhlmann, H.-D. Meyer and K. Schügerl, High productivity ethanol fermentations with cross flow membrane separation techniques for continuous cell recycling, J. Membrane Sci., 22 (1985) 235.
13 M.A. Mehaia and M. Cheryan, Ethanol production in a hollow fiber bioreactor using *Saccharomyces cerevisiae,* Applied Microb. Technol., 20 (1984) 100.
14 D.S. Inloes, D.P. Taylor, S.N. Cohen, A.S. Michaels and C.R. Robertson, Ethanol production by *Saccharomyces cerevisiae* immobilized in hollow fiber membrane bioreactors, Appl. Microbiol., July (1983) 264.
15 S.-I. Nakao, F. Saitoh, T. Asakura, K. Toda and S. Kimura, Continuous ethanol extraction by pervaporation from a membrane bioreactor, J. Membrane Sci., 30 (1987) 273.
16 W.C. MacGregor, Membrane Separations in Biotechnology, Marcel Dekker, Inc., New York and Basel, 1986.
17 K.C. Hoover and S.-T. Hwang, Pervaporation by a continuous membrane column, J. Membrane Sci., 10 (1982) 253.
18 S. Aiba, A.E. Humphrey and N.F. Mills, Biochemical Engineering, Academic Press, Inc., NY, 1973.
19 A.A. Andreasen and T.J. Stier, Anaerobic nutrition of *Saccharomyces cerevisiae,* J. Cell. Comp. Physiol., 41 (1953) 23.
20 V.R. McDonald, Direct microscopic technique to detect viable yeast cells in pasteurized orange drink, J. Food Sci., 28 (1963) 135.
21 J.H. Luong, Kinetics of ethanol inhibition in alcohol fermentation, Biotechnol. Bioeng., 27 (1985) 280.
22 A. Converti, P. Perego, A. Lodi, F. Parisi and M.d. Borghi, A kinetic study of *Saccharomyces* strains: Performance at high sugar concentrations, Biotechnol. Bioeng., 27 (1985) 1108.
23 J.H. Luong, Generalization of Monod kinetics for analysis of growth data with substrate inhibition, Biotechnol. Bioeng., 29 (1987) 242.
24 M.T. Walton and J.L. Martin, Production of butanol acetone by fermentation, in: H.J. Peppler and D. Perlman (Eds), Microbial Technology Vol. 1, 2nd edn., Academic Press, New York, NY, 1979, pp. 187–209.
25 R. Bar, J.L. Gainer and D.J. Kirewan, An unusual pattern of product inhibition: batch acetic acid fermentation, Biotechnol. Bioeng., 29 (1987) 796.

Journal of Membrane Science, 57 (1991) 43–56
Elsevier Science Publishers B.V., Amsterdam

A stability model for the striping phenomenon in ultrafiltration

Poul S. Larsen

Department of Fluid Mechanics, Technical University of Denmark, DK-2800 Lyngby, Denmark

(Received January 24, 1990; accepted in revised form September 24, 1990)

Abstract

The appearance of stripes near the membrane in cross-flow filtration of dyed solutes in water is modeled as a hydrodynamic stability problem of parallel shear flow in a channel of small width.

Spanwise harmonic perturbations in thickness of the concentration boundary layer give spanwise variations in permeate flux which cause cells of streamwise vorticity that are sustained by the shear flow. States of neutral stability are determined by linear theory, giving the spacing of stripes as function of a modified Reynolds number based on permeate flux, channel width, and its ratio to the boundary layer thickness. The present simple model predicts instability to occur at considerably higher values of modified Reynolds number than those prevailing in experiments showing stripes.

Keywords: concentration polarization; theory; ultrafiltration; hydronamic stability

1. Introduction

In the process of membrane filtration a liquid solution at elevated pressure flows through a channel whose walls are permeable to the solvent. As solvent permeates through the membrane the solute builds up as a concentration boundary layer (polarization) along the membrane. Mass transfer and resulting permeate flux depend on resistances in boundary layer and membrane.

The practice of this type of cross-flow filtration, the design and fabrication of membranes and the performance of plate-and-frame filtration units is quite well known [1]. The transport processes in fluid and membrane and the fouling of membranes, however, are not well understood [2,3].

For many plate-and-frame applications the flow rate and channel dimensions (typically 16×1 mm or 16×0.5 mm) are such that an adequate description is provided by laminar flow between parallel, permeable plates. Simple laminar boundary layer theory predicts a permeate flux that decreases with axial position, say as the minus one-third power of distance in the Levêque approximation which is appropriate for large Pèclet numbers.

Experimental results [4] for hollow fiber ducts of circular cross section do confirm a decreasing flux versus position, but property variations, notably the

0376-7388/91/$03.50 © 1991 — Elsevier Science Publishers B.V.

increase of viscosity with concentration, tend to diminish the decrease. However, experimental results for plate-and-frame ducts [1] show nearly constant flux versus position. Apparently, the axially increasing concentration polarization is counteracted by some other phenomenon, such as local mixing.

Further insight has been gained by visualization experiments using large-molecule solutes that are color dyes, such as brown (iron) dextran or blue dextran. Employing flow through a narrow rectangular duct with membrane on one side-wall, the other side-wall being transparent, patterns of non-uniform coloration have been observed elsewhere [1,5,6,7] and in our laboratory. The typical pattern is that of steady colored stripes near the membrane, aligned with the direction of the flow (Fig. 1). Such structures suggest convection cells similar to those of Görtler vortex flows, to those driven by buoyancy in a horizontal fluid layer heated from below, or to those that may be at play in some electroplating processes [8].

Observations at no flow, and a pressure difference yielding permeate flux through the membrane, show the formation of an irregular marbled pattern, apparently on or very close to the membrane. The appearance of stripes, following the sudden establishment of appropriate favorable conditions, is a slow process, lasting on the order of many seconds. Observable stripes vanish either if the flow rate is increased to transitional or turbulent flow or if the driving pressure difference for permeate flux is removed. The disappearance of stripes, following a sudden establishment of conditions appropriate for no stripes, is a rapid process, lasting only seconds or less.

The foregoing observations suggest that stripe formation is a coupled problem of mass transfer and shear flow. Also, a regular spanwise periodic array of cells of streamwise vorticity could yield a nearly constant permeate flux by slowing or halting streamwise boundary layer growth.

Since the intensity of coloration of a dyed solution is proportional to the integral of concentration of solute over depth it is conjectured that observed streamwise stripes represent stable, wave-like variations in thickness and/or concentration in the boundary layer along the membrane. Consequently, since the local permeate flux varies inversely with boundary layer resistance, say, the boundary layer thickness for constant membrane resistance, the observed stripe pattern implies a wave-like variation in permeate flux. This variation, relative to the uniform permeate flux for undisturbed boundary layer thickness, implies in effect a periodic inflow and outflow between boundary and bulk (Fig. 2). Such perturbations represent cells of streamwise vorticity of alternating sign, distorting the bulk flow by bringing high momentum fluid to wave troughs. This provides a mechanism for sustaining initial perturbations and suggests the striping phenomenon to be a stability problem.

Clearly, in the absence of permeate flow there is no basis for sustaining the hypothesized secondary flows, so no stripes should appear. Also, stripes should

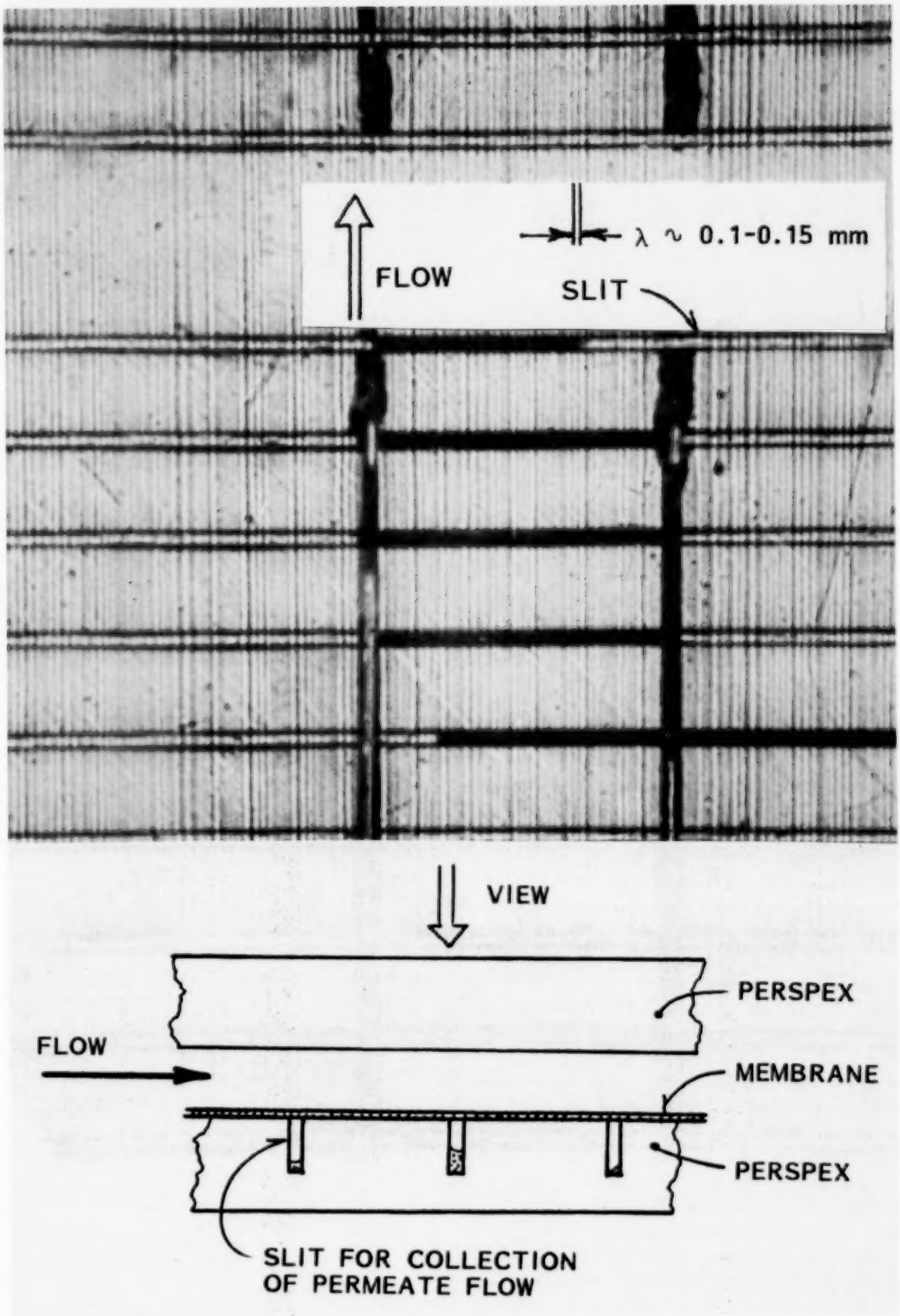

Fig. 1. Photograph of stripe pattern (vertical lines, indicating also the direction of flow), viewed from above the membrane. Double lines are regularly spaced slits (1.0 mm apart) for collecting permeate flow under membrane.
Test conditions: 0.2% blue dextran in water, 16×0.5 mm straight channel with CA-600 transparent membrane, $\Delta p = 4$ bar, $l = 0.25$ mm, $U_m = 0.083$ m/sec, 157 mm downstream of inlet.

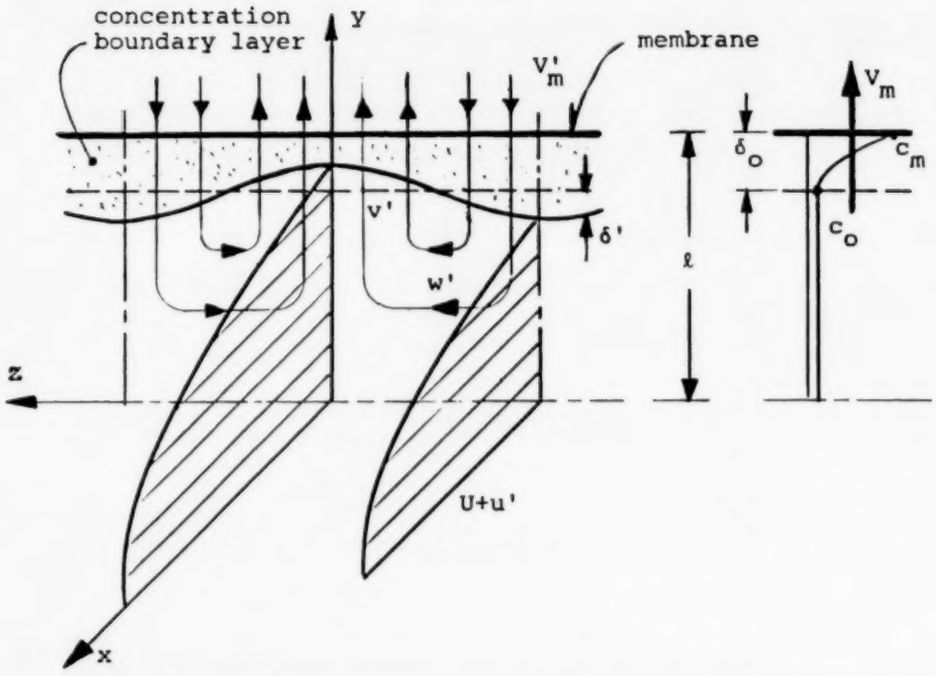

Fig. 2. Model for striping phenomenon, showing perturbed concentration boundary layer and resulting secondary flows and bulk flow (schematic).

disappear in the absence of bulk flow since this flow is responsible for the formation of a steady concentration boundary layer.

Since the phenomenon is observed for solutions of blue dextran, which are largely Newtonian, the effect is probably not rheological, i.e. one of shear induced normal stresses driving secondary flows. The viscosity increases markedly with concentration, typically by one or two orders of magnitude in the boundary layer of blue dextran, but this effect in itself does not seem to provide a mechanism for driving secondary flows.

Presently, the significant increase of viscosity and the small thickness of the boundary layer are used in the formulation of a simplified hydrodynamic stability model in which cells of streamwise vorticity are driven by boundary layer mass transfer and sustained by a channel shear flow. The starting point is a simple model for the base flow, treating the mass transfer as a boundary condition for the bulk flow. The model assumes the base solutions of flow and mass transfer to be disturbed by spanwise harmonic perturbations whose stationary solutions at neutral stability determine the spacing between stripes. Results are compared to observations and limitations of the model are discussed in the concluding section.

2. Physical model and base solution

The starting point for a stability analysis is to establish the duct flow, concentration boundary layer and permeate flow to be subjected to perturbations.

Being concerned with flow in rectangular ducts of large aspect ratio, end effects are ignored.

We therefore consider the steady laminar flow between parallel permeable plates spaced a distance $2l$ apart. Figure 2 shows the quasi-developed velocity and concentration distributions in the symmetric half of this duct flow. Due to the pressure difference Δp over the membrane of permeability K_p a concentration boundary layer of thickness δ_0 is established. The mass fraction of solute is C_0 and C_m in the bulk and at the membrane, respectively. The permeate flux of solute through the membrane is V_m.

To first approximation the base flow is that of steady, incompressible Poiseuille flow,

$$U = P_0(1-\eta^2) \tag{1}$$

$$P_0 = \frac{(-\mathrm{d}p/\mathrm{d}x)l^2}{2\mu}, \quad \eta = y/l, \tag{2}$$

where $(-\mathrm{d}p/\mathrm{d}x)$ denotes the imposed constant pressure gradient. The mean velocity $U_m = (2/3)P_0$ is of the order 0.1–1.0 m/sec, to be compared to a permeate flux V_m of the order 10^{-5} m/sec or less. The weak transversal flow associated with permeation at the wall may therefore be approximated by

$$V \approx \frac{1}{2}\eta(3-\eta^2)V_m, \tag{3}$$

which satisfies the conservation of mass for quasi-developed Poiseuille flow with weak wall suction, hence slowly changing mean velocity.

Essential features of the mass transfer process may be described by considering the somewhat artificial, steady, one-dimensional problem shown in Fig. 2. The uniform velocity V_m is the permeate flux which for osmotic pressure limited permeation at the membrane is given by

$$V_m = K_p(\Delta p - \pi_m). \tag{4}$$

Here, the excess pressure Δp is assumed to exceed the osmotic pressure π_m which depends on the concentration at the membrane through a virial expansion such as, for example, for dextran T-70 [4],

$$\pi_m = (0.6353\, C_m + 12.64\, C_m^2 + 49.55\, C_m^3)\cdot 10^5, \tag{5}$$

where units are π_m(Pa) and C_m(kg/l) $\approx$ [mass fraction]. The solution to the convection–diffusion problem in the layer of thickness δ_0 (Fig. 2), subject to eqn. (5) and bulk concentration C_0 is

$$C_m = C_0 \exp(Pe\, V_m/V_0), \tag{6}$$

where $V_0 = K_p\, \Delta p$ denotes the pure water flux and

$$Pe = V_0\, \delta_0/D \tag{7}$$

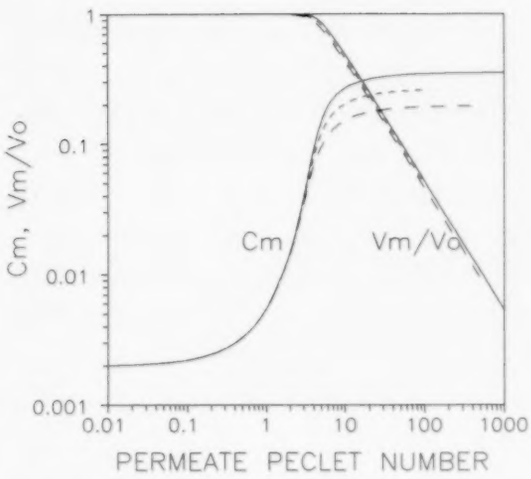

Fig. 3. Concentration at membrane C_m and dimensionless flux V_m/V_0, where V_0 equals the pure water flux, versus permeate Peclet number $V_0\delta_0/D$, the ratio of boundary layer resistance to membrane resistance.
Data for T-70 dextran, bulk concentration $C_m = 0.002$, driving pressure difference Δp: (- - -) 1 bar; (----) 2 bar; (—) 4 bar.

denotes the ratio of resistances to mass transfer in boundary layer and membrane, a water flux Peclet number.

Solutions to eqns. (4)–(7) for $C_0 = 0.002$ and three values of excess pressures, $\Delta p = 1$, 2 and 4 bar, are shown in Fig. 3 in terms of V_m/V_0 and C_m versus Pe. Examination of the asymptotic behavior of eqns. (4)–(7) shows, as suggested by Fig. 3, that $Pe \to 0$ leads to $C_m \to C_0$ and V_m approaches a constant value which in turn approaches the water flux V_0 for vanishing C_0. Also, $Pe \to \infty$ shows C_m to have an upper bound while $V_m/V_0 \to 0$ as $1/Pe$. The latter behavior implies

$$V_m \approx D/\delta_0, \tag{8}$$

being a good approximation for $Pe > 5$ according to Fig. 3. Since our experiments typically show $V_m/V_0 < 0.5$, eqn. (8) will be used to describe the typical behavior.

To exemplify orders of magnitude of parameters, let $Pe \approx 10$, $D \approx 10^{-11}$ m^2/sec and $V_0 \approx 10^{-5}$ m/sec, then $\delta_0 \approx 10^{-5}$ m from eqn. (7). Of course, δ_0 should be determined by solving the convection–diffusion problem of a developing concentration boundary layer in shear flow, but such an analysis would give comparable values of δ_0 (see, for example, [4]). For a stability analysis, however, it suffices to describe the essential physics, and in the present analysis δ_0 and V_m are retained as the characterizing parameters for mass transfer.

3. Perturbation equations

Considering infinitesimal two-dimensional perturbations in y and z, the resulting problem of flow and mass transfer is described by

$$U+u', V+v', w', p+p', \delta_0+\delta', V_m+V'_m. \tag{9}$$

The linearized equations of motion of perturbations become

$$\frac{\partial v'}{\partial y}+\frac{\partial w'}{\partial z}=0 \tag{10}$$

$$\frac{\partial u'}{\partial t}+v'\frac{\partial U}{\partial y}+V\frac{\partial u'}{\partial y}=-\frac{1}{\rho}\frac{\partial p'}{\partial x}+\nu\left[\frac{\partial^2 u'}{\partial y^2}+\frac{\partial^2 u'}{\partial z^2}\right] \tag{11}$$

$$\frac{\partial v'}{\partial t}+v'\frac{\partial V}{\partial y}+V\frac{\partial v'}{\partial y}=-\frac{1}{\rho}\frac{\partial p'}{\partial y}+\nu\left[\frac{\partial^2 v'}{\partial y^2}+\frac{\partial^2 v'}{\partial z^2}\right] \tag{12}$$

$$\frac{\partial w'}{\partial t}+V\frac{\partial w'}{\partial y}=-\frac{1}{\rho}\frac{\partial p'}{\partial z}+\nu\left[\frac{\partial^2 w'}{\partial y^2}+\frac{\partial^2 w'}{\partial z^2}\right] \tag{13}$$

where U is given by eqn. (1) and V by eqn. (3). Boundary conditions are, at the centerline of symmetry,

$$y=0: \qquad \partial u'/\partial y=v'=\partial w'/\partial y=0 \tag{14}$$

and, at the edge of the concentration boundary layer, $y=l-\delta_0-\delta'\approx l$,

$$y\approx l: \qquad u'=\partial v'/\partial y=w'=0 \tag{15}$$

The no-slip condition $u'(l)=0$ of eqn. (15) is a reasonable first-order approximation for a vanishingly thin boundary layer, being much more viscous than the bulk fluid. Also it is consistent with the base flow assumptions.

Permeation at the wall, however, can not be ignored. Linearizing eqn. (8) gives

$$y\approx l: \qquad v'/V_m=-\delta'/\delta_0. \tag{16}$$

Finally, we consider the condition of a constant axial pressure gradient acting on a quasi-developed flow. From the foregoing no-slip condition the channel has effectively a laterally wavy wall represented by the concentration boundary layer. The effect on the axial flow will be of order δ'/l, yielding mean values that are larger at troughs and smaller at crests. The corresponding effect in velocity gradient at the boundary layer edge is evaluated from eqn. (1), linearized to

$$y\approx l: \qquad \partial u'/\partial y=2P_0\,\delta'/l^2. \tag{17}$$

The boundary conditions of eqns. (16) and (17) in effect represent the mass transfer problem and its coupling to the bulk flow perturbations.

According to a usual normal mode analysis, perturbations are assumed in the form

$$(\bar{U}', \bar{v}', \bar{w}', \bar{p}', \bar{\delta}', \bar{V}'_m)=(\bar{u}, \bar{v}, \bar{w}, \bar{p}, \bar{\delta}, \bar{v}_m)\exp(st+ikz), \tag{18}$$

where $k=2\pi/\lambda$ denotes the wavenumber in spanwise direction, λ being the wavelength, i the imaginary unit, and s the amplification factor, generally a complex quantity; $\bar{u}$, $\bar{v}$, $\bar{w}$ and $\bar{p}$ are functions of y only and, they are, along with $\bar{\delta}$ and $\bar{V}_m$, the amplitudes of the normal modes. An overbar refers to the dimensionless notation below.

Introducing the notation

$$\zeta=ky,\ \zeta_1=kl,\ D=d/d\zeta,\ \sigma=s/(\nu k^2),\ Re=V_m l/\nu$$
$$\bar{u}'=u'\zeta_1^3/(2ReP_0),\ \bar{v}'=v'/V_m,\ \bar{w}'=w'/V_m,\ \bar{\delta}=\delta'/\delta_0 \tag{19}$$

where Re denotes the usual Reynolds number associated with suction (permeation) at a wall, eqns. (10)–(13), after eliminating $\bar{w}$, reduce to

$$[D^2-(fRe/\zeta_1)D-1-\sigma]\bar{u}=-\zeta\bar{v}, \tag{20}$$

$$\{(D^2-1)[D^2-(fRe/\zeta_1)D-1-\sigma]+f'Re/\zeta_1^2\}\bar{v}=0. \tag{21}$$

Here, f equals V/V_m of eqn. (3) and f' its derivative with respect to $\eta=\zeta/\zeta_1$. These terms represent the effect of transversal bulk flow associated with permeation. When these terms can be neglected (see below) eqns. (20) and (21) reduce to

$$(D^2-1-\sigma)\bar{u}=-\zeta\bar{v}, \tag{22}$$

$$(D^2-1)(D^2-1-\sigma)\bar{v}=0, \tag{23}$$

which readily accept closed-form analytical solutions.

From eqns. (14)–(17), boundary conditions are, at the centerline of symmetry,

$$\zeta=0: \qquad D\bar{u}=\bar{v}=D^2\bar{v}=0, \tag{24}$$

where eqn. (10), in the form $D\bar{v}+i\bar{w}=0$, has been used, and at the edge of the concentration boundary layer,

$$\zeta\approx\zeta_1: \qquad \bar{u}=D\bar{v}=0, \tag{25}$$

$$\bar{v}=-\bar{\delta}, \tag{26}$$

$$(Re'/\zeta_1^2)D\bar{u}=\bar{\delta}, \tag{27}$$

where the modified permeate Reynolds number is defined by

$$Re'=Re\,l/\delta_0=(V_m l/\nu)(l/\delta_0). \tag{28}$$

4. Solutions to the stability problem

Assuming the principle of the exchange of stabilities holds for this problem we set $\sigma=0$ to determine the states of neutral stability. Furthermore, noting that $V\ll U$, and considering V to be of the same order as perturbations, con-

vective terms of the base flow associated with permeation should be of second order.

Therefore, for weak permeation, $Re/\zeta_1 \ll 1$ and $Re/\zeta_1^2 \ll 1$, we consider first the boundary value problem posed by eqns. (22)–(27) for which analytical solutions are,

$$\bar{v} = A[\zeta \cosh \zeta - (1+\zeta_1 \tanh \zeta_1) \sinh \zeta] \tag{29}$$

$$\bar{u} = A[g(\zeta) - g(\zeta_1) \cosh \zeta / \cosh \zeta_1], \tag{30}$$

where A is a constant of integration and $g(\zeta)$ denotes the particular solution to eqn. (22),

$$g(\zeta) = \frac{1}{4}(2+\zeta_1 \tanh \zeta_1)(\zeta^2 \cosh \zeta - \zeta \sinh \zeta) - \frac{1}{6}\zeta^3 \sinh \zeta. \tag{31}$$

Then, inserting eqns. (29) and (30) into the boundary conditions of eqns. (26) and (27), the solution to the eigenvalue problem is obtained by requiring that the determinant vanishes for the resulting homogeneous equations in the arbitrary amplitudes A and $\bar{\delta}$. This gives

$$Re' = \frac{\zeta_1{}^2\{\zeta_1 \cosh \zeta_1 - (1+\zeta_1 \tanh \zeta_1)\sinh \zeta_1\}}{g(\zeta_1) \tanh \zeta_1 - g'(\zeta_1)} \tag{32}$$

where a prime denotes differentiation with respect to ζ. Considering the limits of eqn. (32) for small and large wavenumber gives the asymptotic solutions

$$\lim_{\zeta_1 \to 0} Re' = \frac{5}{2}; \quad \lim_{\zeta_1 \to \infty} (Re'/\zeta_1) = \frac{4}{3}. \tag{33}$$

The solution valid for weak permeation, eqn. (32), is shown in Fig. 4, in terms of the dimensionless wavenumber, $\zeta_1 = kl$ at neutral stability as function

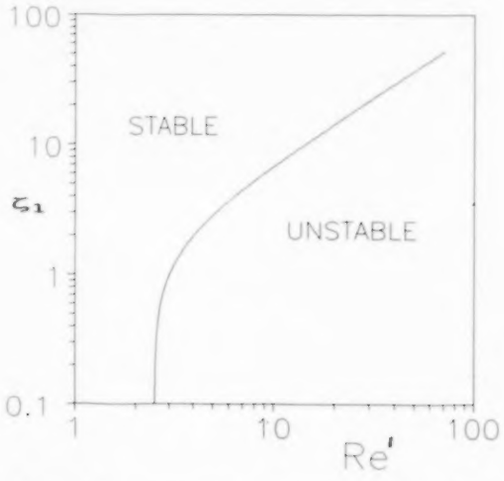

Fig. 4. Dimensionless wavenumber $\zeta_1 = kl$ at neutral stability versus modified permeate Reynolds number, $Re' = (V_m l/\nu)(l/\delta_0)$.

of modified permeate Reynolds number Re'. The nature of the perturbation flow associated with stripes is illustrated in Fig. 5, showing the streamlines in the y,z-plane for $\zeta_1 = 1, 5, 10$ and 50. Note that the depth to which the secondary flow penetrates into the bulk decreases, as does the wavelength, with increasing values of wave number.

Next, including the effect of transversal bulk flow associated with permeation, eqns. (20) and (21), subject to eqns. (24)–(27), have been solved numerically. Sample results for two values of the usual permeate Reynolds number, $Re = 0.1$ and 0.5, are shown in Fig. 6 in terms of dimensionless wave number versus modified permeate Reynolds number. The figure also shows the solution for weak permeation, eqn. (32). At low wavenumbers the transversal flow has a negligible effect while at high wavenumbers it acts stabilizing, as ex-

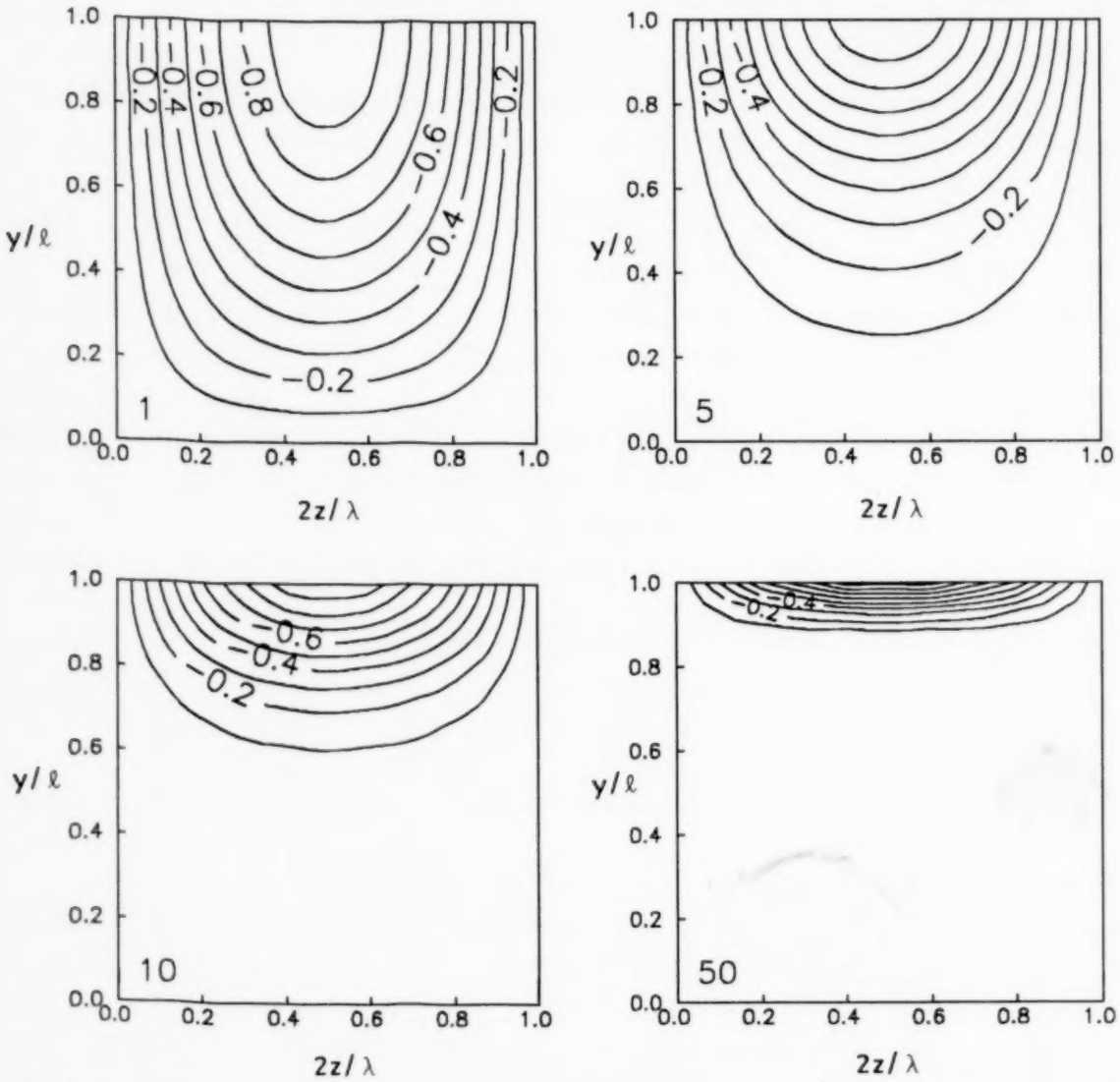

Fig. 5. Streamlines of perturbation flow in y,z-plane (streamfunction normalized to max. value). Cases of dimensionless wavenumber $\zeta_1 = 1, 5, 10$ and 50.

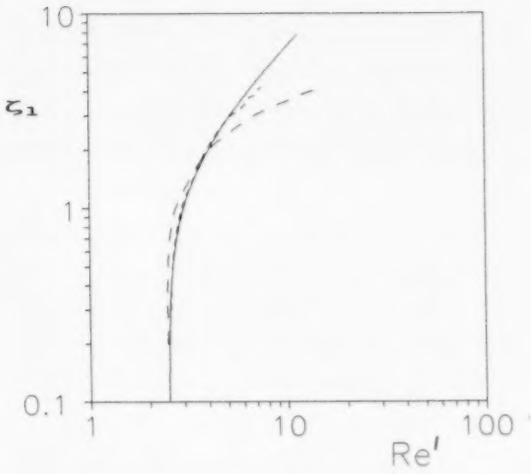

Fig. 6. Dimensionless wavenumber ζ_1 at neutral stability versus modified permeate Reynolds number, Re'.
Effect of transversal bulk flow owing to permeation.
(—) no flow; (----) $Re=0.1$; (- - -) $Re=0.5$.

pected for suction. However, for a value of $Re<0.01$, which is appropriate for the present study, the effect is negligible.

5. Experimental observations

Because available experimental results are limited it is only possible to estimate the order of magnitude of the parameters appearing in the stability analysis.

Thus, for a range of flow conditions of a mixture of 0.2% blue dextran in water, our observations indicate a typical wavelength of stripes of 0.1–0.15 mm. For a channel width of $2l=0.5$–1.0 mm this implies a dimensionless wavenumber of about $\zeta_1 \approx 10$–30.

Other quantities known with some certainty include the permeate flux, $V_m \approx 10^{-5}$ m/sec and the kinematic viscosity of the bulk fluid $\nu \approx 10^{-6}$ m^2/sec. Therefore, the usual permeate Reynolds number is quite small, $Re \approx 0.003$–0.005, and terms of order Re/ζ_1 and Re/ζ_1^2, which account for the effect of transversal bulk flow associated with permeation, should be negligible. Consequently, the asymptotic solution, eqn. (33) for ζ_1 large, should apply, yielding the theoretical prediction $Re' \approx (4/3)\zeta_1 \approx 13$–$40$.

Experimentally, δ_0 is not known directly but estimates based on boundary layer theory (see also [4]) suggest $\delta_0 \approx 0.01$–0.05 mm. Hence, the modified permeate Reynolds number at which stripes are observed is estimated to be $Re' \approx 0.01$–0.25, which is much less than the critical values predicted by the model. This discrepancy is probably due to the simplicity of the present model, particularly with regard to its lack of detailed description of the mass transfer. Also, the model is based on linear, infinitesimal theory.

In view of the estimated large values of ζ_1 the penetration of secondary flow into the duct flow will be small (Fig. 5). Considering also the expected magnitude of these velocity perturbations it is not surprising that they have not been detected in exploratory velocity measurements using laser Doppler velocimetry.

6. Discussion and conclusions

A simplified stability model has been formulated for the striping phenomenon observed in the quasi-developed mass transfer process of cross-flow ultrafiltration in a parallel plate channel. The boundary layer mass transfer process has been simplified, and in effect reduced to boundary conditions imposed on the bulk flow. The necessary coupling that sustains perturbations in boundary layer thickness, hence in permeate flux, is associated with the primary bulk flow which is assumed to be subjected to a constant axial pressure gradient. In this way, an increased boundary layer thickness implies a reduced bulk velocity and a reduced velocity gradient at the boundary layer.

The present stability problem, as formulated and solved for the case of weak permeation, has some mathematical similarities with that of Görtler vortices arising in boundary layer flows over concave walls, see, for example Ref. [9]. In the latter problem, the centrifugal body force, through its coupling of $\bar{u}$ and $\bar{v}$, provides a volume source, yielding non-trivial solutions with no distinct minimum on the curve of neutral stability. In the former problem, a volume term is absent but the mass transfer provides a coupling between $\bar{u}$ and $\bar{v}$ at the boundary (eqns. 26 and 27), affording a closed form solution, eqn. (32), also having no distinct minimum on the stability curve.

From experimental observations of stripe spacing and permeate flux this simplified case of weak permeation should apply to the experimental conditions. Hence, neutral stability is governed by a single parameter, the modified permeate Reynolds number, eqn. (28). Accordingly, instability is promoted by low bulk viscosity, high permeate flux (high permeability and high excess pressure), and, compared to channel width, a thin concentration boundary layer (low mass diffusivity, high bulk flowrate, and low viscosity of wall layer).

While the foregoing parametric trends appear physically reasonable, numerical values based on observation (see foregoing section) do not confirm the quantitative results of the model. One reason for the discrepancy may be the simplicity of the model formulation with regard to the mass transfer process. Another is the linear analysis which may be expected to yield too large critical values for the governing parameter [9]. Further study is required to resolve the discrepancy.

Acknowledgements

This research was partially supported under the BRITE/EURAM program in collaboration with DDS Filtration, Nakskov, Denmark. The author is in-

depted to Messrs. E.M. Christensen and C.B. Hansen for the photograph in Fig. 1.

List of symbols

A	integration constant
C_0	mass fraction of solute in bulk
C_m	mass fraction of solute at membrane
D	mass diffusivity (m^2/sec)
g	particular solution, eqn. (31)
i	imaginary unit, $\sqrt{-1}$
k	wave number (1/m)
K_p	membrane permeability (m-sec^{-1}-Pa^{-1})
l	duct half-width (m)
p	pressure (Pa)
P_0	Coefficient, eqn. (2) (m/sec)
Δp	driving pressure difference (Pa)
Pe	water flux Peclet number, eqn. (7)
Re	permeate Reynolds number, eqn. (19)
Re'	modified Reynolds number, eqn. (28)
s	amplification factor (1/sec)
U,u	velocity, streamwise (m/sec)
U_m	bulk (mean) velocity (m/sec)
V,v	velocity, transveral (m/sec)
V_0	water flux (m/sec)
V_m	permeate flux (m/sec)
w	velocity, spanwise (m/sec)
x	streamwise coordinate (m)
y	transversal coordinate (m)
z	spanwise coordinate (m)

Greek letters

δ	boundary layer thickness (m)
δ_0	unperturbed thickness (m)
η	dimensionless coordinate, y/l
λ	wavelength, $2\pi/k$ (m)
μ	dynamic viscosity of bulk fluid (kg/sec-m)
ν	kinematic viscosity, μ/ρ (m^2/sec)
π	osmotic pressure (Pa)
π_m	osmotic pressure at membrane (Pa)
ρ	mass density (kg/m)
σ	amplification factor, eqn. (19)

ζ dimensionless coordinate, ky
ζ_1 dimensionless wavenumber, kl

References

1 R.F. Madsen, Hyperfiltration and Ultrafiltration in Plate-and-Frame Systems, Elsevier, New York, NY, 1977.
2 G. Jonsson and C.E. Boesen, Polarization phenomena in membrane processes, in: G. Belfort (Ed.), Synthetic Membrane Processes, Academic Press, New York, NY, 1984, pp. 101–130.
3 G.B. van den Berg and C.A. Smolders, Flux decline in membrane processes, Filtr. Sep., (March/April) (1988) 115–121.
4 M.J. Clifton, N. Abidine, P. Aptel and V. Sanchez, Growth of the polarization layer in ultrafiltration with hollow-fibre membranes, J. Membrane Sci., 21 (1984) 233–246.
5 G. Jonsson, Transport phenomena in ultrafiltration: Membrane selectivity and boundary layer phenomenon, Pure Appl. Chem., 158 (1984) 1647–1656.
6 G. Jonsson, Boundary layer phenomena during ultrafiltration of dextran and whey protein solutions, Desalination, 151 (1984) 61–77.
7 D.K. Dienesen, DDS Filtration, (personal communication) (1988).
8 M.M. Jakšic and V.P. Komnenic, Hydrodynamic flow visualization by an electrochemical method, in: R.K. Shah, E.N. Ganic and K.T. Yang (Eds.), Experimental Heat Transfer, Fluid Mechanics and Thermodynamics, Elsevier, New York, NY, 1988, pp. 1156–1176.
9 P.G. Drazin and W.H. Reid, Hydrodynamic Stability, Cambridge University Press, Cambridge, 1981, p. 116, chap. 7.

Journal of Membrane Science, 57 (1991) 57–68
Elsevier Science Publishers B.V., Amsterdam

Transport properties of anion exchange membranes in contact with hydrochloric acid solutions. Membranes for acid recovery by electrodialysis

Maguelone Boudet-Dumy, Arlette Lindheimer and Claude Gavach

Laboratory of Physical Chemistry of Polyphasic Systems, CNRS, USTL, BP 5051, 34033 Montpellier Cedex (France)

(Received March 20, 1990; accepted in revised form September 24, 1990)

Abstract

The transport numbers of chloride ion as well as unidirectional fluxes under a constant current are measured by the radiotracer technique. The studied anion exchange membranes are in contact on both sides with hydrochloric acid at the same concentration. The membranes are the commercial membranes AAV Selemion and ARA Morgane, specially designed for the recovery of acids by electrodialysis. In addition, measurements of the electrical conductances of the membrane and of the amount of sorbed electrolyte at equilibrium have been carried out. The analysis of the results suggests a low dissociation degree of the acid present in the membrane phase.

Keywords: ion-exchange membrane; electrochemistry; electrodialysis; Selemion membrane; Morgane membrane; chloride ion transport; radiotracer technique

Introduction

Nowadays electrodialysis can be used for the treatment of acid effluents from industry (chemical, hydrometallurgy, electroplating). By this process, concentrated acid can be obtained with anion exchange membranes showing a low permeability towards protons.

The recovery of acids by electrodialysis can be performed with sulfuric acid [1–5], hydrofluoric acid [6], chromic acid [7] and phosphoric acids [8,9]. Concerning hydrochloric acid, some studies have been carried out in order to improve the electrodialysis efficiency. For this purpose, bipolar membranes [10] as well as modified anion exchange membranes [11] have been used. The aim of this work is to compare the transport properties of two polymeric anion exchange membranes which have been specially manufactured for the recovery of acid by electrodialysis: the AAV Selemion membrane produced by Asahi Glass and the ARA membrane produced by Morgane.

Radiotracers are used for measuring the transmembrane unidirectional fluxes

0376-7388/91/$03.50 © 1991 — Elsevier Science Publishers B.V.

of Cl^- when the membranes are maintained between two symmetrical HCl solutions. By this technique the values of the Cl^- self diffusion fluxes as well as the transport number can be evaluated. The study is completed by measurements of the membrane conductance and of the amount of the HCl sorbed in membranes equilibrated with HCl solutions. The analysis of the experimental results provides a better understanding of the factors responsible for the reduced permeability of the membranes towards protons.

Experimental

Two anion exchange membranes expressly manufactured for the recovery of acid by electrodialysis are studied:

- the ARA membrane, which is an experimental membrane produced by Morgane and has an exchange capacity of 0.6 mequiv-g^{-1} of dry membrane;
- the AAV Selemion membrane, a commercial membrane produced by Asahi glass, which is 110 μm thick and has an exchange capacity of 0.54 mmol-g^{-1} of dry material.

Before utilization, the membranes are soaked in water for more than 48 hr and before the experiments, they are maintained in the studied solution for 24 hr. Measurements are carried out at 25° C; ^{36}Cl-labelled HCl was obtained from Amersham Radiochemical Centre. All the solutions are prepared with deionized water.

Self-diffusion flux measurements and transport number measurements

For these measurements, the same cell has been used; the experimental technique has been described elsewhere [12].

Electrical resistance of the membrane

The electrical resistance of the membrane equilibrated with the aqueous solutions is measured at 1000 Hz by means of a Rhone–Poulenc clip cell. The electrodes are platinized-platinum discs. The solution into which the clip cell dips is carefully thermostated. The membrane resistance is the difference between the measured values of the resistance with the membrane and without it.

Desorption kinetics and determination of the amount of sorbed electrolyte

The general principle of the method has been described by Glueckauf and Watts [13]. In order to determine the amount of sorbed HCl, the membrane is immersed in an aqueous solution of HCl labelled with ^{36}Cl until the equilibrium state is reached. The membrane is then removed from the solution and its surface is wiped with blotting paper, and the membrane is then immersed in a given volume of pure water with a vigorous stirring. By measuring the variation of radioactivity in the water at regular intervals of time, it is possible

to determine the kinetics of release of the sorbed electrolyte in the membrane and its total amount.

Results

The water content (WC) is defined by the following formula:

$$WC = \frac{m_W - m_D}{m_W} \times 100$$

where m_W is the weight of the membrane sample equilibrated with HCl 10^{-1} N aqueous solution and m_D is the weight of the dried membrane in the chloride form, the membrane having been maintained under vacuum at 35 °C until a constant weight was attained. For the two membranes, the water content corresponds to about eight water molecules per anion exchange group. In Table 1 are collected the main characteristics of the two studied membranes.

Exchange ionic fluxes and unidirectional fluxes

The values of the unidirectional fluxes, at equilibrium and under an applied current, are obtained from the slopes of the curves of the variation of the number of chloride ions appearing in the second aqueous side, the labelled chloride ions having been added to the first aqueous side. An example of such a determination is shown in Fig. 1.

During these experiments, it was not possible to note any significant water transport.

The values of the zero current exchange fluxes (J_0) and of the unidirectional fluxes J, under a constant electrical current, are given in Table 2. When a constant current is applied, the value of the total flux for a given ion transported through the membrane is equal to the difference between the two unidirectional fluxes $\vec{J}$ and $\overleftarrow{J}$, where $\vec{J}$ corresponds to the unidirectional flux from the cathode to the anode and $\overleftarrow{J}$ to the flux in the opposite direction. In Table

TABLE 1

Properties of the two studied membranes

Code	Type	Thickness (μm)	Water content (%)	Exchange capacity (mequiv-g^{-1})
AAV Selemion	Anion exchange membrane	114	8.6	0.54
ARA Morgane	Anion exchange membrane	159	8.7	0.60

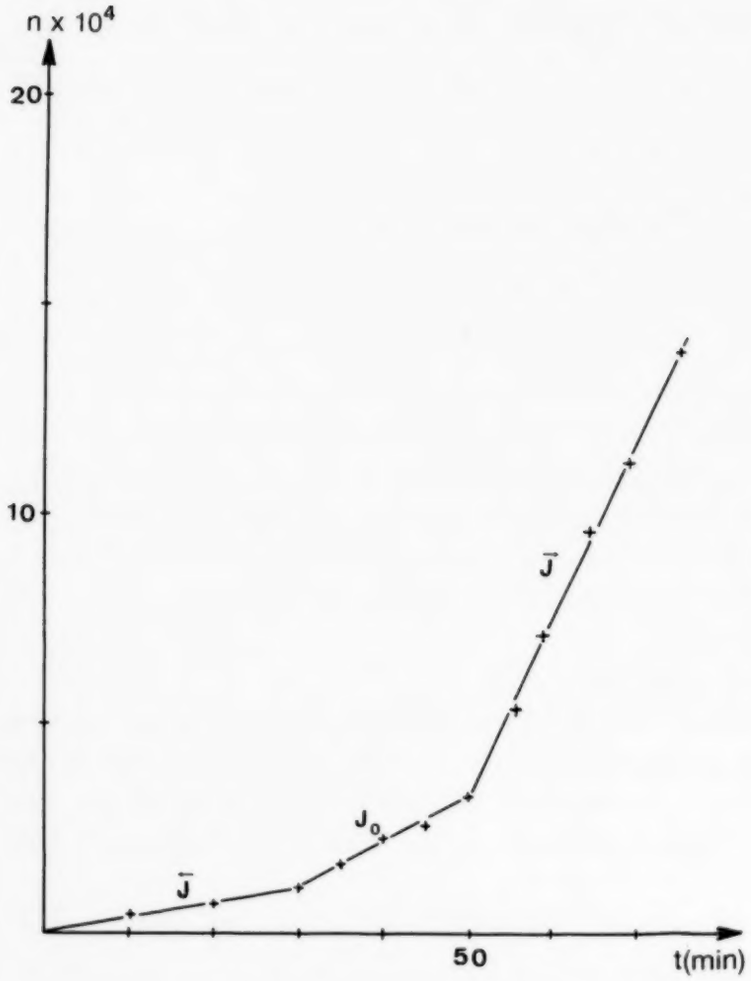

Fig. 1. Variation of the number of Cl^- ions crossing the ARA membrane equilibrated with two 2 *M* HCl solutions as a function of time. Current density $I=30$ mA-cm^{-2}. J_0 is the self-diffusion flux; $\vec{J}$ is the unidirectional flux from the cathode to the anode; $\overleftarrow{J}$ is the unidirectional flux from the anode to the cathode.

2, *I* is the density of the applied current. In order to compare the behaviour of Cl^- and SO_4^{2-}, some measurements have been carried out with H_2SO_4 solutions; in Table 3 the results obtained for 4 *N* solutions are given.

Membrane conductivity measurements

The electrical conductivities of membranes equilibrated with different HCl solutions have been measured. In Table 4, the values of these conductivities are given for various external electrolyte concentrations.

Determination of the amount of sorbed electrolyte

Figure 2 shows the variation with time of the number of Cl^- anions which are released into a given volume of 4 *N* HCl solution. The membrane has been previously equilibrated with a ^{36}Cl-labelled 2 *N* solution of HCl. One may consider that, when the plateau is reached, the total amount of Cl^- initially pres-

TABLE 2

Zero current exchange fluxes (J_0) and unidirectional fluxes $\vec{J}$ and $\overleftarrow{J}$ of Cl^- ions through the membranes separating two HCl solutions at the same concentration. $\vec{J}$ is the unidirectional flux from the cathode to the anode and $\overleftarrow{J}$ the flux in the opposite direction

C_{HCl} (mol-dm^{-3})	$I=0$	$I=30$ mA-cm^{-2}	
	$10^8 J_0$ (mol-sec^{-1}-cm^{-2})	$10^8 \vec{J}$ (mol-sec^{-1}-cm^{-2})	$10^9 \overleftarrow{J}$ (mol-sec^{-1}-cm^{-2})
AAV membrane			
0.5	2.1	28.0	4.3
1	1.4	26.8	7.9
2	2.2	22.5	8.2
4	3.5	16.4	9.1
5	1.4	14.6	9.6
6	1.5	12.8	8.7
ARA membrane			
0.5	6.1	28.6	3.2
1	5.0	26.8	2.9
2	6.4	25.6	17.2
3	7.3	21.3	28.6
4	6.7	17.3	26.2
5	4.6	14.6	22.6
6	4.8	12.5	51.4

TABLE 3

Comparison between Cl^- and SO_4^{2-} fluxes obtained with 4 N HCl solutions and 4 N H_2SO_4 solutions; current density = 30 mA-cm^{-2}

	Cl^-	SO_4^{2-}
AAV membrane	$10^8 \vec{J}=16.4$ mol-sec^{-1}-cm^{-2} $10^8 \overleftarrow{J}\simeq 0.9$ mol-sec^{-1}-cm^{-2}	$10^8 \vec{J}=8.5$ mol-sec^{-1}-cm^{-2} $10^8 \overleftarrow{J}\simeq 0$ mol-sec^{-1}-cm^{-2}
ARA membrane	$10^8 \vec{J}=17.3$ mol-sec^{-1}-cm^{-2} $10^8 \overleftarrow{J}= 2.6$ mol-sec^{-1}-cm^{-2}	$10^8 \vec{J}=9.1$ mol-sec^{-1}-cm^{-2} $10^8 \overleftarrow{J}\simeq 0$ mol-sec^{-1}-cm^{-2}

ent inside the membrane sample has been transferred into the aqueous phase. The total number of Cl^- ions, $N^*_{Cl^-}$, present inside the membrane is related to the exchange capacity through the equation:

$$N^*_{Cl^-} = X + N_s$$

where N_s is the number of HCl molecules which are sorbed inside the membrane. Table 5 shows, for the two studied membranes, the values of $N^*_{Cl^-}$ and N_s expressed as mequiv-g^{-1} and mmol-g^{-1} of dry membranes.

TABLE 4

Electrical conductivity of membranes equilibrated with HCl solutions: $K \times 10^3\ \Omega^{-1}\text{-cm}^{-1}$

[*HCl*] (mol-l^{-1})	AAV membrane	ARA membrane
0.5	2.97	7.03
1	3.50	7.50
2	4.02	9.19
3	4.68	11.19
3.5	4.98	11.53
4	2.45	11.19
5	2.76	10.75
6	3.23	9.75

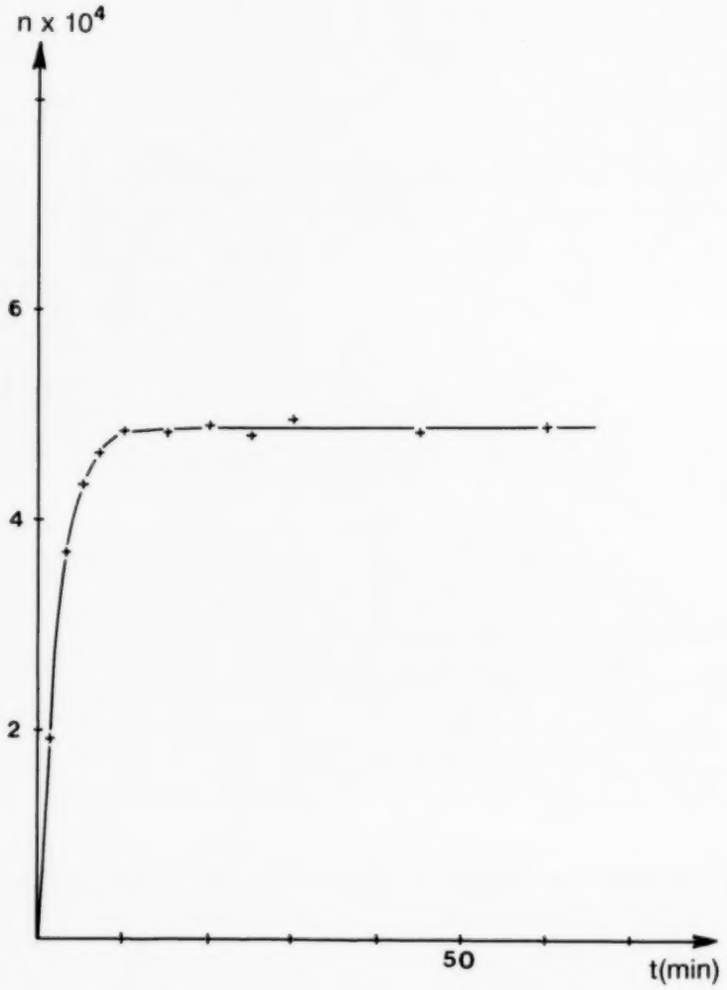

Fig. 2. Variation with time of the number of Cl^- ions released into 4 *N* HCl solution from an ARA membrane previously equilibrated with 2 *N* $H^{36}Cl$ solution.

TABLE 5

Amount of total Cl^- ions of sorbed HCl in the membranes

$[HCl]$ (mol-l^{-1})	AAV membrane		ARA membrane	
	N^* (mequiv-g^{-1})	N_s (mmol-g^{-1})	N^* (mequiv-g^{-1})	N_s (mmol-g^{-1})
0.1	1.18	0.64	0.74	0.14
0.5	1.50	0.96	0.91	0.31
1	1.94	1.40	1.22	0.62
2	2.18	1.64	1.33	0.73
3	2.55	2.01	1.43	0.83
4	2.67	2.13	1.66	1.06
5	3.21	2.67	1.95	1.35
6	4.54	4.00	2.48	1.88

Discussion

When a constant current is applied, the value of the total flux for a given ion transferred through the membrane is equal to the difference between the two unidirectional fluxes $\vec{J}$ and $\overleftarrow{J}$. The transport number of an ion i through the membrane is then given by the following equation.

$$t_i = \frac{|\vec{J}_i - \overleftarrow{J}_i| F}{I} \tag{1}$$

where I is the density of the applied current and F is the Faraday constant. The values of t_{Cl^-} and $t_{SO_4^{2-}}$ deduced from eqn. (1) are given in Table 6.

TABLE 6

Values of Cl^- and SO_4^{2-} transport numbers

	AAV membrane	ARA membrane
$[HCl]$ (mol-l^{-1})		
0.5	0.92	0.94
1	0.87	0.87
2	0.74	0.82
3	0.62	0.66
4	0.54	0.55
5	0.46	0.48
6	0.41	0.41
$[H_2SO_4]$ (mol-l^{-1})		
2	0.28	0.59
4	0.16	0.36

In order to analyse the results of transport number measurements, the gel model for the membrane phase can be used. The membrane is assimilated to a polyelectrolyte solution; considering that the moving electrical species are only H_3O^+ and Cl^-, the expressions for the transport numbers in the case of complete dissociation are:

$$t_{H_3O^+} = \frac{\bar{m}_u \bar{u}_{H_3O^+}}{\bar{m}\bar{u}_{H_3O^+} + (\bar{m}+\bar{X})\,\bar{u}_{Cl^-}} \tag{2}$$

and

$$t_{Cl^-} = \frac{(\bar{X}+\bar{m})\,\bar{u}_{Cl^-}}{(\bar{X}+\bar{m})\,\bar{u}_{Cl^-} + \bar{m}\bar{u}_{H_3O^+}} \tag{3}$$

where $\bar{m}$ is, at the sorption equilibrium, the molality of the electrolyte which is present in the membrane, $\bar{X}$ is the molality of fixed charges, and $\bar{u}$ is the apparent mobility of ions in the membrane.

Assuming that the ion mobilities do not depend on the molalities of the sorbed HCl, eqn. (3) gives:

$$\frac{1}{t_{Cl^-}} = 1 + \frac{\bar{u}_{H_3O^+}}{\bar{u}_{Cl^-}} \cdot \frac{\beta}{1+\beta} \tag{4}$$

with $\beta = \frac{\bar{m}}{\bar{X}} = \frac{n_{HCl}}{n_{sites}}$

The β values are given in Table 7.

One notices the very high values of β, especially with the AAV membrane, even at low concentrations. In Fig. 3, $1/t_{Cl^-}$ is plotted as a function of $[\beta/(1+\beta)]$; it may be observed that the experimental results do not fit eqn. (4) in the molality range considered.

This result must be related to the results of conductivity measurements.

TABLE 7

Values of β for HCl solutions

[*HCl*] (mol-l^{-1})	AAV membrane	ARA membrane
0.1	1.19	0.23
0.5	1.78	0.52
1	2.59	1.03
2	3.04	1.22
3	3.72	1.38
4	3.94	1.77
5	4.94	2.25
6	7.41	3.13

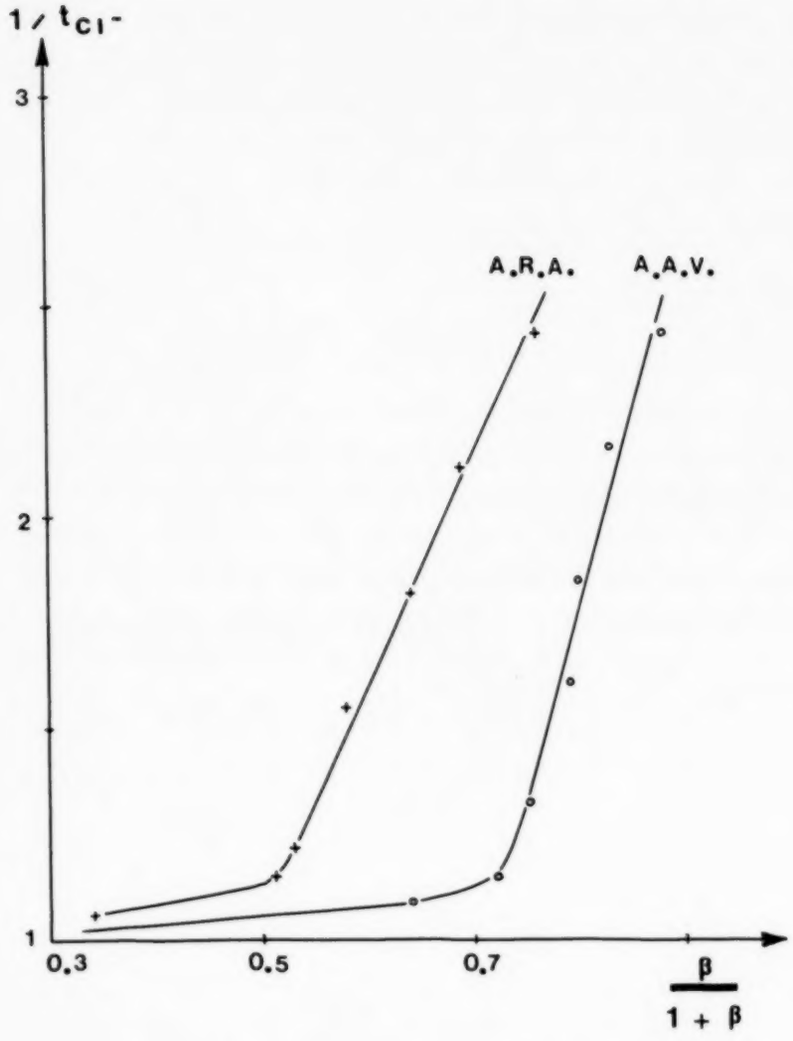

Fig. 3. Variation of $1/t_{Cl^-}$ as a function of $\beta/(1+\beta)$.

Figure 4 shows the variation of the membrane conductivity as a function of the external HCl concentration. A sharp maximum is observed for $\beta \approx 1.4$ with the ARA membrane and a smooth maximum is observed for $\beta = 3.8$ with the AAV membrane.

The results show that the theoretical model – the membrane considered as a gel phase and complete ion dissociation – does not fit to the studied system. One notes the very high amount of sorbed electrolyte in the membrane with respect to the amount of water. For instance, in the membranes equilibrated with 6 *N* HCl solutions, the number of sorbed HCl molecules over the number of fixed sites ($N_s/\bar{X}$) is 3.13 for the ARA membrane and 7.4 for the AAV membrane; the number of water molecules over the number of total chloride ions is 3.46 for the ARA membrane and less than 1.9 for the AAV membrane.

These data strongly suggest an incomplete ionic dissociation inside the membrane phase. A fraction of sorbed HCl probably remains in the neutral molecule form. Under these conditions, another expression applies:

$$t_{Cl^-} = \frac{(\bar{X}+\gamma\bar{m})\,\bar{u}_{Cl^-}}{(\bar{X}+\gamma\bar{m})\bar{u}_{Cl^-} + \gamma\bar{m}\bar{u}_{H_3O^+}} \tag{5}$$

where γ is the dissociation coefficient of sorbed HCl. Equation (5) can be rearranged into the following form:

$$\frac{1}{t_{Cl^-}} = 1 + \frac{\bar{u}_{H_3O^+}}{U_{Cl^-}} \cdot \frac{\gamma\beta}{1+\gamma\beta} \tag{6}$$

Equation (6) shows that the values of the transport number of the moving ions inside the membrane phase are dependent not only on the ratio of their mobilities and the amount of sorbed acid but also on the dissociation coefficient of sorbed acid.

If the ratio of the mobilities of the free ions $\bar{u}_{H_3O^+}/\bar{u}_{Cl^-}$ maintains a constant value, $1/t_{Cl^-}$ will have the same variations as $\gamma\beta/(1+\gamma\beta)$. In Fig. 5 the calcu-

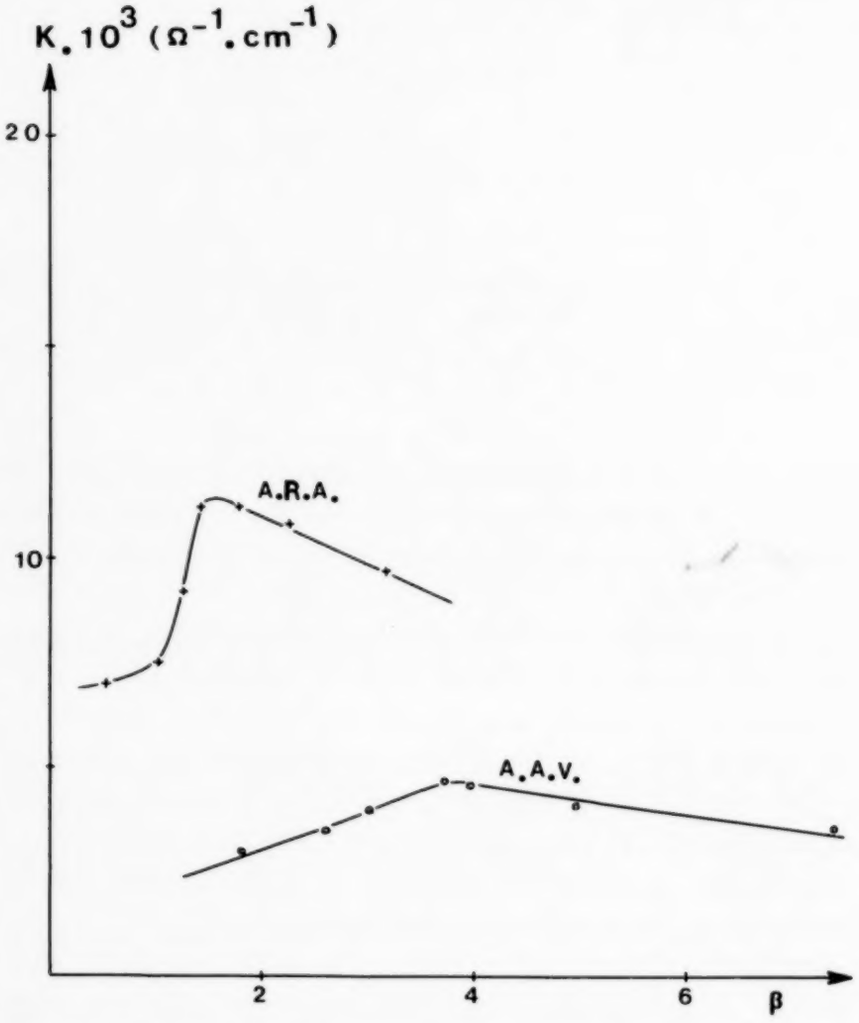

Fig. 4. Variation of membrane conductivities as a function of β.

lated variations of this expression are plotted as a function of β for four different values of γ. From this curve, we can deduce that $1/t_{Cl^-}$ is lowered when the dissociation coefficient γ is low.

We can conclude that the lower dissociation of sorbed HCl is a factor which decreases the proton leakage of the anion exchange membrane.

As for the variation of the ratio of the mobilities of H_3O^+ and Cl^-, no direct information can be deduced from the experimental data. We can only observe a maximum in the curves of the membrane conductivity (Fig. 4). Considering again an incomplete dissociation of the sorbed hydrochloric acid in the membrane phase, we can only conclude that the mobilities of the free ions have decreased because the expression of the membrane conductance is:

$$\Lambda = F[(\bar{X} + \gamma\bar{m})\,\bar{u}_{Cl^-} + \gamma\bar{m}\bar{u}_{H_3O^+}] \tag{7}$$

The decrease of the values of free ion mobilities has two distinct origins: the increase of the local viscosity of the hydrophilic pathways in the membrane phase, and the increase of the interionic interactions, these two effects being

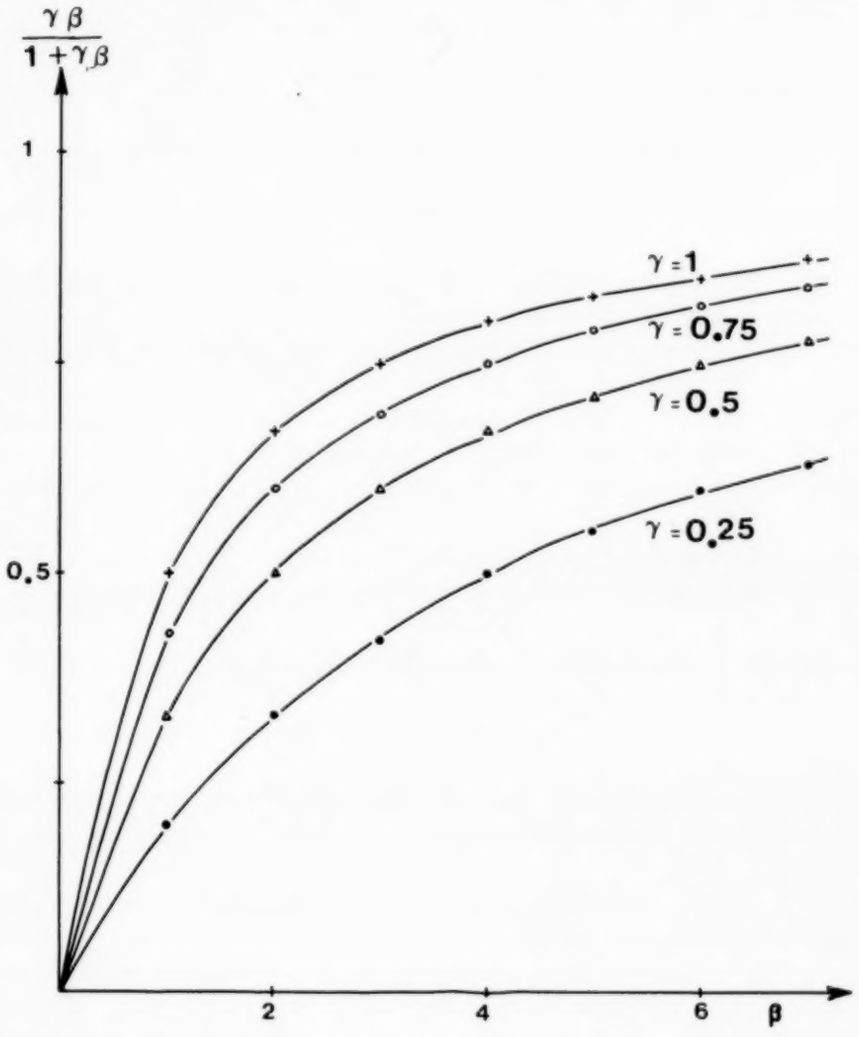

Fig. 5. Variation of $\gamma\beta/(1+\gamma\beta)$ as a function of β for several values of γ.

due to the high value reached by the mobility of hydrochloric acid in the membrane phase.

From the data given in Table 2, one may note that, for a current density of 30 mA-cm^{-2}, the unidirectional flux $\vec{J}$ of Cl^- through the ARA membrane from the anode to the cathode steadily increases as the amount of sorbed electrolyte increases. This result means that chloride ions are associated with the movement of positively charged species. This fact may be due to the formation of an aggregate form such as $(H_4OCl)^+$ resulting from the solvation of a proton by a water molecule and an HCl molecule, ion association inside the membrane overcoming the state of a neutral HCl molecule. This result confirms the role of ion association in this membrane.

Acknowledgement

This work has been financially supported by "Electricité de France" (convention No. 2J0722).

References

1 K. Urano, T. Ase and Y. Naito, Recovery of acid from wastewater by electrodialysis, Desalination, 51 (1984) 213.
2 A.T. Cherif and C. Gavach, Sulfuric acid concentration with an electrodialysis process, Hydrometallurgy, 21 (1988) 191.
3 T.C. Huang and R.S. Juang, Recovery of sulfuric acid with multicompartment electrodialysis, Ind. Eng. Chem. Process Des. Dev., 25 (1986) 537.
4 B.R. Nott, Electrodialysis for recovering acid and caustic from ion exchange regeneration wastes, Ind. Eng. Chem. Prod. Res. Dev., 20 (1981) 170.
5 V.D. Grebenyuk, I.I. Penkalo and L.M. Chalaya, Desalination of water with simultaneous production of alkali and acid, Khim. Tekhnol. Vody, 8 (1986) 76.
6 F.B. Leitz, Electrodialysis for industrial water cleanup, Environ. Sci. Technol., 10 (1976) 136.
7 J.L. Eisenmann, Membrane processes for metal recovery from electroplating rinse water, Second Conference on Advanced Pollution Control for the Metal Finishing Industry, E.P.A., Cincinnati, OH, 1979, p. 99.
8 T. Yoshihara, Recovery of phosphoric acid by electrodialysis, Japanese Patent Kokai No Sho, 53 96 994, 1978.
9 T.R. Hanley, H.K. Chiu and R.J. Urban, Phosphoric acid concentration by electrodialysis, AIChE Symp. Ser., 82 (1985) 121.
10 G.A. Bobrinskaya, T.V. Pavlova, Y.G. Freidlin and A.Y. Shatalov, Production of acid and alkali from sodium chloride by using bipolar membranes, Teor. Prakt. Sorptionnykh Protsessov, 17 (1985) 111.
11 T. Gunjima, Y. Sugaya and T. Ichiki, Anion exchange resin membrane hardly permeable to hydrogen ion, Jpn. Kokai Tokyo Koho, 76 103 089, 1975.
12 A. Lindheimer and C. Gavach, A study of the superselectivity of Nafion perfluorosulfonic membranes, J. Electroanal. Chem. Interfacial Electrochem., 216 (1987) 71.
13 E. Glueckauf and R.E. Watts, Donnan law and its application to ion exchanger polymers, Proc. R. Soc. London, Ser. A, 268 (1962) 339.

Journal of Membrane Science, 57 (1991) 69–81
Elsevier Science Publishers B.V., Amsterdam

A two step mechanism of diffusion-controlled ethylene vinyl alcohol membrane formation

Tai-Horng Young and Leo-Wang Chen*

Chemical Engineering Department, National Taiwan University, Taipei 10764 (Taiwan)

(Received March 21, 1990; accepted in revised form September 13, 1990)

Abstract

The coagulation of ethylene vinyl alcohol (EVAL) copolymer membranes was investigated with a solvent/nonsolvent mixture. A two step mechanism model is presented which describes mass transfer processes occurring for specified membrane formation systems. The various morphology structures can be reasonably explained by this model by changing the solvent content of the coagulation bath. It clearly shows that the membrane structure actually depends on the local composition at phase transition and is controlled mainly by kinetic and structural factors rather than thermodynamic equilibrium. This model also points out some aspects neglected of membrane formation in published research. This analysis provides better understanding and correct control of membrane formation techniques.

Keywords: membrane preparation and structure; two step mechanism model; phase transition; ethylene vinyl alcohol membrane

Introduction

Since the development of asymmetric type membranes by Loeb and Sourirajan [1], the field of membrane science and technology has experienced an increasing growth. The asymmetric membranes are generally produced by the so-called phase inversion technique [2]. In this process, a polymer solution is immersed into a coagulation bath containing nonsolvent miscible with the solvent. A solvent/nonsolvent diffusional interchange between the polymer solution and the coagulation bath causes the polymer to precipitate, and a 'gel' containing considerable amounts of solvent and nonsolvent is formed. Finally, the gel solidifies to form a membrane film.

From the technological point of view, the most important problem is to obtain membranes of optimum morphological structure to meet with the requirements for a wide range of applications, such as gas permeation and blood dialysis. In a previous paper [3], we have described the relationship between the

*To whom correspondence should be addressed.

0376-7388/91/$03.50 © 1991 — Elsevier Science Publishers B.V.

structure of EVAL membranes and experimental variables, including temperature and solvent effects. Our present discussion will be confined to an isolated problem: the addition of solvent to the coagulation bath in an attempt to gain a clear understanding of the membrane formation mechanism.

Theory

It is obvious that an explanation for the phase inversion technique should be based on two factors: (1) the thermodynamic equilibrium properties, involving the ternary phase diagram for the system polymer/solvent/nonsolvent (P/S/NS), and (2) the kinetic properties, involving the mass transfer rates of solvent and nonsolvent.

An isothermal ternary phase diagram is represented in Fig. 1. It is divided into three regions according to their thermodynamic state. Two different types of phase transition can be distinguished.

(1) Liquid–liquid phase separation (from I to II): the completely miscible solution crosses the binodal boundary (the solid line, see Fig. 1), i.e. from a stable homogeneous solution region into a two-phase region.

(2) Solidification (from I to III or from II to III): a hypothetical boundary is located in the diagram since the viscosity of polymer solution increases to a certain value, the polymer motion will be limited, and then the membrane structure is specified. This boundary (the dotted line, see Fig. 1) moves across the diagram from left to right while descending slightly since the viscosity in concentrated polymer solution is higher in a poor solvent than in a good one (not the same as suggested by Mulder et al. [4]). This is rationalized by postulating tighter coiling in good solvents as concentration is increased, where, since polymer–solvent interaction ≫ polymer–polymer interaction, intermolecular contact between polymer chains is forbidden. The coils must as a result become smaller as they are crowded together with increasing concentration. The result is that each coil contributes progressively less to overall viscosity. In poor solvents, on the other hand, intermolecular contacts are not so strongly

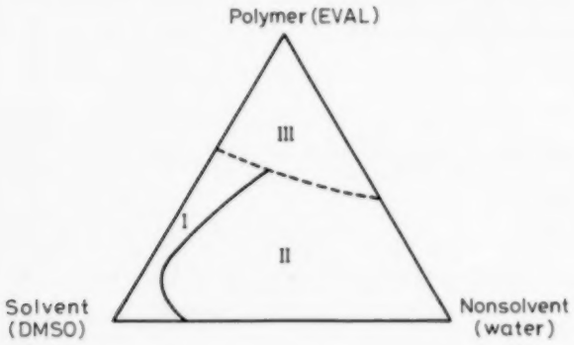

Fig. 1. Ternary phase diagram of EVAL–DMSO–WATER system. I: homogeneous solution region; II: two-phase region; III: solidification region. (data are given in Ref. [3]).

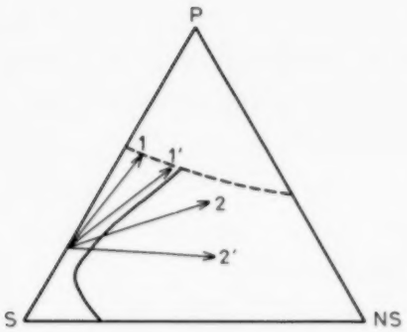

Fig. 2. Schematic route of composition for dense structure (1), and microporous structure (2) of a membrane.

forbidden and the increasing size of the polymer network owing to chain interpenetration results in increased viscosity [2]. (The above result is opposite in diluted polymer solution.) From the phase diagram it follows that the resulting structure of the membrane does not only depend on the average composition but also on the route by which this composition was reached (Fig. 2). Therefore, the morphology is determined by the local polymer solution in each layer of nascent membrane gel, whether the coagulation path follows the line 1 or 2 (Fig. 2). The line 1 (from I to III) occurs at higher polymer concentrations. A dense structure is formed in this way. Line 2 (from I to II) occurs at lower polymer concentrations. The result is a porous structure. Therefore, it is important to know how the rates of transfer of the individual mobile components affect the route of composition change.

A very important controllable factor is the addition of solvent to the coagulation bath in order to change its composition. This does not effect phase equilibrium but does control the kinetics of mass transfer. Generally, an increase of solvent content in the coagulation bath reduces the driving force for diffusion. The same observations have been made by Strathmann et al. [5], Wijmans et al. [6] and Yilmaz and McHugh [7]. But their results are either restricted to a short distance from the membrane surface or not consistent with the overall membrane properties. The aim of this study is to get a better understanding of the membrane formation process by providing a two step mechanism model based on experimental observations.

Experimental

Materials

The ethylene–vinyl alcohol (EVAL) copolymer which has a content of 56 mol% of vinyl alcohol monomeric units was obtained using previously reported techniques [3]. De-ionized and ultrafiltrated water was used in our experiments. Other reagents are of chemical reagent grade and were used without purification.

Membrane preparation

EVAL copolymers were dissolved in DMSO to form a 25% polymer solution at 60°C. The resulting solution was kept at 25°C for 24 hr and was subsequently spread on glass plates to a uniform thickness. The glass plates were immersed immediately in a 25°C coagulation bath of varying DMSO/water composition (see Table 1). After standing overnight, the membrane was removed from the glass plate and was kept in a pure water bath.

Membrane characterization

The morphology of the membranes was examined using a scanning electron microscope (Philips Model-515). The water permeability was measured using a type 8050 Amicon Filter at 25°C.

The water content of the membrane was determined from the weight difference between an equilibrated membrane in a pure water bath and that of the membrane dried to constant weight at 60°C. This content equals approximately the percent porosity of the membrane and indicates a diffusional interchange between the polymer solution and the coagulation bath.

Results and discussion

Porosity and absorption equilibrium

Figure 3 shows the liquid content of the membranes as a function of the DMSO content of the coagulation bath. It shows that the liquid content after

TABLE 1

Details of coagulation baths (D: DMSO, W: water)

Notation of membrane	G1	G2	G3	G4	G5	G6
D/W ratio	0/1	1/4	2/3	1/1	2/1	3/1

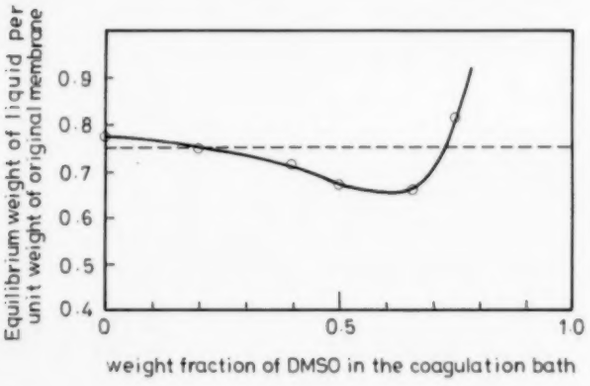

Fig. 3. The effect of the composition of the coagulation bath on the liquid content of EVAL membranes.

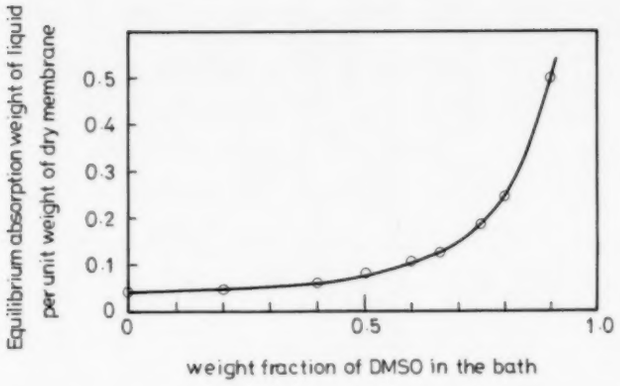

Fig. 4. Absorption equilibrium of dense EVAL membranes in the water/DMSO bath.

coagulation in a pure water bath (membrane G-1, see Table 1) is more than the original liquid content (75%; see the dashed line), which indicates that the DMSO loss by diffusion is less than the water gain. As the DMSO content of the coagulation bath increases, the liquid content initially decreases slightly, then goes through a minimum, and finally rises. As the DMSO content of the coagulation bath is 20% (membrane G-2), the liquid content is about equal to the original liquid content, which indicates that the diffusional interchange is about the same.

The minimum point is at a DMSO content of the coagulation bath of 66% (membrane G-5). The original liquid content is surpassed as the DMSO content of the coagulation bath reaches 75%. In fact, the membrane is swollen by the coagulation bath and almost dissolves the polymer. Membranes produced in this way have very little mechanical strength.

Figure 4 shows an absorption equilibrium curve as mentioned below. A dry-dense EVAL membrane, which is free of any voids by SEM visualization, is immersed in coagulation baths of different DMSO concentrations. Because there are not many pores in the membrane, the solvent can only slowly dissolve into the membrane. Membranes are weighted after equilibration and the change in weight from the dry-dense membrane is drawn in Fig. 4. It shows that the absorption equilibrium amount increases monotonously with the DMSO content in the coagulation bath.

The outcome of Fig. 4 is different from Fig. 3. No minimum peak can be seen in Fig. 4. It shows that membrane formation mechanism and morphology structure do not change monotonously according to the solvation power (i.e. the DMSO content) of the coagulation bath.

The chemical potential variation of the coagulation bath

The SEM pictures (Figs. 5–10) reveal that the DMSO content exerts an influence upon the structure of membranes. This can be explained by the fact that due to the presence of DMSO the membrane formation mechanism is changed. Therefore, it is very important to know the effect of the DMSO con-

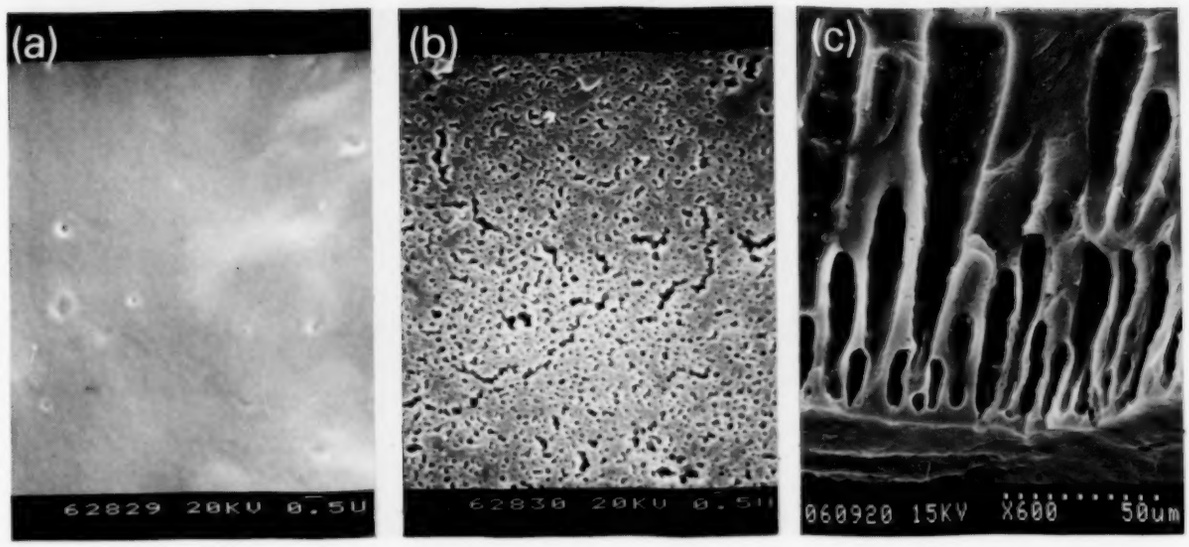

Fig. 5. SEM picture of the G-1 membrane in a 100% water coagulation bath: (a) top, (b) bottom and (c) cross section.

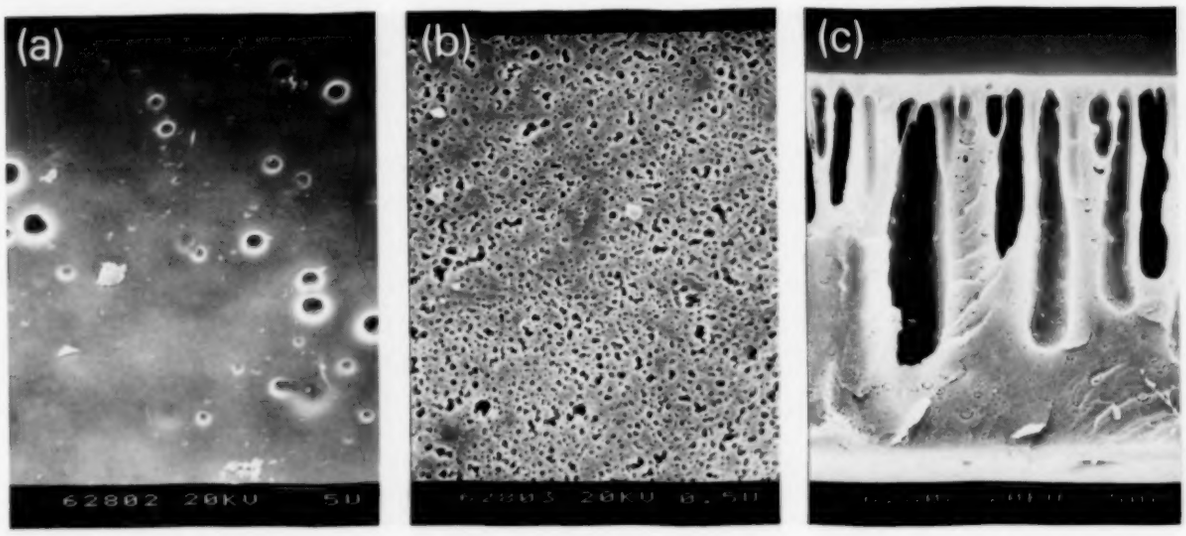

Fig. 6. SEM picture of the G-2 membrane in a water/DMSO coagulation bath, containing 20% DMSO: (a) top, (b) bottom and (c) cross section.

tent on the chemical potential changes of the coagulation bath since it directly influences the driving force for the diffusional interchange between the coagulation bath and polymer solution [6]. The relation between flux J_i and chemical potential difference $\Delta\mu_i$ can be represented by a simplified phenomenological equation:

$$J_i = L_i \Delta\mu_i \tag{1}$$

L_i is the permeability coefficient which may be a function of concentration. Since the polymer solution system is fixed, we only consider the chemical potential variation of the coagulation bath (we disregard the influence of L_i). For

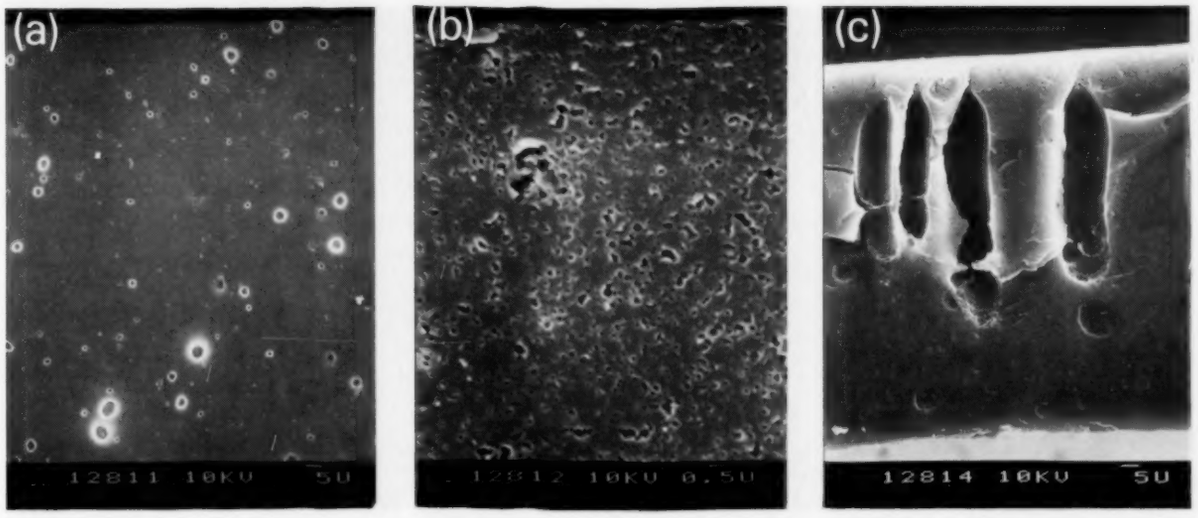

Fig. 7. SEM picture of the G-3 membrane in a water/DMSO coagulation bath, containing 40% DMSO: (a) top, (b) bottom and (c) cross section.

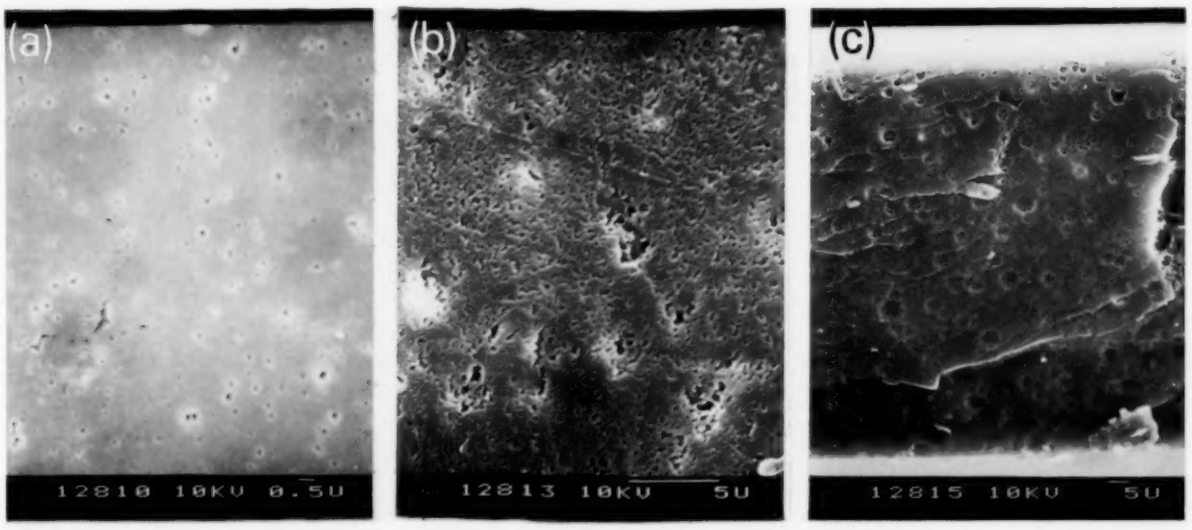

Fig. 8. SEM picture of the G-4 membrane in a water/DMSO coagulation bath, containing 50% DMSO: (a) top, (b) bottom and (c) cross section.

the chemical potential of DMSO and water as a function of DMSO content in the coagulation bath, the expression used is:

$$\mu_i = \mu_i^0 + RT \ln \gamma_i x_i \tag{2}$$

where μ_i^0 is the chemical potential of component i in a pure (standard) state at the same temperature and pressure as that of the mixture. The index i indentifies DMSO or water. The activity coefficients, γ_i, used to calculate the chemical potential, are taken from Lam et al. [8] and listed in Table 2. Using these quantities, $(\mu_i - \mu_i^0)$ was calculated from eqn. (2) and is shown in Table 2. Examining the results (see Table 2 or Fig. 11), one finds that the chemical potential of DMSO increases very rapidly and that of water decreases slightly

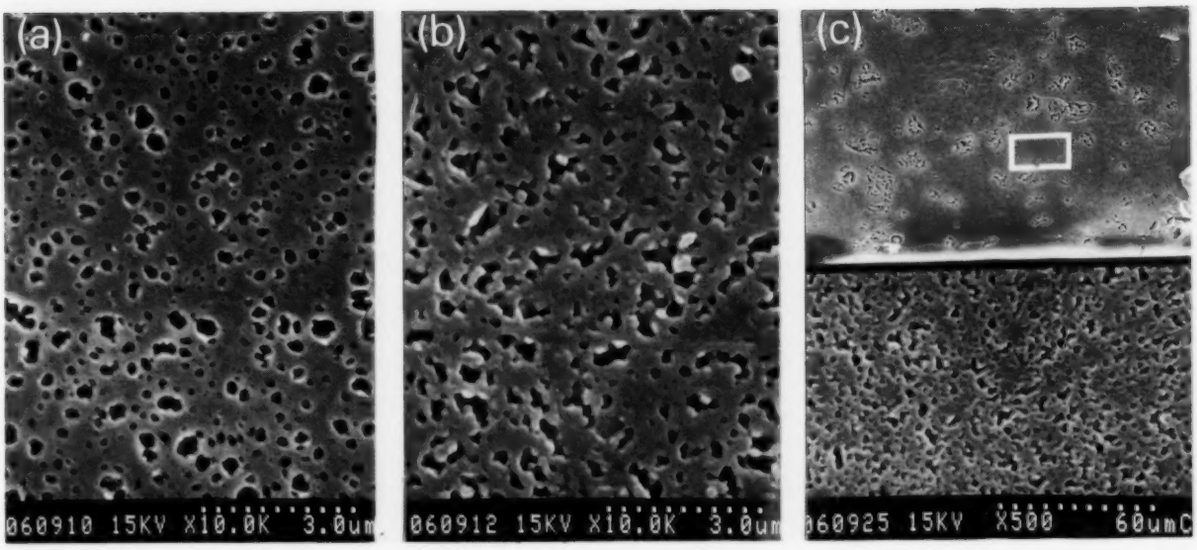

Fig. 9. SEM picture of the G-5 membrane in a water/DMSO coagulation bath, containing 66% DMSO: (a) top, (b) bottom and (c) cross section.

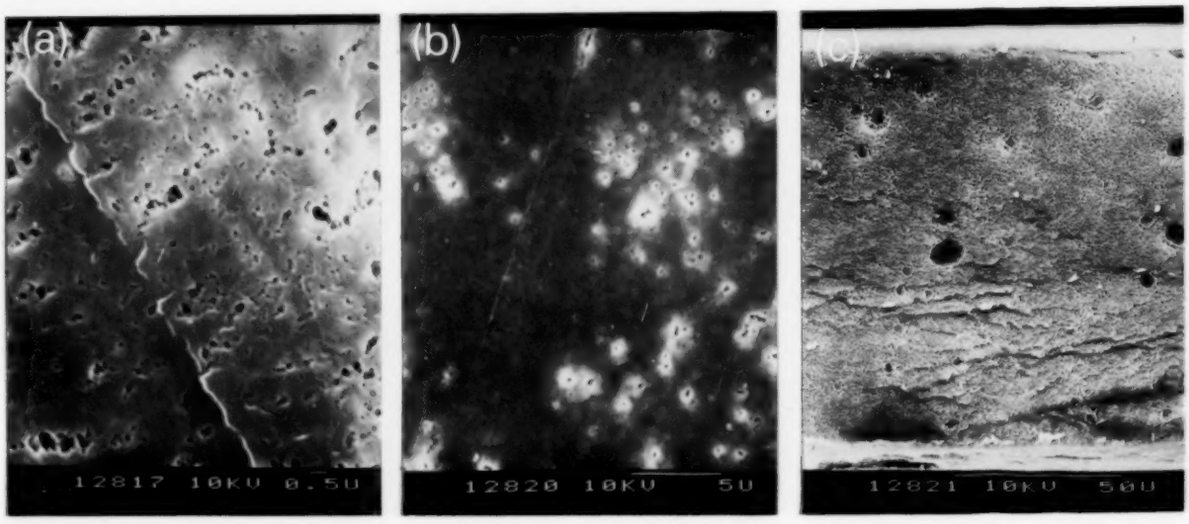

Fig. 10. SEM picture of the G-6 membrane in a water/DMSO coagulation bath, containing 75% DMSO: (a) top, (b) bottom and (c) cross section.

upon increasing the DMSO concentration. It is clear that the outdiffusion rate of DMSO is reduced very rapidly and the indiffusion rate of water is reduced slightly by adding solvent to the coagulation bath (Fig. 12). Therefore, the DMSO outflow decreases appreciably and the water inflow decreases slightly. In other words, the DMSO outflow decreases more rapidly than the decreasing water inflow. This result should lead to a more porous polymer structure in the resulting membrane with increasing DMSO content in the coagulation bath. However, it provides a poor prediction for the membrane porosity (see Fig. 3) while presenting a good fit for the determination of skin structure from SEM pictures (see Figs. 5–10). So we investigate the overall membrane formation

TABLE 2

Activity coefficients and chemical potential of DMSO-water system at 25 °C

D/W ratio	γ_o	γ_w	$\mu_D - \mu_D^0$ (cal/mole)	$\mu_W - \mu_W^0$ (cal/mole)
0/1	0.05	1.00	$-\infty$	0.0
1/4	0.10	0.99	−3029	−43.8
2/3	0.16	0.93	−2249	−132.3
1/1	0.24	0.86	−1810	−221.4
2/1	0.49	0.66	−1061	−492.0
3/1	0.65	0.56	−755	−676.2

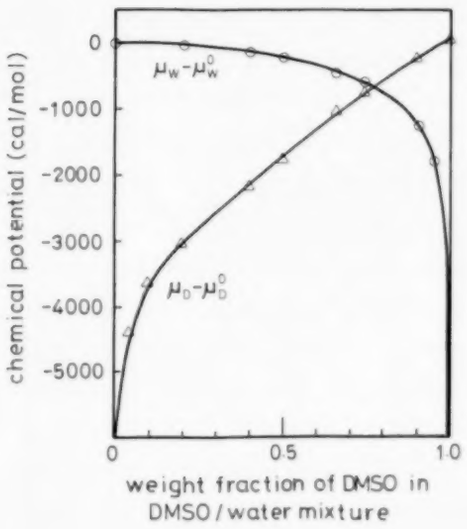

Fig. 11. The chemical potential of DMSO and water relative to their pure state in the coagulation bath.

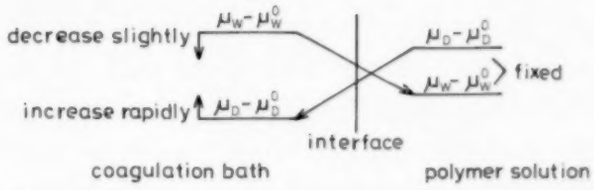

Fig. 12. The variation of the chemical potential of DMSO and water with increasing DMSO content in the coagulation bath.

mechanism in the discussion below. This analysis is an important step towards a better understanding of the diffusion process during membrane formation.

The mechanism of diffusion-controlled formation

Immediately the casting solution becomes turbid when DMSO is absent in the coagulation bath, caused by a rapid diffusion of DMSO from the polymer

solution to the coagulation bath. At the same time, relatively little water penetrates since it is a nonsolvent for the EVAL copolymer. This means that the local polymer concentration increases and hence the viscosity also increases rapidly at the surface. When the viscosity increases to a certain extent, the homogeneous polymer solution undergoes phase transition into a gel and the system is solidified (line 1 in fig. 2). A high polymer concentration gel is formed in this way, i.e. a dense skin is formed. Figure 5 shows the near absence of pores in the toplayer of membrane G-1. The skin formed at the surface of the initial membrane is believed to control the rate of mass transfer by having a permeability considerably lower than the inner portions of fresh solution. Thus, the structure below the skin is determined by the diffusion rate of solvent and nonsolvent through the skin layer.

The DMSO outdiffusion rate is thus hindered due to the presence of the skin. Water, which has smaller molecular size, penetrates the dense skin layer by a molecular diffusion mechanism causing phase transition at a lower polymer concentration (line 2′ in Fig. 2) resulting in the so-called finger structure. So the membrane G-1 formation mechanism has two steps and the structure is determined by the local composition in each step. In the first step, the DMSO outdiffusion rate is faster, and in the second step, water indiffusion rate is faster. The skin is very thin, so the liquid content of the membrane G-1 is larger than that of the original solution. Its porosity is about 77%.

With increasing DMSO content in the coagulation bath, the initial tendency of DMSO diffusion from the film slows down since the chemical potential of DMSO increases very steeply in the coagulation bath. Therefore, the viscosity increases less rapidly and it takes more time for the surface solution to undergo phase transition and more water will diffuse into the surface solution, thus affecting the skin composition. It follows from line 1′ in Fig. 2 that the resulting skin will be less compact. The Figs. 6 and 7 show that some pores occur in the top skin layer.

Below the less dense skin layer, the DMSO outdiffusion rate increases, and the finger cavities gradually become smaller as shown in the SEM picture of the cross section. Upon increasing the DMSO content to 66% in the coagulation bath, the finger structure disappears and the sponge structure emerges. Membrane G-5 from this coagulation bath does not have a skin layer. Since the tendency of DMSO outdiffusion becomes smaller, the phase transition of the surface solution is slow rather than rapid and water has enough time to diffuse into the polymer solution to cause liquid–liquid phase separation (line 2 in Fig. 2). The average pore size of the toplayer is about 0.4 μm. Because this is larger than the size of diffusing component, the microporous toplayer does not influence the diffusion rate, and the solvent and nonsolvent can diffuse freely through the toplayer. Therefore, the diffusion rate of solvent and nonsolvent below the toplayer is the same as that of solvent and nonsolvent in the initial period and the polymer solution below the toplayer will go through the

same phase separation as the top layer. Therefore, membrane G-5 is regarded to have a one step formation mechanism and a homogeneous structure with pores uniformly distributed through the entire membrane (see Fig. 9). Hence, the DMSO diffusion rate from the interior polymer solution is higher than when a skin is present. Finally, the porosity of membrane G-5 becomes smaller and is ca. 66%. Upon increasing the DMSO content in the coagulation bath to 75%, DMSO presents good solvent power. So the porosity of membrane G-6 increases, no skin and no finger structure appear, but the membrane does not have enough mechanical strength for any application.

It is obvious from the above discussion that with increasing DMSO content in the coagulation bath the toplayer structure follows the line 1 to 1′ or 2, and the sublayer structure follows the line 2′ to 2 in Fig. 2. This phenomenon can clearly be ascribed to the variation of the diffusion rate of solvent and nonsolvent during the membrane formation process. So the membrane formation process clearly has two different mechanisms and the porosity as well as function of the membranes is determined by both toplayer and sublayer.

Membrane performances

Figure 13 shows the water flux experiment at low pressure difference (<0.9 kg/cm^2). The water flux increases with increasing DMSO content in the coagulation bath, except for membrane G-5. This can be explained by the fact that the skin becomes less dense with increasing DMSO content in the coagulation bath. But the porosity of membrane G-5 is lower resulting in a lower water flux than for membranes G-3 and G-4.

Figure 14 shows the dynamic creatinine dialysis experiment with membrane G-1, G-5 and the commercial membrane "Gambro". It is obvious from the

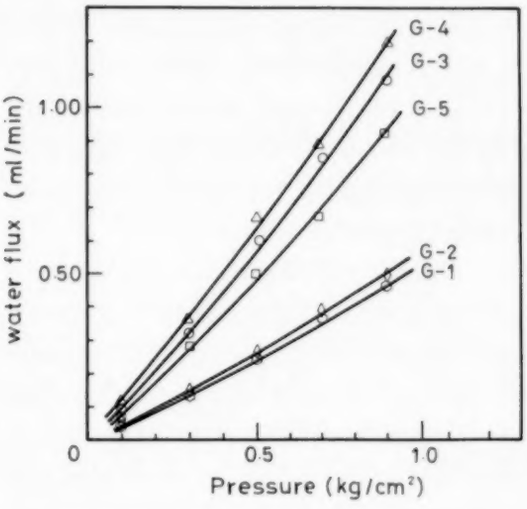

Fig. 13. Influence of DMSO content of the coagulation bath on the water flux of EVAL membranes at different operating pressure.

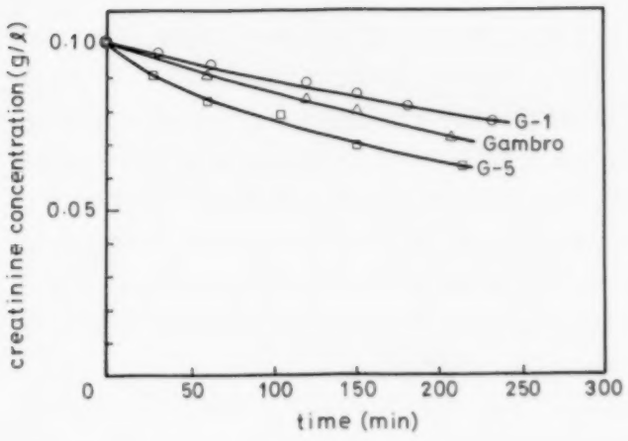

Fig. 14. The creatinine dialysis experiment for G-1, G-5 and Gambro membrane.

figure that membrane G-5 is better than Gambro. Therefore, membrane G-5 is a potential film for the application in dialysis.

Conclusion

In this paper we have presented the mass transfer processes responsible for the membrane formation mechanism. The ultimate determining factor for membrane structure is the local composition of each layer in the casting solution at the moment that a phase transition is reached. Progressing solidification actually depends on the diffusional interchange of solvent and nonsolvent. As shown, the mass transfer rate influences membrane formation, which can be considered as a two step mechanism.

(1) The ratio of nonsolvent inflow and solvent outflow is of the utmost importance for the toplayer structure, more specifically, the compactness of the toplayer actually depends on the local composition at phase transition. If the toplayer enters the solid phase directly, a dense skin is formed. If the toplayer crosses the binodal boundary to cause liquid–liquid phase separation, the result is a porous layer. The structure of the toplayer is thus related to the chemical properties of the polymer/solvent/nonsolvent system, and especially the variation in chemical potential has a remarkable influence.

(2) If the toplayer structure is relatively compact, it will increase the barrier for diffusion of solvent from and nonsolvent into the sublayer of polymer solution. Therefore, mass transfer in the dense toplayer (skin) occurs at a much slower rate, and it will determine the overall diffusion rate through the film below the toplayer. On the other hand, if the toplayer structure is microporous, mass transfer rate is only slightly influenced by the toplayer. As a consequence, the sublayer structure is the same as the toplayer structure and the two step mechanism is reduced to a one step mechanism. Thus, the sublayer structure can be predicted from the chemical and physical properties of the toplayer/

solvent/nonsolvent complex, and especially the toplayer structure plays an important role.

Applying the above result, we are able to govern membrane structure by suitably regulating the solvent content in the coagulation bath. Asymmetric and symmetric, finger type or sponge type membranes can be obtained by the phase inversion technique. Finally, our results demonstrate that the two step mechanism model leads to a good prediction, which is consistent with existing experimental observations.

Acknowledgement

The authors wish to thank the National Science Council of Taiwan (ROC) for their financial support of this project.

References

1 S. Loeb and S. Sourirajan, Sea water demineralization by means of an osmotic membrane, Adv. Chem. Ser., 38 (1963) 117.
2 R.E. Kesting, Synthetic Polymeric Membranes, John Wiley and Sons, New York, NY, 1985.
3 L.W. Chen and T.H. Young, EVAL membranes for blood dialysis, Macromol. Symp., 33 (1990) 183.
4 M.H.V. Mulder, J.O. Hendrikman, J.G. Wijmans and C.A. Smolders, A rationale for the preparation of asymmetric pervaporation membranes, J. Appl. Polym. Sci., 30 (1985) 2805–2820.
5 H. Strathmann, K. Kock, P. Amar and R.W. Baker, The formation mechanism of asymmetric membranes, Desalination, 16 (1975) 179–203.
6 J.G. Wijmans, J.P.B. Baaij and C.A. Smolders, The mechanism of formation of microporous or skinned membranes produced by immersion precipitation, J. Membrane Sci., 14 (1983) 263–274.
7 L. Yilmaz and A.J. McHugh, Modelling of asymmetric membrane formation. I. Critique of evaporation models and development of a diffusion equation formalism for the quench period, J. Membrane Sci., 28 (1986) 287–310.
8 S.Y. Lam and R.L. Benoit, Some thermodynamic properties of the dimethylsulfoxide–water and propylene carbonate–water system at 25 °C, Can. J. Chem., 52 (1974) 718–722.

Journal of Membrane Science, 57 (1991) 83–94
Elsevier Science Publishers B.V., Amsterdam

Electrode responses to phenolic species through cellulosic membranes

Zahra Koochaki, Ian Christie and Pankaj Vadgama

University of Manchester, Department of Clinical Biochemistry, Hope Hospital, Eccles Old Road, Salford, M6 8HD (UK)

(Received May 22, 1990; accepted October 8, 1990)

Abstract

The responses of an amperometric electrochemical cell to species of interest in the field of clinical biosensors, including hydrogen peroxide, ascorbate and phenolics were investigated. The effects of covering the electrode surface with polycarbonate and cellulose-based membranes on the response were determined, in order to assess the suitability of such membranes for use in biosensors.

The addition of an amino or a further hydroxyl group in the *ortho* or *para* positions to a phenol group, enhanced the electroactivity of the phenolic group. A polycarbonate membrane of 2 μm pore size imparted no selectivity, with all phenolic, ascorbate and hydrogen peroxide electrode responses being 10–20% of the bare electrode value.

Cellulose acetate membranes gave smaller responses, but were selective, being relatively more permeable to hydrogen peroxide and to phenol than to other phenolics, and excluding ascorbate to a large extent. Such membranes thus have a useful selectivity for use in certain biosensors. Cellulose acetate butyrate membranes showed a further reduction in signal size, but an unchanged pattern of selectivity.

Keywords: biosensors; electrochemistry; cellulose based membranes

Introduction

In recent years, considerable interest has been focussed on biosensors in which an enzyme or whole-cell coated sensor produces a signal in response to a substrate [1]. Many such systems utilise amperometric detection, and covering membrane layers are important in this respect. Thus a semi-permeable membrane is often required between the enzyme layer and the electrode surface to furnish the desired degree of selectivity for the chosen analyte in biological fluids. Avoidance by this procedure of complicated separation steps makes feasible invasive or "dipstick" sensors, suitable for clinical use [2].

A commonly used membrane is a dense cellulose acetate layer. This for example is utilised in a commercial glucose analyser [3], where H_2O_2 is the detected end product of a glucose oxidase catalysed reaction. In this situation,

0376-7388/91/$03.50 © 1991 — Elsevier Science Publishers B.V.

the inner selective membrane needs to be permeable to hydrogen peroxide, while excluding electrochemically interfering species from blood, notably ascorbate, urate, certain amino acids and small peptides, such as glutathione [4].

The successful use of such hydrogen peroxide selective membranes [4] in the glucose sensor has stimulated their incorporation into other oxidase based, direct responding electrodes. In reverse osmosis experiments, phenol and certain of its derivatives are known to permeate dense cellulose acetate membranes more readily than inorganic species [5–7]. This offers scope for biosensor construction in situations where there is a need to detect a phenolic compound.

A number of phenolic compounds are of clinical interest. Paracetamol ideally should be directly measured without the intervention of an enzyme [8–10]. Serum levels of both acid and alkaline phosphatase enzymes can be monitored by the dephosphorylation of phenolic compounds [11]. The resulting unconjugated phenols being electroactive, detection with an electrode is therefore feasible, but as yet, not achieved in serum without a prior separation step, due to problems of background interference.

Alkaline phosphatase is commonly used as a label in enzyme immunoassays, and electrochemical detection can also be applied here [12,13]. A number of substrates are suitable for the enzyme, e.g. phosphates of phenol and *p*-aminophenol, but these differ considerably in the ease of electrochemical product detection [13,14].

The work described here combines the phenol permeability of cellulose acetate membranes indicated by reverse osmosis, with the selectivity properties of previous biosensors. The responses of a polarised platinum electrode obtained through such cellulose acetate (CA) and cellulose acetate butyrate (CB) membranes are investigated. Comparison is made to the responses of a bare electrode and of one covered by an unselective microporous polycarbonate membrane (PCM). The phenolic species of clinical interest are considered along with a common biological interferent, ascorbate. Hydrogen peroxide and various other phenolics are investigated in order to correlate the structure and the permeation characteristics through the membrane.

Experimental

Materials

Figure 1 shows the structures of the species investigated. Measurements were performed in isotonic phosphate buffer at pH 7.3, containing 2.44 g NaH_2PO_4, 7.5 g Na_2HPO_4, 3 g NaCl and 0.6 g EDTA per litre. A pH of 7.3 was chosen as being appropriate for oxidase enzyme electrodes and paracetamol measurements in serum. It was also adopted as the standard assay pH throughout the studies comparing the other species of interest. Polycarbonate membranes with

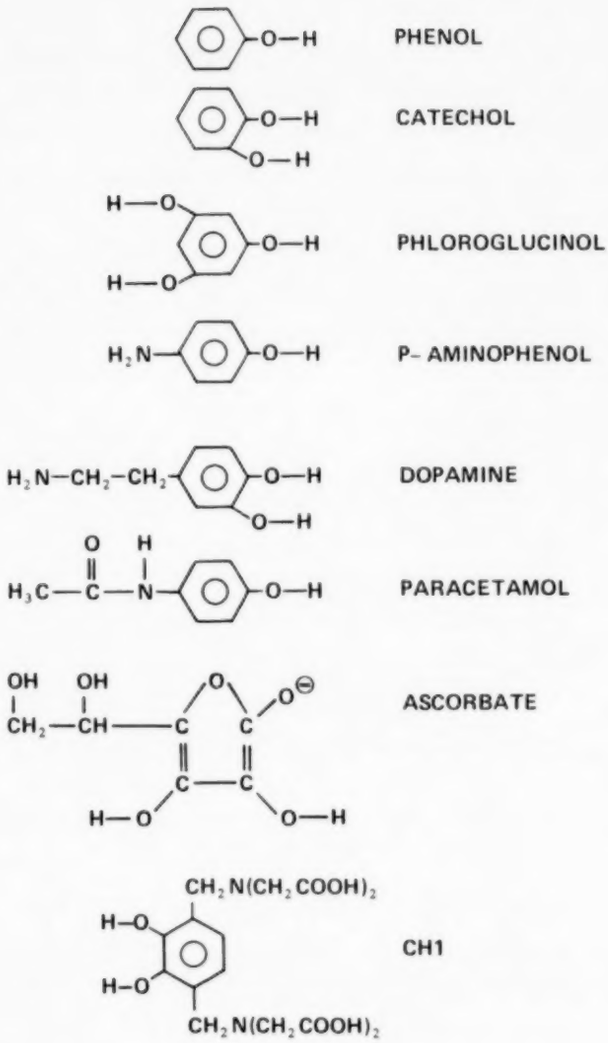

Fig. 1. Structures of species studied.

track-etched pores of 2 μm diameter were obtained from Nuclepore® (Pleasanton, CA).

Preparation of membranes

Solutions of cellulose acetate (39.8% acetyl content) and cellulose acetate butyrate (17% butyryl) were prepared by dissolving 1.5 g polymer in 100 ml acetone. One ml of the solution was evenly spread over a glass plate ($5 \times 5\,cm^2$). The glass plate was manually rotated, approximately once every two seconds during a two minute evaporation period; more rapid rotation led to uneven membranes being formed. Membranes were left to dry at room temperature for one hour. Membrane batches were prepared and stored for later study. Average thickness, as assessed by a micrometer screw gauge, and by scanning electron microscopy in a limited number of membranes, was ca. 10 μm.

Measurement procedure

A two electrode cell was used, based on an oxygen electrode (Rank Brothers, Bottisham Cambridge, UK) (Fig. 2), with a platinum anode and silver cathode. For bare electrode measurements, the O-ring and membrane were omitted. Membranes covering the sensor were held in place by the O-ring to provide a

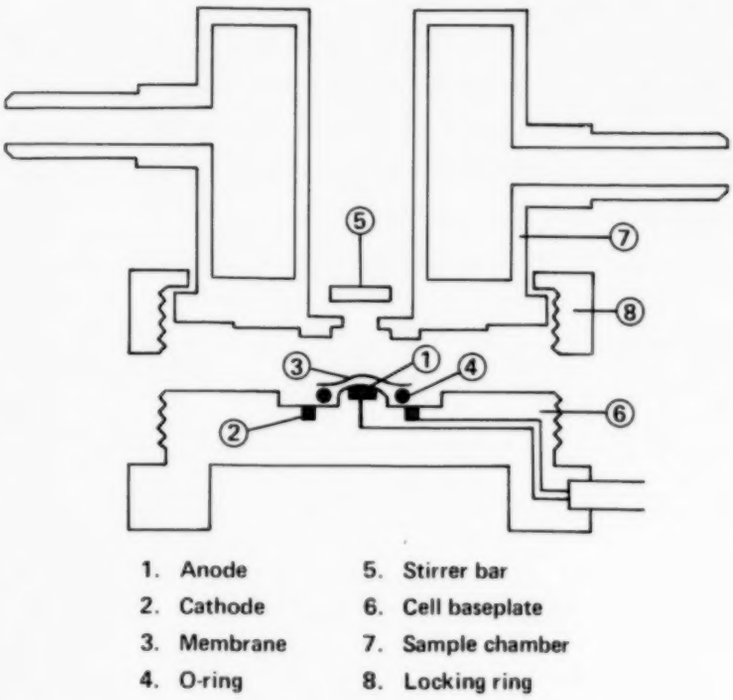

Fig. 2. Cross section of the Rank electrochemical cell.

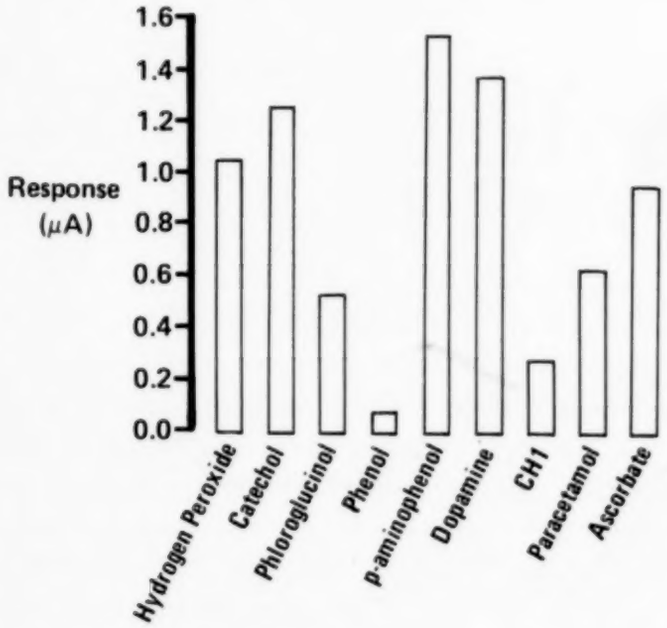

Fig. 3. Responses obtained to 0.04 m*M* solutions, using a bare electrode.

seal so that all responses were solely due to diffusion through the membrane. The platinum anode was polarized at 650 mV against the silver cathode, which acted as a pseudo reference, using an "in-house" potentiostat (School of Chemistry Workshops, University of Newcastle-upon-Tyne). This allowed control of polarising voltages (+/−1.2 V) and detection of current flow in the range 0.1nA–2.0mA. A recorder output was connected to a Lloyd Instruments (Fareham, Hants) type CR652s strip chart recorder.

The electrode was allowed to condition in buffer before use, until a stable base line was achieved (2 hr). Measurements were made by adding small volumes of stock buffered solutions to the assay buffer in the cell. A step change in current output resulted, and responses were recorded at the plateau value; the cell was rinsed with buffer between each measurement.

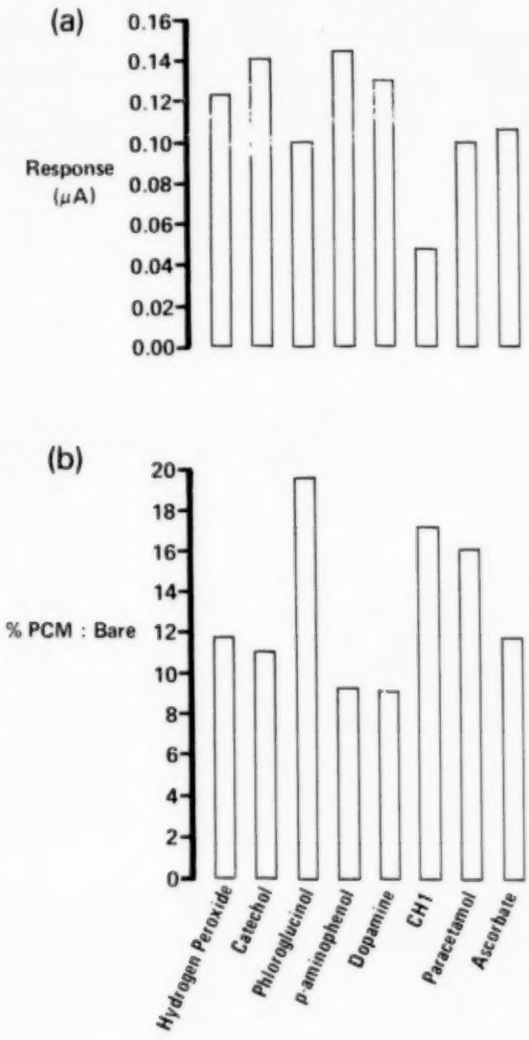

Fig. 4. Polycarbonate membrane; (a) responses obtained to 0.04 m*M* solutions, (b) responses using PCM, expressed as a percentage of the bare electrode responses.

Results

The responses of the bare electrode to 0.04 m*M* solutions are shown in Fig. 3. Both ascorbate and hydrogen peroxide were strongly electroactive, and selective membranes would be required to measure peroxide in samples containing ascorbate.

The relative responses are shown in Fig. 3. Phenol itself had the lowest electroactivity, compared to the other monohydroxy derivatives *p*-aminophenol and paracetamol. The dihydroxy compounds catechol, dopamine and CH1 also gave larger responses, while the trihydroxy species phloroglucinol was also electroactive, but less so than most catechol derivatives.

When a PCM was used (Fig. 4a), the responses were reduced by approximately 90% (Fig. 4b). Though the relative order of activities was unchanged, responses to the less active compounds were attenuated to a lesser degree.

Cellulose membranes decreased the electrode signal to a greater extent. For both CA and CB membranes (Figs. 5a and 6a), peroxide responses were proportionally less reduced. The effects of cellulose membranes on the responses

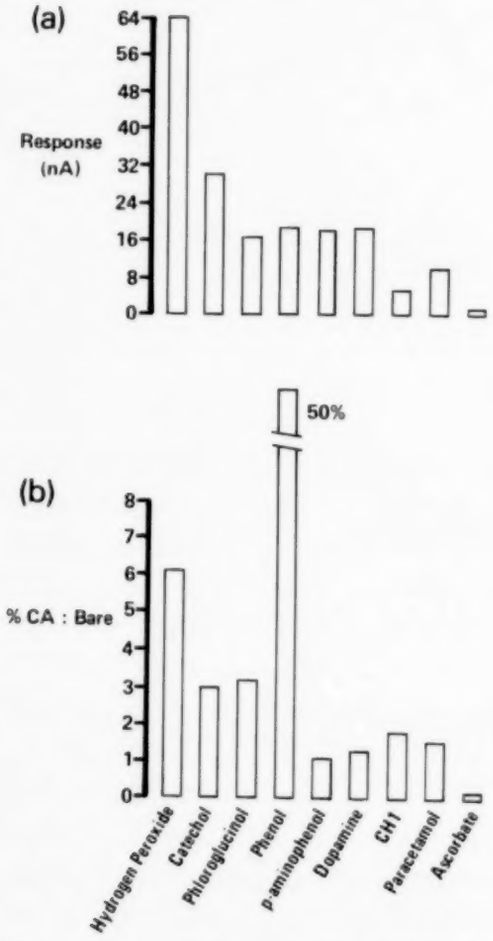

Fig. 5. Cellulose acetate membrane; (a) responses obtained to 0.04 m*M* solutions, (b) responses using CA membranes expressed as a percentage of the bare electrode responses.

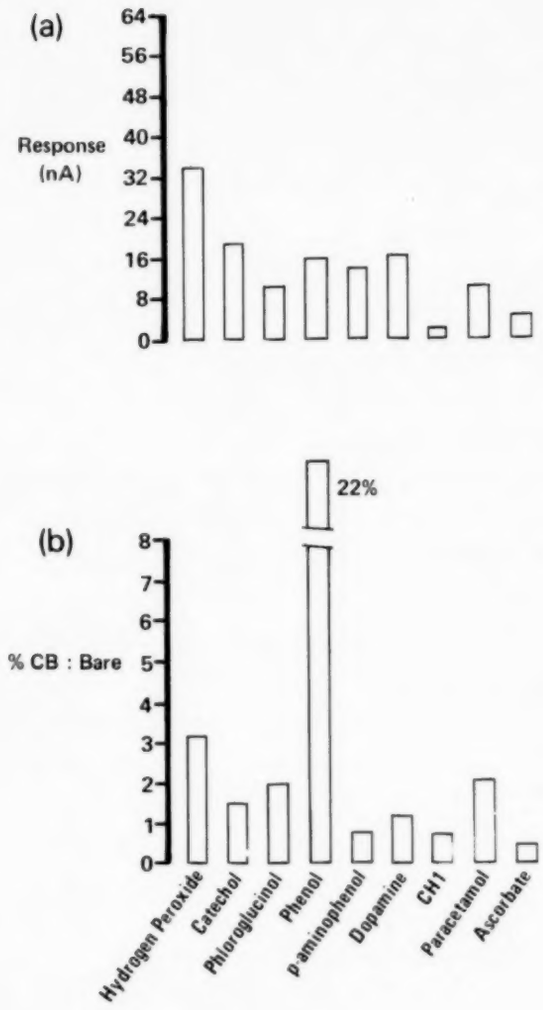

Fig. 6. Cellulose acetate butyrate membrane; (a) responses obtained to 0.04 m*M* solutions, (b) responses using CB membranes expressed as a percentage of the bare electrode responses.

to different phenols were further assessed by determining the percentage of the residual signal with the membrane in place, compared to the bare electrode (Figs. 5a and 6b). This showed relatively little effect on the phenol signal, while those of the other species were greatly reduced. For a CA membrane phloroglucinol, catechol and particularly peroxide were less reduced than the other species. The results on CB were similar, but with all responses reduced to around half the value obtained with CA. The phloroglucinol, peroxide and catechol response was closer to that of the other compounds with this membrane. Figures 7 and 8 are calibration curves demonstrating a general linear dependence on concentration. This is critical for electrode calibration; the results confirm that relative solute permeation through the membranes was concentration independent, and up to 0.1 m*M* did not show saturation behaviour.

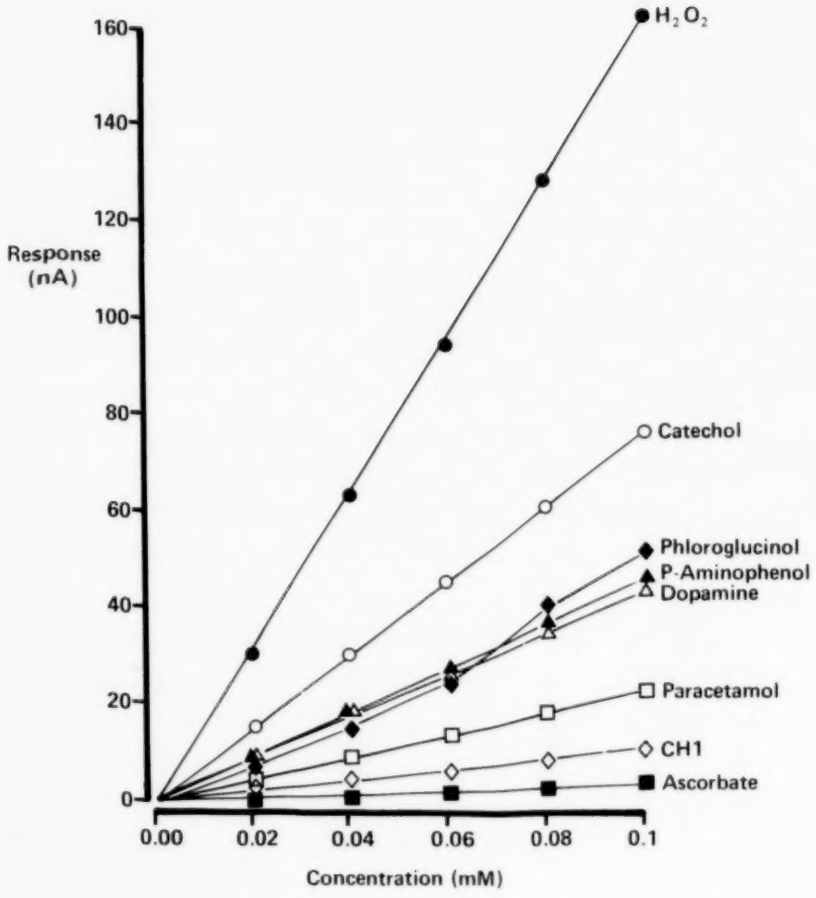

Fig. 7. Calibration curves obtained using cellulose acetate membranes.

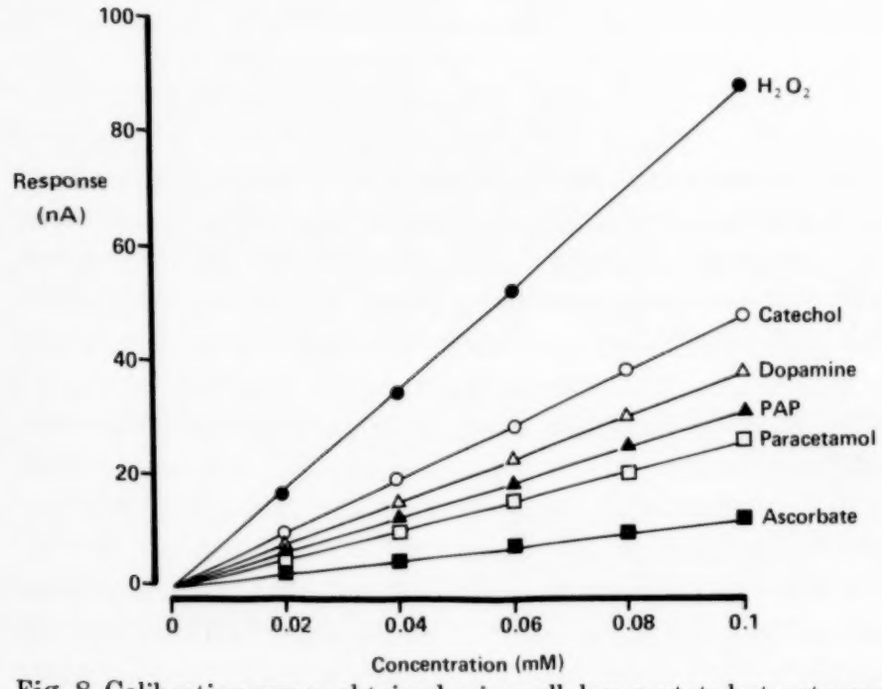

Fig. 8. Calibration curves obtained using cellulose acetate butyrate membranes.

Discussion

Initial results were consistent with the observations of Tang et al. [13], and Koile and Johnson [15], that phenolic compounds can foul the surface of the electrode during oxidation. However, by adopting a low concentration (0.04 m*M*), this problem was eliminated; no loss of signal in this study was experienced at this concentration.

The electroactivity of the phenolics shown in Fig. 3 appears to show a relationship to structure. The substituents –OH and $-NH_2$ have lone pair electrons adjacent to the ring, tending towards increased electron density in *ortho* and *para* positions, with the result that phenols with –OH or $-NH_2$ groups in *ortho* or *para* positions are more readily oxidisable. Hence the dihydroxy molecules catechol and dopamine and also the amines paracetamol and *p*-aminophenol gave larger responses than phenol. In the case of CH1, which is a substantially larger molecule, the relatively low response was due to its larger size which probably resulted in more restricted diffusion to the electrode surface. Phloroglucinol has three –OH groups, but these are in *meta* positions, which are less enhancing of functional group activity than either *ortho* or *para* configurations.

The use of any membrane restricts diffusion to an electrode; the steady state concentration gradient at the electrode surface is correspondingly reduced, giving proportionately lowered currents.

A PCM brought about a general reduction in signal for all species. Such a membrane is microporous, and the effect can be attributed simply to a reduction in area available for diffusion.

The situation with cellulose membranes is somewhat different. These membranes constitute a homogeneous phase, and any permeation involves intimate solute contact with the membrane polymer. The distinction between homogeneous dense membranes formed by a casting procedure similar to ours, and the Loeb–Sourirajan type with a dense surface layer, but porous bulk, has been demonstrated by electron microscopy [16,17]. The nature of the interaction will determine the flux through the membrane [5–7]. There are no large pores by which the diffusing molecules can avoid the influence of the membrane material. Cellulose membranes brought about a great reduction in signal size for all the species investigated. Hydrogen peroxide gave the greatest signal through both membranes and the ascorbate responses were amongst the lowest. This is ideal for use in oxidase enzyme electrodes, and the cellulose acetate membrane seems particularly suited. Reverse osmosis membranes of cellulose acetate were used by Matsuura and Sourirajan [18–20] with a range of phenolic and other organic species in aqueous solution, and a correlation of permeation with pK_a and hydrogen bonding ability was found. Nonionised molecules with a proton available for hydrogen bonding were more permeable than cations. Matsuura and Sourirajan [20] also described cellulose acetate as hav-

ing a proton acceptor character. Their results are in agreement with our data showing ascorbate to be excluded relative to the phenolics and hydrogen peroxide.

A further general effect of cellulosic membranes is to reduce the high variability of responses to various phenolics (Fig. 3), although catechol responses were the largest, and those to CH1, the smallest with both membranes. In particular, the already small phenol responses of the bare electrode were little reduced by the cellulosic membranes. For phenol, the low reactivity of the molecule itself led to relatively small signals at the bare electrode, whereas for the membrane covered electrode, the decreased flux was a less drastic limiting factor on signal size than for the more electroactive species. There was relatively little difference between the phenol derivatives. Charged dopamine, *p*-aminophenol and CH1, and uncharged catechol, phloroglucinol and paracetamol did not fall into two readily discernable groups, the variation within each class being quite considerable. Cellulose acetate reverse osmosis membranes were found by Matsuura and Sourirajan to reject certain charged species, while allowing uncharged molecules to permeate [18,19]. They found that the cellulose acetate had a certain degree of proton acceptor character, which was responsible for the rejection of anions. Since *p*-aminophenol and dopamine are cationic, their charge does not restrict membrane entry. In view of the anionic nature of CH1, the mechanism of its permeation is less clear, but is possibly explained by a partitioning effect, in which the anionic nature of the acid groups is offset by the uncharged part of the molecule. In addition to the rejection of ascorbate on the basis of charge, its non-aromatic nature may have been important in diminishing membrane partitioning.

Conclusion

The behaviour of phenolic species on a bare electrode is directly related to their structure. Microporous membranes can act as a diffusion barrier, but without any selectivity properties. The use of cellulose based membranes can impact selectivity.

For practical biosensors, it is the signal/interference ratio that is important. CA membranes are thus likely to be more appropriate than PCM or CB for selectivity, particularly for peroxide, against ascorbate (plasma [*ascorbate*] $\leqslant 0.1$ m*M*), which is the desired situation for oxidase based sensors.

Similar results apply to *p*-aminophenol, phenol and paracetamol detection in the presence of biological fluids. It should however be noted, that paracetamol remains a serious interferent in glucose determination with cellulosic membranes, and alternative polymers need to be developed for this problem. To exclude paracetamol by rendering it charged, would necessitate highly alkaline conditions sufficient to hydrolyse cellulosic membranes.

Acknowledgements

This work was supported by ICI and SERC. The authors also wish to thank Dr. G.J. Kontoghiorghes of the Royal Free Hospital, London, for donating CH1.

References

1 A.P.F. Turner, I. Karube and G.S. Wilson, Biosensors, Oxford University Press, Oxford, 1987.
2 S.J. Churchouse, C.M. Battersby, W.H. Mullen, P.M. Vadgama, Needle enzyme electrodes for biological studies, Biosensors, 2 (1986) 325.
3 K.S. Chua and I.K. Tan, Plasma glucose measurement with Yellow Springs glucose analyser, Clin. Chem., 24 (1978) 150.
4 G. Palleschi, M.A.N. Rahni, G.J. Lubrano, J.N. Ngwainbi and G.G. Guilbault, A study of interferences in glucose measurements in blood by hydrogen peroxide based glucose probes, Anal. Biochem., 159 (1986) 114.
5 H.K. Lonsdale, U. Merten and M. Tagami, Phenol transport in cellulose acetate membranes, J. Appl. Polym. Sci., 143 (1967) 1807.
6 J.E. Anderson, S.J. Hoffman and C.R. Peters, Factors influencing reverse osmosis rejection of organic solutes from aqueous solution, J. Phys. Chem., 76 (1972) 4006.
7 H.G. Burghoff, K.L. Lee and W. Pusch, Characterization of transport across cellulose acetate membranes in the presence of strong solute–membrane interactions, J. Appl. Polym. Sci., 25 (1980) 323.
8 G.J. Wang, L.D. Hutchins, S. Selim and L.B. Cumming, Long voltammetric microelectrode for *in vivo* monitoring of acetaminophen in primate species, Bioelectrochem. Bioenerg., 12 (1984) 193.
9 G.J. Wang, L.D. Hutchins, B. Selim and L.B. Cumming, Catheter microelectrode assembly for *in vivo* and *in vitro* voltammetric analysis of body fluids, Talanta, 30 (1983) 121.
10 D.J. Miner, J.R. Rice, R.M. Riggin and P.T. Kissinger, Voltammetry of acetaminophen and its metabolites, Anal. Chem., 53 (1981) 2258.
11 N.W. Tietz, A.D. Rinker and L.M. Shaw, IFCC methods for the measurement of catalytic concentration of enzymes, part 5. IFCC method for alkaline phosphatase, Clin. Chim. Acta, 135 (1983) 339F.
12 S.H. Jenkins, W.R. Heineman and H.B. Halsall, Extending the detection limit of solid-phase electrochemical enzyme immunoassay to the attomole level, Anal. Biochem., 168 (1988) 292.
13 H.T. Tang, C.E. Lunte, H.B. Halsall and W.R. Heineman, *p*-aminophenyl phosphate: an improved substrate for electrochemical immunoassay, Anal. Chim. Acta, 214 (1988) 187.
14 V.J. Razumas, J.J. Kulys and A.A. Malinauskas, Kinetic amperometric determination of hydrolase activity, Anal. Chim. Acta, 117 (1980) 387.
15 R.C. Koile and D.C. Johnson, Electrochemical removal of phenolic films from a platinum anode, Anal. Chem., 51 (1979) 741.
16 H.K. Lonsdale, U. Merten and R.L. Riley, Transport properties of cellulose acetate osmotic membranes, J. Appl. Polym. Sci., 9 (1965) 1341.
17 R. Riley, J.O. Gardner and U. Merten, Cellulose acetate membranes: electron microscopy of structure, Science, 143 (1964) 801.
18 T. Matsuura and S. Sourirajan, Physicochemical criteria for reverse osmosis separation of alcohols, phenols and monocarboxylic acids in aqueous solutions using porous cellulose acetate membranes, J. Appl. Polym. Sci., 15 (1971) 2905.

19 T. Matsuura and S. Sourirajan, Physicochemical criteria for reverse osmosis separation of aldehydes, ketones, ethers, esters and amines in aqueous solutions using porous cellulose acetate membranes, J. Appl. Polym. Sci., 16 (1972) 1663.
20 T. Matsuura and S. Sourirajan, Reverse osmosis separation of phenols in aqueous solutions using porous cellulose acetate membranes, J. Appl. Polym. Sci., 16 (1972) 2531.

Journal of Membrane Science, 57 (1991) 95–113
Elsevier Science Publishers B.V., Amsterdam

Formaldehyde production from methanol using a porous Vycor glass membrane reactor

Jin-Young Song and Sun-Tak Hwang

Department of Chemical Engineering, University of Cincinnati, Cincinnati, OH 45221 (USA)

(Received August 17, 1990; accepted in revised form October 29, 1990)

Abstract

The feasibility of using a membrane reactor to shift the equilibrium of formaldehyde production from methanol is investigated. Formaldehyde production from methanol over a silver catalyst is an endothermic, reversible, and conversion-limited dehydrogenation reaction. In the membrane reactor, the equilibrium is further shifted by removing the hydrogen through the membrane. This enables the membrane reactor to be operated economically at a lower temperature. The permeabilities are measured using a porous Vycor glass membrane. The reaction kinetics are investigated over the temperature range of 300–400°C at atmospheric pressure in a fixed-bed differential reactor over 99.998% silver needle catalyst. The membrane reactor performance is experimentally analyzed at atmospheric pressure to study the effect of changing operating variables such as temperature, space velocity, air/methanol feed ratio, and membrane surface area. A theoretical model is derived and a computer simulation is carried out based on the Runge–Kutta method to verify the above experimental data. Using an isothermal cocurrent model, a parametric study is conducted to provide basic information regarding scale-up and optimum operating conditions. The experimental study and parametric analysis of the present study point to the necessity of developing an improved permselective inorganic membrane material. Such a new membrane will make the membrane reactor method an attractive alternative in many industrial applications.

Keywords: glass membranes; membrane reactor; Vycor; formaldehyde production; porous membranes

Introduction

Equilibrium-limited conversion is common in chemical reactions. A number of industrial reactions show incomplete conversions because of equilibrium limitations. As these limitations seriously hinder or prevent commercial utilization of potentially useful reactions, there is enormous economic incentive to find technologies that can drive these reactions toward completion. A reaction is most simply driven to completion by removing the reaction products from

0376-7388/91/$03.50 © 1991 — Elsevier Science Publishers B.V.

the reaction zone. Formaldehyde production from methanol over a silver catalyst is an endothermic, reversible, and conversion-limited dehydrogenation reaction [1–3]. In conventional formaldehyde production, the hydrogen is oxidized with air to drive the equilibrium position resulting in increased production of formaldehyde. The conversion of methanol depends markedly on the temperature of the reaction [4–6]. The conversion improves as the temperature increases, with the side-reactions (formation of carbon dioxide and carbon monoxide) increasing at the same time. In the membrane reactor method, the equilibrium is shifted by removing hydrogen through the membrane. This enables the membrane reactor to be operated at a lower temperature, since the equilibrium shift induced by the removal of hydrogen through the membrane would eventually drive the reaction toward completion. At lower reaction temperatures, selectivity increases owing to the lesser extent of side-reactions and thermal decomposition of the reactant and the product. Therefore, the expected low operating temperatures in the membrane reactor might provide a higher yield.

The partial oxidation of methanol is the principal commercial route to formaldehyde production. In general, this process is carried out by passing a mixture of methanol and air over a heated stationary catalyst at approximately atmospheric pressure and scrubbing the off-gases with water to obtain aqueous formaldehyde. The formation of formaldehyde from methanol and air was first believed to be a gas phase oxidation process, as indicated by the following equation:

$$CH_3OH + 1/2\ O_2 \rightarrow CH_2O + H_2O + 38\text{kcal} \qquad (1)$$

This is still believed to be the mechanism followed when an oxide catalyst is employed. However, studies of the reaction mechanism and examination of the products obtained by the metal-catalyzed process demonstrated that under these conditions the mechanism is either dehydrogenation followed by oxidation of hydrogen to the extent that oxygen is present in the gaseous mixture as shown below, or a combination of the dehydrogenation and oxidation reactions [1,3,7].

$$CH_3OH \rightleftarrows CH_2O + H_2 - 20\ \text{kcal} \qquad (2)$$

$$H_2 + 1/2\ O_2 \rightarrow H_2O + 58\ \text{kcal} \qquad (3)$$

Oxidation reactions supply heat to make the process self-sustaining and are also believed to keep the catalyst active and displace the dehydrogenation equilibrium to the right. Newton and Dodge [2] quantitatively determined the equilibrium relation for this reaction and found that

$$K_p = P_{CH_2O} P_{H_2} / P_{CH_3OH} = \log^{-1}(-4600/T + 6.470) \qquad (4)$$

The above experimental values of the equilibrium constants are compared with their thermodynamic values [8–10] and used in the calculation of the equilibrium conversions.

In recent years, many researchers have studied the feasibility of producing hydrogen by enhancing the conversion of dehydrogenation and decomposition reactions. Dokiya et al. [11], Fukuda et al. [12], and Kameyama et al. [13] employed a porous Vycor glass membrane to selectively separate the hydrogen produced in the decomposition of hydrogen sulfide. In a separate study using the same reaction, Kameyama et al. [14] showed the possibility of using porous alumina membranes. Shindo et al. [15] conducted similar studies for the hydrogen iodide reaction using a porous Vycor glass membrane. Ito et al. [16], in a theoretical study of the decomposition of hydrogen iodide, showed that a significant equilibrium shift is possible when a porous Vycor glass membrane is used to separate the hydrogen. Shinji et al. [17] and Ito [18], using a porous Vycor glass membrane and palladium, respectively, enhanced the dehydrogenation of cyclohexane. Ito et al. [19] simulated the membrane reactor with the above reaction and showed that for given rates of permeation and reaction, there is an optimum thickness of membrane at which maximum conversion is obtained. In a separate parametric study by Mohan and Govind [20], it is known that for a membrane that is permeable to both products and reactants, the maximum equilibrium shift possible is limited by the loss of reactant from the reaction zone. Sun [21] studied the same reaction using a platinum-impregnated Vycor glass catalytic membrane reactor. A propylene disproportionation reaction has been studied by Chang [22] in a porous Vycor glass membrane reactor. This reaction is particularly interesting because it is reversible at room temperatures. Recently, Chen [23] studied the direct oxidation of ethylene to acetaldehyde in an aqueous solution of palladium (II) chloride–cupric chloride catalyst with a silicone rubber membrane reactor and a polypropylene membrane reactor.

Experiments

Permeabilities of gases and vapors were measured using a porous Vycor glass permeation cell which was the same as the membrane reactor but without the catalyst and outlet. For gases (hydrogen, oxygen, nitrogen, and carbon dioxide), the pure gas was used as feed and the volumetric flow rate of the permeate gas was measured with a bubble flow meter. To measure the permeabilities of the vapor components, pure methanol, pure water, and a 37% formaldehyde solution (mixture of formaldehyde, water, and methanol) was vaporized in a separate heating vessel and each vapor component or a mixture of vapors was collected in a condenser using liquid nitrogen and a vacuum pump.

The reaction rate constants were independently measured using a differential fixed-bed reactor. The reactor was made small enough with a 1/4 inch

(O.D.) stainless steel tube to eliminate mass and heat transfer effects. The reactor was packed with 2.1 g of heat-treated 99.998% silver needle catalyst (mesh size 16×30). The catalyst was commercially available from Metz Metallurgical Corp., South Plainfield, NJ. The system operated at low conversion at atmospheric pressure so that the composition as well as the reaction rate could be considered constant at any point in the reactor. No appreciable catalyst deactivation was observed during the measurement of reaction rate constants between 300°C and 400°C. After initial operation for 1.5 hr to ensure attainment of the steady-state condition, the actual run was conducted for 1 hr, during which the liquid and gaseous products were collected. The conversions were measured at various feed flow rates.

A schematic diagram of the apparatus for the studies of the membrane reactor is shown in Fig. 1. The membrane cell has a double-pipe configuration. The membrane is a porous Vycor glass tube (Corning Vycor brand glass, No. 7930, code 742081, O.D. 10 mm, I.D. 8 mm) with one end connected to a 10 mm ordinary Pyrex glass tube using a Vycor–Pyrex graded seal (Corning Cat. No. 6466). The other end of the inner tube is closed by glass fusion only. The porous section of the inner tube is ca. 8 to 21 cm in length. The outer shell is an ordinary Pyrex glass tube 16 mm outside diameter and 30 cm in length. One end of the inner tube is suspended in order to prevent breakage due to the uneven thermal expansions of the inner tube and the outer shell. No inlet line is installed in the permeate side chamber; thus the input molar flow to the permeate side is effectively kept at zero throughout the experiments. The tem-

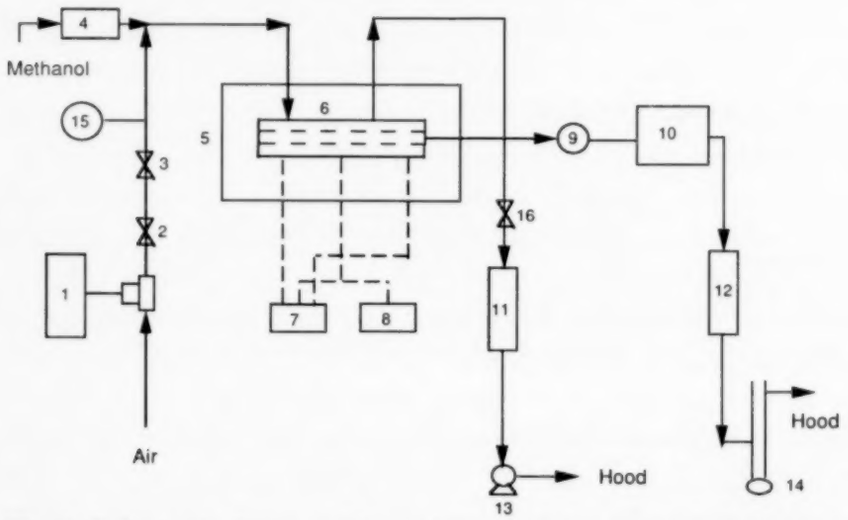

Fig. 1. Schematic diagram of membrane reactor apparatus; (1) mass flow meter, (2) regulating valve, (3) metering valve, (4) syringe pump, (5) electric furnace, (6) porous Vycor glass membrane reactor packed with silver catalyst, (7) temperature indicator, (8) temperature indicator, (9) six-port valve, (10) GowMac 550 TCD gas chromatograph, (11) condenser with liquid nitrogen, (12), ice-trap, (13) vacuum pump, (14) bubble flow meter, (15) pressure gauge, (16) plug valve.

perature is measured with three K-type thermocouples attached to the outside wall of the reactor cell, and is controlled within $\pm 1\,^{\circ}C$ of the desired value by an electric furnace and a Cole–Parmer digital temperature controller. The gas feed (dry air) is from a gas cylinder and the flow rate is measured with a mass flow meter. The liquid feed (methanol) is injected at a constant flow rate using a syringe pump, heated, and evaporated so that the vapor can be carried to the shell side (catalyst) by the feed gas. Heating tapes are used to preheat the input stream and prevent condensation in the output stream. The outlet gas flow rate in the rejected stream is measured with a bubble flow meter, and the liquid outputs in both streams are collected in two separate condenser systems. A vacuum is applied to the permeate stream and feed side pressure is maintained at atmospheric pressure. A pressure gauge is used to measure the feed side pressure. The output stream was sampled with an on-line sampling valve and analyzed for the compositions of vapors (formaldehyde, water, and methanol) using a Gow-Mac series 550 TCD gas chromatograph equipped with an Alltech $6' \times 1/8''$ SS (80/100 mesh size) Porapak T column. Helium was used as the carrier gas (55 ml/min) and column temperature was $145\,^{\circ}C$. The composition of the exhaust gas stream (hydrogen, nitrogen, and oxygen) was determined using the same G.C. with an Alltech $3' \times 1/8''$ SS (65/100 mesh size) Molecular Sieve 5A column. Argon was employed as the carrier gas (25 ml/min) and the column temperature was $25\,^{\circ}C$. Carbon dioxide content was measured using a Porapak T column at $25\,^{\circ}C$ with a helium flow rate of 65 ml/min and compositions of carbon monoxide and methane were analyzed using a Molecular Sieve 5A column at $25\,^{\circ}C$ with a helium flow rate of 35 ml/min. The feed composition of methanol and air is about 0.3 and 0.7, respectively, and the vapor compositions of the permeate and reject streams are checked every hour with the on-line sampling G.C. The liquid output flow rates are calculated based on the amounts of liquid collected after the experiment is finished. To obtain enough steady-state data, each experiment is allowed to last for 5 to 6 hr. Just before the end of each run, the compositions and flow rates of the exhaust gases are to be measured. A plug valve is installed at the end of the permeate stream to allow comparison of the membrane reactor data with those of the packed-bed reactor. After each run, the valve is closed, and the packed-bed reactor performance is checked.

Modelling

For isothermal cocurrent model, the shell side of the membrane reactor is packed with a catalyst and becomes the reaction zone. The flow rate change at any intermediate point within the cell can be determined from a differential material balance as shown in Fig. 2.

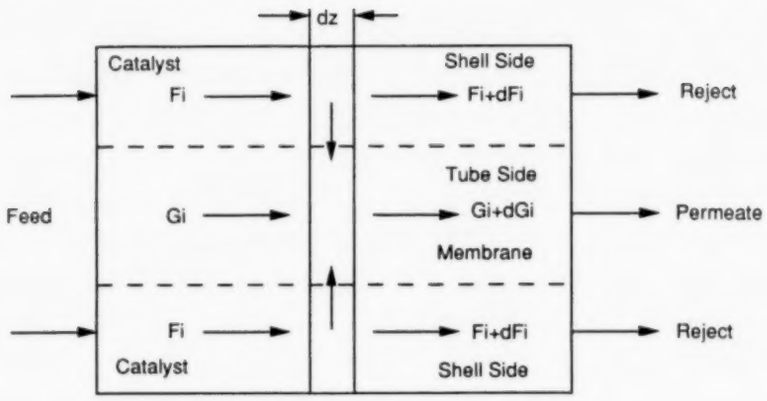

Fig. 2. Cocurrent tube-and-shell membrane reactor.

On the shell side:

$$\frac{dF_j}{dz} = r_j L_c - 2\pi Q_j P_H (x_j - P_r y_j)/\ln(R_o/R_i) \tag{5}$$

On the tube side:

$$\frac{dG_j}{dz} = 2\pi Q_j P_H (x_j - P_r y_j)/\ln(R_o/R_i) \tag{6}$$

The first term on the right-hand side of eqn. (5) represents the mass generated by reaction, where L_c can be termed "catalyst linear density" with a measured value of 1.75 g/cm inside the tube. The second term accounts for the contribution from membrane permeation. Equation (6) implies that the flow rates on the tube side change solely due to permeation through the membrane wall. With the initial composition known, a fourth-order Runge–Kutta method is then used for the integration of the simultaneous differential eqns. (5) and (6).

Results and discussion

A. Permeability measurements

The temperature dependences of the permeabilities in the porous Vycor glass membrane are plotted in Fig. 3 for the gases (hydrogen, oxygen, nitrogen, and carbon dioxide) and in Fig. 4 for the vapors (methanol, water, and formaldehyde). The ratio of permeabilities of hydrogen and nitrogen in the studied temperature range (573–723°K) is 3.72, which is very close to the theoretical value of 3.74 predicted by the Knudsen flow mechanism in which the permeability ratio of two gases is inversely proportional to the ratio of the square roots of their molecular weights. Similarly, the permeability ratio of hydrogen to oxygen is 3.92, for which the theoretical value is 4.00. The permeability of carbon dioxide also conforms to the theoretical calculation with ±3% error. However, the permeabilities of methanol, water, and formaldehyde do not fol-

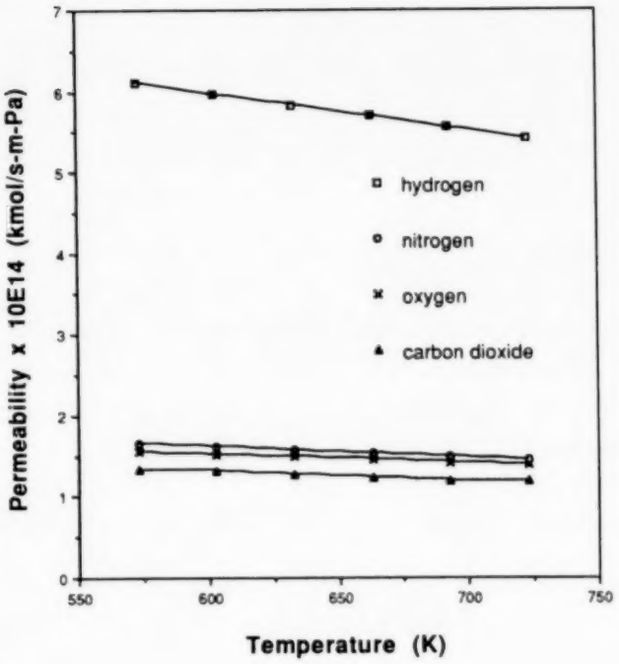

Fig. 3. Gas permeabilities measured in porous Vycor glass membrane.

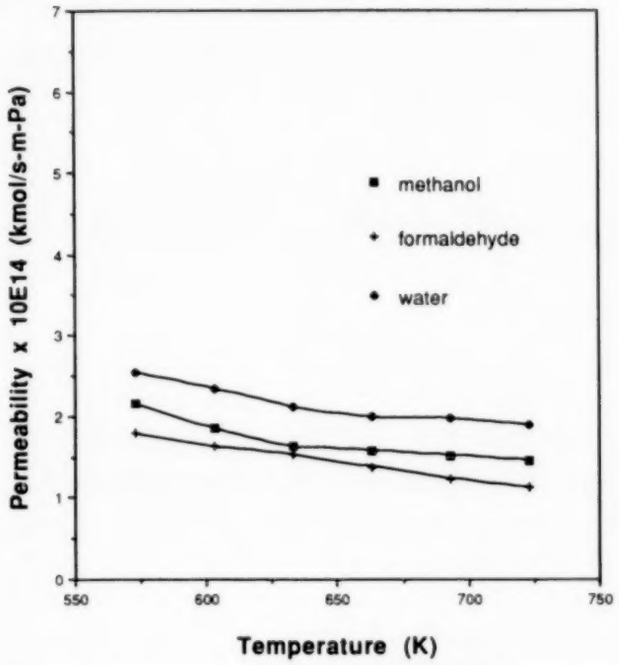

Fig. 4. Vapor permeabilities measured in porous Vycor glass membrane.

low the prediction given by the Knudsen flow mechanism. For example, the experimental data for methanol deviate up to 39% from the predicted values at 573°K. The above deviations for those three vapor components could be explained by the mechanism of surface diffusion and condensation flow in this temperature range [24–26].

B. Kinetic study

Robb and Harriot [27] proposed the following kinetic equation, which is based on competitive adsorption of methanol and hydrogen on sites formed by reversible chemisorption of oxygen on silver and reaction of adsorbed methanol with underlying oxygen atoms:

$$r_m = \{kP_m/(1+K_mP_m+K_hP_h)\}\{K_oP_{oi}^{0.5}/(1+K_oP_{oi}^{0.5})\} \quad (7)$$

This rate expression allows for a variable fractional order with respect to methanol and takes into account the effect of product inhibition and oxygen inlet partial pressure. Hydrogen is assumed to be the inhibiting product. If the oxygen adsorption constant is large, then the rate expression simplifies to

$$r_m = \{kP_m/(1+K_mP_m+K_hP_h)\} \quad (8)$$

In order to obtain the constants in the rate expression the integrated form of eqn. (8) is fitted to the kinetic data using a nonlinear regression program (Marquardt's).

$$k\tau' = (K_hP_{mi}+1)\ln(1/(1-X)) + (K_m-K_h)P_{mi}X \quad (9)$$

A separate set of experimental data was gathered to see the effect of oxygen inlet partial pressure [28]. When P_{mi} is kept constant (0.95 atm) and the conversion level is very low, eqn. (7) can be reduced to

$$r_m = A\{K_oP_{oi}^{0.5}/(1+K_oP_{oi}^{0.5})\} \quad (10)$$

where A is assumed to have a constant value. The linearized form of eqn. (10) can be rewritten as:

$$1/r_m = 1/A\{1+(1/K_o)(1/P_{oi}^{0.5})\} \quad (11)$$

From the plot of $1/r_m$ vs. $1/P_{oi}^{0.5}$, K_o is obtained. The results are summarized in Table 1. The values of k, K_m, and K_h have the same order of magnitude with the literature value [27]. For the calculation of the activation energy, log k has been plotted against $1/T$; the activation energy was found to be 10,942 kcal/kmol.

TABLE 1

Values of rate constants

Temp. (°C)	$k\times10^5$ (kmol/kg-atm-sec)	K_m (1/atm)	K_h (1/atm)	K_o (1/atm$^{0.5}$)
300	0.2868	1.3	16.5	18.75
350	0.5974	2.6	31.8	70.68
400	1.1982	3.9	48.4	160.13

C. Performance of membrane reactor

The membrane reactor performance was experimentally analyzed at atmospheric pressure to study the effect of changing operating variables. Atmospheric pressure was employed to maintain a high conversion level (fraction of reactant converted). Temperatures between 300°C and 400°C were chosen to maximize the extent of equilibrium shift and also to minimize any possible deactivation of the catalyst. Four different sizes of syringes were used to vary the space velocity (number of reactor volumes of feed treated in unit time).

3 ml syringe; 0.009 ml/min, 0.3710×10^{-8} kmol/sec
10 ml syringe; 0.025 ml/min, 1.0306×10^{-8} kmol/sec
30 ml syringe; 0.057 ml/min, 2.3498×10^{-8} kmol/sec
50 ml syringe; 0.086 ml/min, 3.5453×10^{-8} kmol/sec

Conversion improves as the temperature and the space time (time required to process one reactor volume of feed) increase. In general, beyond a certain temperature the methanol conversion rises only slightly, whereas the side reactions show a more marked increase. The maximum yield (fraction of reactant converted into desired product) lies at the temperature at which the sum of the losses through the unreacted methanol and from the formation of carbon dioxide and carbon monoxide is at a minimum. Up to 400°C carbon monoxide is not detected and the formaldehyde selectivity increases. The yield increases with the increase in space velocity. This remarkable effect of the space velocity is apparently connected with the higher gas velocity in the catalyst bed. This may be explained by the fact that the turbulence of the gas molecules increases as they flow past the silver crystals, which increases the probability of their undergoing reaction [5]. The oxygen in the incoming air is almost completely consumed and a high hydrogen content must be maintained to obtain good yields at constant feed flow rate. This means that the dehydrogenation reaction should be encouraged as much as is consistent with practical conversion. When the temperature goes up and the space velocity increases, the water content decreases. In the membrane reactor, the thermodynamic equilibrium is displaced by burning the hydrogen with air and further shifted by removing the hydrogen through the membrane. As expected, a longer space time gives a larger equilibrium shift as shown in Figs. 5, 6, and 13.

D. Effect of air/methanol feed ratio

The experiment was conducted at 60%, 70%, and 80% of air in the feed mixture to observe the influence of air/methanol feed ratio. The efficiency of the process depends to a large extent on maintaining an optimum ratio of methanol to air. Thomas [29] demonstrated that with the silver catalyst, gaseous mixtures containing 0.5–0.3 gram oxygen per gram of methanol give better yields. A methanol–air mixture of the type cited contains 30–41 vol.% of methanol. Figures 5 and 6 show experimental results using a 12 cm long, 10 mm O.D. porous Vycor glass membrane reactor at a temperature of 350°C.

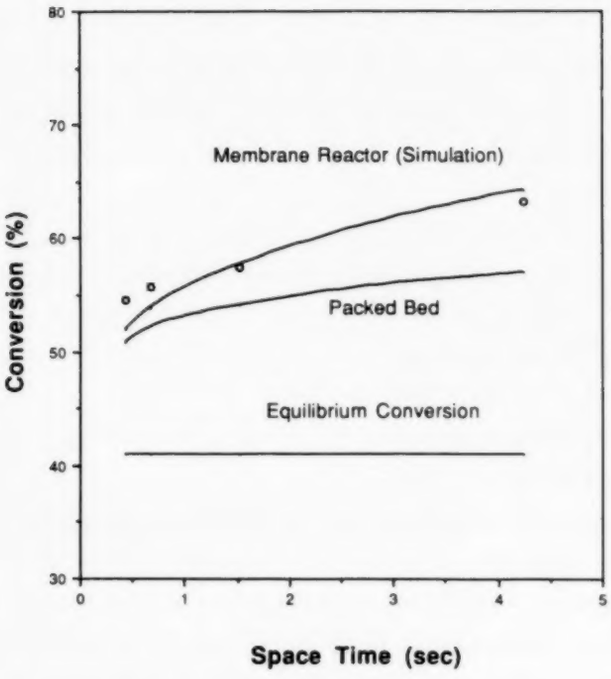

Fig. 5. Effect of space time on conversion at 60% air (350°C, 10 mm O.D., length = 12 cm porous Vycor glass membrane).

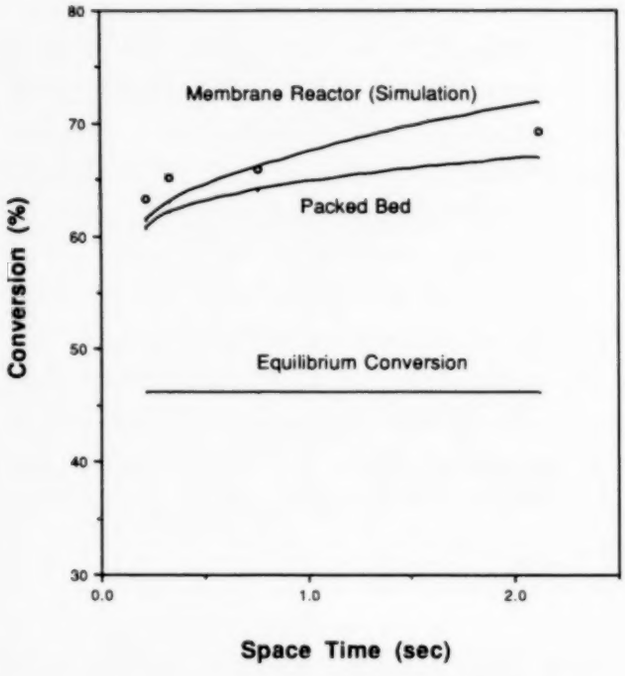

Fig. 6. Effect of space time on conversion at 80% air (350°C, 10 mm O.D., length = 12 cm porous Vycor glass membrane).

Comparison of these data with the computer simulation and the packed-bed reactor data is also included. At a higher percentage of air, the conversion and the selectivity increased while the equilibrium shift decreased. In other words, with increasing concentrations of methanol the manufacturing yields gradu-

ally fell off, but the net yield increased. Although the experimental data are scattered around the prediction given by the theoretical model depending on the space time, the isothermal cocurrent model simulates quite well the general trend of the actual membrane reactor system.

E. Effect of membrane surface area

To determine the effect of permeation area, four different lengths of membrane reactors were made with 10 mm O.D. porous Vycor glass membrane.
10 mm O.D., 8 cm long porous Vycor glass; 22.3 cm^2
10 mm O.D., 12 cm long porous Vycor glass; 33.4 cm^2
10 mm O.D., 17 cm long porous Vycor glass; 47.3 cm^2
10 mm O.D., 21 cm long porous Vycor glass; 58.4 cm^2
Figures 7 and 8 illustrate experimental results using two different sizes of syringes at a temperature of 350°C. Higher conversions were obtained using longer membrane reactors. In Table 2, at a 70:30 air/methanol feed ratio 33.7%, 25.9%, and 16.0% of the maximum possible equilibrium shift was achieved at 300°C, 350°C, and 400°C, respectively by the combination of the longest space time (6.0 sec) and the largest permeation area (58.4 cm^2). In the above mentioned figures, the enhanced equilibrium shift by the membrane was 3.1%, 4.0%, and 5.7% at 300°C, 350°C, and 400°C, respectively. It is apparent that the effect of the membrane reactor becomes greater at higher reaction temperatures as more hydrogen can permeate through the membrane because of its higher partial pressure.

In this research, the catalyst linear density was fixed at 1.75 g/cm for all

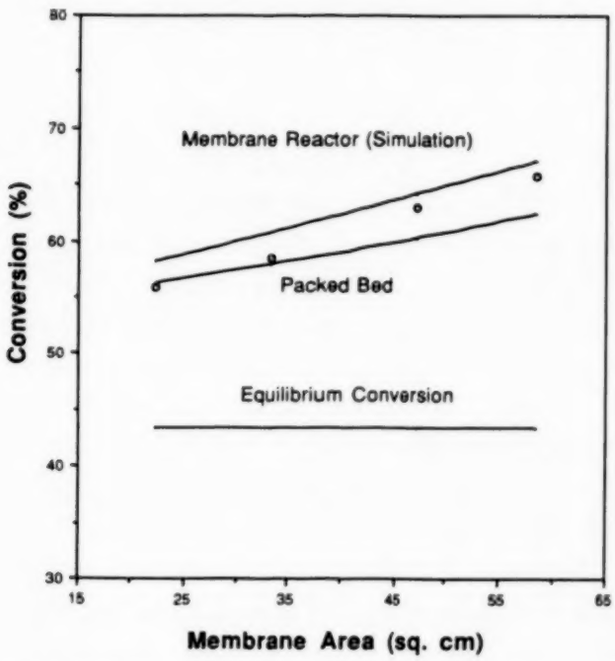

Fig. 7. Effect of membrane surface area on conversion (350°C, 10 ml syringe, catalyst density = 0.63 g/cm^2, 70% air).

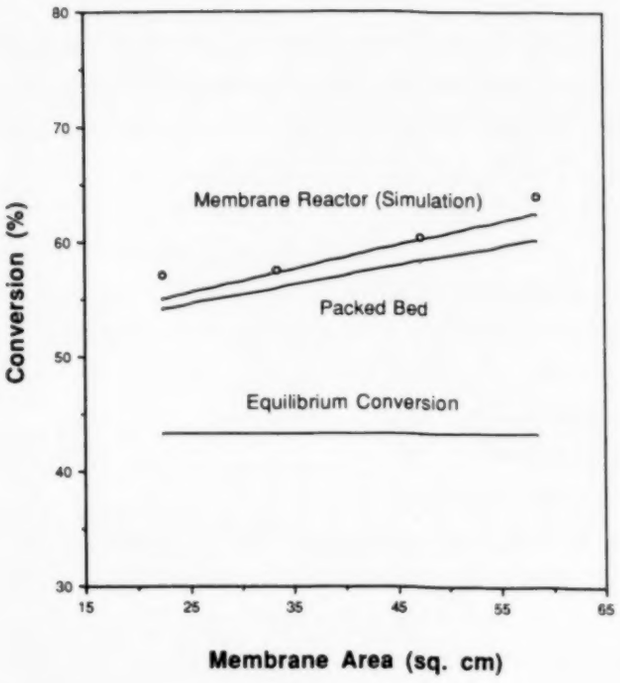

Fig. 8. Effect of membrane surface area on conversion (350°C, 30 ml syringe, catalyst density = 0.63 g/cm^2, 70% air).

TABLE 2

Equilibrium shift by membrane reactor (21 cm Vycor, 70% air, 3 ml syringe)

Temp. (°C)	X_{eq}	X_{pb}	X_{mr}
300	23.1%	53.7%	56.8%
350	43.3%	65.2%	69.2%
400	65.8%	76.1%	81.8%

membrane reactors. Due to this fact, the longer membrane reactor produced an adverse effect on the selectivity owing to the longer space time. For maximum yields under this condition, a membrane length (or area) should be decided through the compromise between conversion and selectivity. Similar to the previous section, at longer space time (3 and 10 ml syringe) the experimental data were slightly lower than the model values. On the other hand, the shorter ones (30 and 50 ml syringe) had slightly higher conversions. This phenomenon implies that even if the outside wall temperature was controlled isothermally, the actual catalyst temperature at the larger space velocity (or shorter space time) might be somewhat higher than that of the smaller space velocity (or longer space time) due to the difference in the amount of air oxidation. For better control of the catalyst temperature, several researchers recommended dilution of the feed mixture with water vapor [5,29–32]. The effect of the water can be explained as follows: some of the reaction heat from the

adiabatic process is absorbed by the water; in this way the oxygen fraction of the reaction mixture may be increased by passing in more air without the catalyst temperature rising. The dehydrogenation equilibrium is thus shifted in the direction of the formation of formaldehyde as a result of greater quantities of hydrogen being burnt. The yield rises to an optimum value as the proportion of water rises. If more water is added the yield drops in spite of increased conversion because more carbon dioxide is formed.

F. Effect of membrane permeability

The effect of membrane permeability was studied using the isothermal co-current model. Based on the experimental data of 12 cm long, 10 mm O.D. porous Vycor glass membrane reactor (catalyst linear density 1.75 g/cm), the permeation flux was increased up to 10 times. Results are shown in Fig. 9 for 10 ml syringe and in Fig. 10 for 30 ml syringe at a temperature of 350°C. As can be seen in the previous section, increasing the membrane permeability (or the permeation flux) has the same effect as that shown by giving more membrane surface area. It is also observed that at higher temperatures the membrane reactor plays a more important role because of the hydrogen partial pressure. If the permeation flux is to be increased infinitely, the conversion reaches a maximum value and then drops gradually to zero since methanol partial pressure almost approaches zero value at some point due to the reaction and the permeation. In other words, the total conversion is attained by the competition of the hydrogen removal and the methanol depletion. Such information should

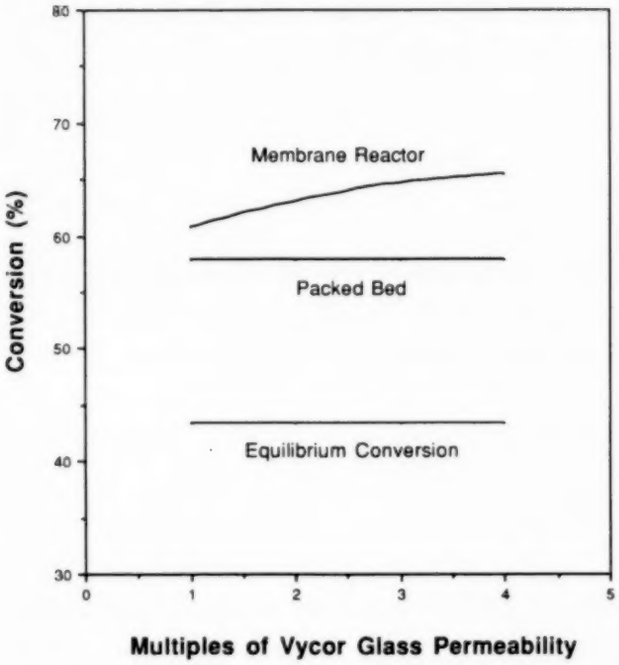

Fig. 9. Effect of membrane permeability on conversion (350°C, 10 ml syringe, membrane area = 33.4 cm^2, 70% air).

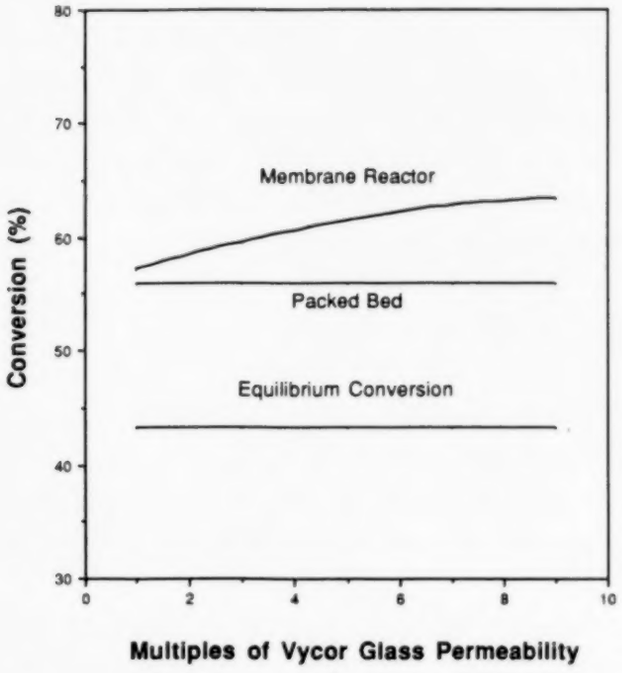

Fig. 10. Effect of membrane permeability on conversion (350°C, 30 ml syringe, membrane area = 33.4 cm^2, 70% air).

be taken into account in determining the permeation flux for a large scale operation.

G. Effect of membrane selectivity

The effect of membrane selectivity (separation factor or index of the relative separability) was examined using the theoretical model. According to the experimental data of 12 cm long, 10 mm O.D. porous Vycor glass membrane reactor (catalyst linear density 1.75 g/cm), the ideal separation factor, α, for this system is defined as

$$\alpha = Q_h/Q_m \tag{12}$$

where Q_h is the permeability of hydrogen through Vycor glass and Q_m is the permeability of methanol through Vycor glass. Results are shown in Fig. 11 for a 3 ml syringe and in Fig. 12 for a 10 ml syringe at a temperature of 350°C. Referring to the results in the previous section, it is found that increasing the membrane selectivity (or the ideal separation factor) gives the same effect as having more permeation flux.

H. Recycle membrane reactor

In a recycle membrane reactor a portion of the product is returned to the feed. As mentioned earlier, methanol is also permeable to the porous Vycor glass membrane and this will diminish the driving force for the forward reaction. If the permeated methanol is recycled, the above limitation of the mem-

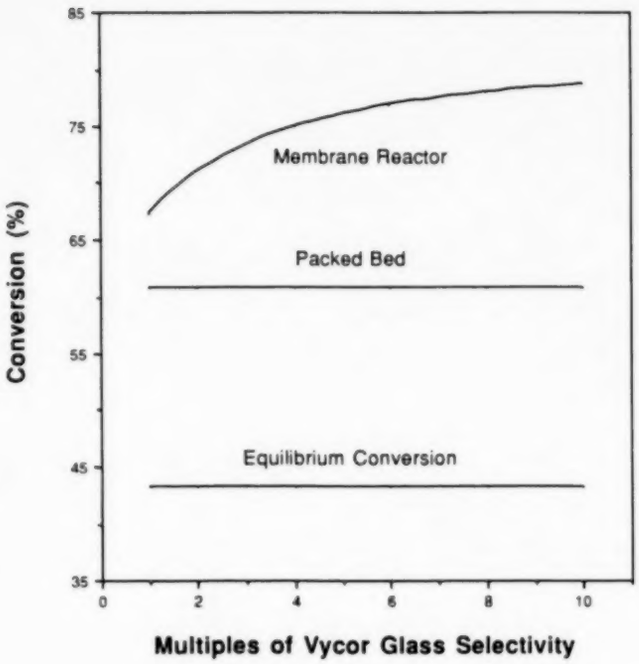

Fig. 11. Effect of membrane selectivity on conversion (350 °C, 3 ml syringe, membrane area = 33.4 cm^2, 70% air).

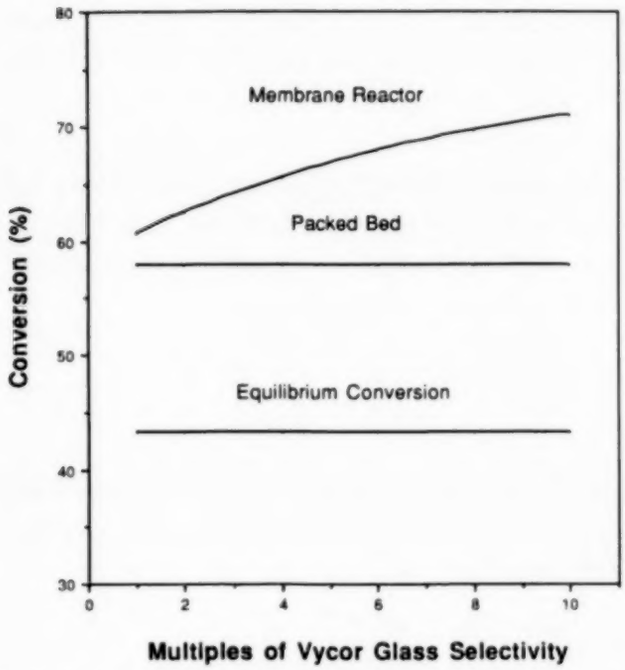

Fig. 12. Effect of membrane selectivity on conversion (350 °C, 10 ml syringe, membrane area = 33.4 cm^2, 70% air).

brane reactor system can be overcome. Figure 13 shows the comparison among the recycle membrane reactor (RMR), membrane reactor (MR) and packed-bed reactor (PR), at 350 °C. All the values are taken from computer simulations using a 12 cm long, 10 mm O.D. porous Vycor glass membrane reactor

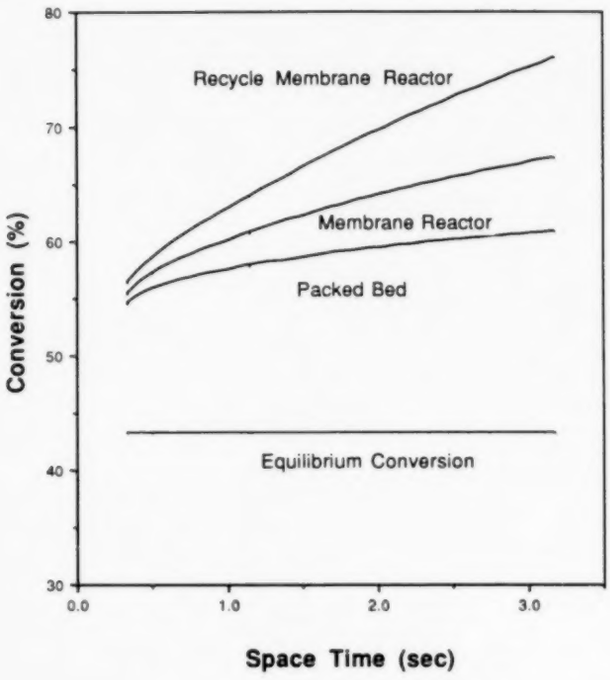

Fig. 13. Recycle membrane reactor (350°C, 10 mm O.D., length = 12 cm Vycor glass membrane, 70% air).

(catalyst linear density 1.75 g/cm). With the existing apparatus and operating procedures, it is difficult to recycle the permeated methanol, since the quantity is small and collected in a frozen state under vacuum and liquid nitrogen conditions. However, those difficulties may be resolved in a large scale process because commercial formaldehyde is obtained as aqueous formaldehyde by scrubbing the off-gas with water. As long as the recycle membrane reactor can be implemented into the real system, it will make up for the shortcoming of the membrane reactor method by a slight process modification.

Conclusions

The membrane reactor is experimentally analyzed and found to outperform the conventional process (the packed-bed reactor). The current study has not only demonstrated the enhanced equilibrium shift by removing the hydrogen through the membrane, but also introduced a new process using a membrane reactor as an economical alternative. Higher conversions are obtained using a longer space time and a larger membrane area. The effect of the membrane reactor becomes greater at higher reaction temperatures since more hydrogen can permeate through the membrane because of its higher partial pressure. The isothermal cocurrent model has been proposed and a computer simulation is made using the Runge–Kutta method to verify the experimental data. Although the experimental data are scattered around the prediction given by the theoretical model due to the heat effect, this model simulates quite well the

general trend of the actual membrane reactor system. The experimental results and parametric analysis of the present study point to the necessity of developing an improved permselective inorganic membrane material, which should also be heat-resistant, inexpensive, and easy to handle. Such a new membrane will make the membrane reactor method an attractive alternative in many industrial application.

List of symbols

G	tube-side molar flow rate (kmol/sec)
F	shell-side molar flow rate (kmol/sec)
k	forward reaction rate constant (kmol/kg-sec-atm)
K	adsorption equilibrium constant (1/atm)
K_p	equilibrium constant (atm)
L_c	catalyst linear density (kg catalyst/m reactor)
P_H	high pressure (Pa)
P_L	low pressure (Pa)
P_r	pressure ratio ($=P_L/P_H$)
Q	permeability (kmol/sec-m-Pa)
R_i	inside radius of membrane (m)
R_o	outside radius of membrane (m)
r	reaction rate expression (kmol/kg cat-sec)
T	temperature (°C or °K)
X	conversion
x	shell-side molar fraction
y	tube-side molar fraction
z	axial position (m)
α	ideal separation factor ($=Q_h/Q_m$)
τ'	weight time (kg-atm-sec/kmol)

Subscripts

eq	equilibrium state
h	hydrogen
i	inlet condition
j	component
m	methanol
mr	membrane reactor
o	oxygen
pb	packed-bed reactor

References

1 J.F. Walker, Formaldehyde, Krieger, New York, NY, 1975.
2 R.H. Newton and B.F. Dodge, The equilibrium between carbon monoxide, hydrogen, formaldehyde, and methanol, J. Am. Chem. Soc., 55 (1933) 4747.
3 P. Sabatier and A. Mailhe, Actions des oxydes métalliques sur les alcools primaires, Ann. Chim. Phys., 8(20) (1910) 344.
4 J. Kollar, Ethylene glycol from syngas, Chemtech, August (1984) 504.
5 U. Gerloff, Compare BASF formaldehyde process, Hydrocarbon Process., 46 (1967) 170.
6 I. Calrati, L. Di Fiore, P. Forzatti, I. Pasquon and F. Trifito, Oxidation of methanol in a fluidized bed, Ind. Eng. Chem., Proc. Des. Dev., 19 (1980) 561.
7 M. Klar and C. Schulze, German Patent 106, 495 (1898).
8 O.A. Hougen and K.M. Watson, Chemical Process Principles. Part 2. Thermodynamics, John Wiley and Sons, New York, NY, 1947.
9 G.N. Lewis and M. Randall, Thermodynamics, 2nd edn., McGraw-Hill, New York, NY, 1961.
10 R.C. Reid, J.M. Prausnitz and T.K. Sherwood, The Properties of Gases and Liquids, 3rd edn., McGraw-Hill, New York, NY, 1977.
11 M. Dokiya, T. Kameyama and K. Fukuda, The application of the effusion on the thermochemically limited reactions, Denki Kagaku, 45 (1977) 701.
12 K. Fukuda, M. Dokiya, T. Kameyama and Y. Kotera, Catalytic decomposition of hydrogen sulfide, Ind. Eng. Chem., Fundam., 17 (1978) 243.
13 T. Kameyama, M. Dokiya, M. Fujishige and H. Yokogawa, Possibility for effective production of hydrogen from hydrogen sulfide by means of a porous vycor glass membrane, Ind. Eng. Chem., Fundam., 20 (1981) 97.
14 T. Kameyama, M. Dokiya, M. Fujishige, H. Yokogawa and K. Fukuda, Production of hydrogen from hydrogen sulfide by means of selective diffusion membranes, Int. J. Hydrogen Energy, 8 (1983) 5.
15 Y. Shindo, K. Haraya, K. Obata, T. Hakuta and H. Yoshitome, Gas diffusion in microporous media in Knudsen's regime, Preprints for 15th Autumn Meeting Soc. Chem. Eng., Kanazawa, Japan (1981), as referred to by Ito et al. (1984, 1985).
16 N. Ito, Y. Shindo, T. Hakuta and Y. Yoshitome, Enhanced catalytic decomposition of HI by using a microporous membrane, Int. J. Hydrogen Energy, 9 (1984) 835.
17 O. Shinji, M. Misono and Y. Yoneda, The dehydrogenation of cyclohexane by the use of a porous-glass reactor, Bull. Chem. Soc. Jpn., 55 (1982) 2760.
18 N. Ito, A membrane reactor using palladium, AIChE J., 33 (1987) 1576.
19 N. Ito, Y. Shindo, K. Haraya, K. Obata, T. Hakuta and H. Yositome, Simulation of a reaction accompanied by separation, Int. Chem. Eng., 25 (1985) 138.
20 K. Mohan and R. Govind, Analysis of a cocurrent membrane reactor, AIChE J., 32 (1986) 2083.
21 Y.M. Sun, Catalytic membrane reactor, Ph.D. Thesis, Univ. of Cincinnati, Cincinnati, OH, 1987.
22 M.Y. Chang, The continuous membrane reactor, Ph.D. Thesis, Univ. of Cincinnati, Cincinnati, OH, 1988.
23 S. Chen, Study of hollow-fiber membrane reactors in homogeneous catalysis involving gas-liquid reactions, Ph.D. Thesis, Univ. of Cincinnati, Cincinnati, OH, 1989.
24 R.M. Barrer and J.A. Barrie, Sorption and surface diffusion in porous glass, Proc. Roy. Soc., A213 (1952) 250.
25 S.-T. Hwang and K. Kammermeyer, Surface diffusion in microporous media, Can. J. Chem. Eng., 44 (1966) 82.
26 K.H. Lee, The transport of condensable vapors through microporous vycor glass membrane, Ph.D. Thesis, Univ. of Iowa, IA, 1984.

27 D.A. Robb and P. Harriott, The kinetics of methanol oxidation on a supported silver catalyst, J. Catal., 35 (1974) 176.
28 S.K. Bhattacharyya, N.K. Nag and N.D. Ganguly, Kinetics of vapor-phase oxidation of methanol on reduced silver catalyst, J. Catal., 23 (1971) 158.
29 M.D. Thomas, Preparation of formaldehyde, J. Am. Chem. Soc., 42 (1920) 867.
30 M.A. Trillat, Appareil d'étude pour les actions de contact (cas de la spirale de platine), Bull. Soc. Chim., III, 27 (1902) 797; Étude de l'oxydation catalytique des alcools (cas de la spirale de platine), 29 (1903) 35.
31 H.B. Uhl and I.H. Cooper, U.S. Patent 2,465,498 (1949).
32 A. Terlecki-Baricevic, B. Grbic and D. Jovanovic, Methanol dehydrogenation and oxidation to formaldehyde on silver crystals of various granulations, Bull. Soc. Chim. Beograd, 49 (1984) 469.

Meetings Calendar

1991

April 7–11
Houston, TX, USA
AIChE's Spring 1991 National Meeting and Petrochemical and Refining Exposition
(For information see Vol. 56, No. 1, p. 122)

April 15–20
Malta
5th World Congress/12th European Symposium on Desalination and Water Re-use
(For details see Vol. 49, No. 1, p. 118)

April 21–26
Minneapolis, MN, USA
201st ACS National Meeting
(For information see Vol. 56, No. 1, p. 122)

April 22–24
Austin, TX, USA
Gas Separation International Conference
(For details see Vol. 49, No. 2, p. 237)

May 29–31
San Diego, CA, USA
Fourth National Meeting of the North American Membrane Society
(For details see Vol. 56, No. 2, p. 235)

June 9–13
Jerusalem, Israel
International Conference on Biomedical Polymers—From Molecular Design to Clinical Applications
(For details see Vol. 56, No. 1, p. 122)

June 25–28
Enschede, The Netherlands
Progress in Membrane Science and Technology
(For details see Vol. 48, Nos. 2+3, p. 350)

July 1–4
Montpellier, France
Second International Conference on Inorganic Membranes, ICIM(2)-91
(For details see Vol. 52, No. 1, p. 118)

July 7–12
Compiègne, France
7th International Conference on Surface and Colloid Science
(For details see Vol. 53, No. 3, p. 305)

July 8–11
Amsterdam, The Netherlands
Controlled Release Society 18th International Symposium on Controlled Release of Bioactive Materials
(For details see Vol. 56, No. 1, p. 122)

July 11–12
Amsterdam, The Netherlands
Controlled Release Society Workshop: Regulatory Affairs Concerning Controlled Release Systems
(For details see Vol. 56, No. 1, p. 122)

July 28–August 2
Plymouth, NH, USA
Gordon Research Conference on Reverse Osmosis, Ultrafiltration and Gas Separation
(For information see Vol. 56, No. 3, p. 359)

August
Boston, MA, USA
AIChE's Summer 1991 Annual Meeting
(For information see Vol. 56, No. 1, p. 122)

August 19–22
Montreal, Que., Canada
VIII World Congress of the International Society for Artificial Organs
IV International Symposium on Blood Substitutes
(For details see Vol. 50, No. 3, p. 330)

August 25–30
New York, NY, USA
202nd ACS National Meeting
(For information see Vol. 56, No. 1, p. 122)

September 17–23
Zvenigorod (Moscow), USSR
9th European Summer School in Membrane Science and Technology, "Fundamentals in Membrane Science and Separation Processes"
(For details see Vol. 54, No. 3, p. 355)

October 21–23
Newton (Boston), MA, USA
Membrane Technology Planning Conference and First High Technology Separation Symposium
(For details see Vol. 56, No. 2, p. 235)

October 20–25
Hawaii, USA
IVth International Conference on "Separation Technology"
(For details see Vol. 51, No. 3, p. 359)

November 17–22
Los Angeles, CA, USA
AIChE's Fall 1991 Annual Meeting
(For information see Vol. 56, No. 1, p. 122)

November 29–30
Bhavnagar, India
National Conference on Synthetic Membranes and their Applications
(For details see Vol. 53, No. 3, p. 305)

December 16–20 Maui, Hawaii, USA
First US-Japanese Symposium on Drug Delivery
(For details see Vol. 56, No. 1, p. 122)

December 19–21 Calcutta, India
International Seminar on Downstream Processing in Biotechnology
(For details see Vol. 56, No. 1, p. 123)

Pervaporation Membrane Separation Processes

edited by **R.Y.M. Huang,** *Department of Chemical Engineering, University of Waterloo, Waterloo, Ont., Canada*

(Membrane Science and Technology, 1)

Covered here are the various aspects of pervaporation: theory and principles, separation characteristics, sorption and diffusion, thermodynamics and evaluation of polymer materials for membranes, as well as plant design and optimization. The book also includes interesting new material on the synthesis of novel copolymer membranes with very high separation potential and future implications for the pervaporation separation of biological sytstems and its applications in the exciting field of biochemical engineering. Special attention is paid to industrial research and applications of pervaporation membranes and plant operations involving new pervaporation processes.

The book also includes a chapter dealing with the development of vapour permeation for industrial applications, which is a new variant of liquid pervaporation processes.

Contents:

Chapter 1. Introduction to Pervaporation *(J. Néel)*. **Chapter 2.** Separation and Characteristics of Pervaporation Membrane Separation Processes *(R.Y.M. Huang, J.W. Rhim)*. **Chapter 3.** Engineering Aspects of Pervaporation: Calculation of Transport Resistances, Module Optimization and Plant Design *(R. Rautenbach, C. Herion and U. Meyer-Blumenroth)*. **Chapter 4.** Thermodynamic Principles of Pervaporation *(M.H.V. Mulder)* . **Chapter 5.** Estimation and Evaluation of Polymeric Materials for Peraporation Membranes *(G.H.Koops and C.A.* Smolders). **Chapter 6.** Sorption and Diffusion in Pervaporation Membranes *(A. Heintz, H. Funke and R.N. Lichtenhaler)*. **Chapter 7.** Synthesis of Novel Copolymer Membranes for Pervaporation *(T. Shimidzu and M. Yoshikawa)*. **Chapter 8.** Pervaporation in Biotechnology *(H. Strathmann and W. Gudernatsch)*. **Chapter 9.** Recent Progress in Pervaporation Membranes for Water/Ethanol Separation *(Y. Maeda and M. Kai)*. **Chapter 10.** Selective Pervaporation of Organics from Water *(K.W. Bödekker and G. Bengtson)*. **Chapter 11.** Plasma Grafted Pervaporation Membranes (*T. Hirotsu)*. **Chapter 12.** Pervaporation Membrane Plant. Industrial Experience and Plant Design in Japan *(T. Asada)*. **Chapter 13.** Development of Vapour Permeation for Industrial Application *(U.H.F. Sander)*. Subject Index.

1991 540 pages

Price: US$ 168.50 / Dfl. 295.00

ISBN 0-444-88227-8

Elsevier Science Publishers

P.O. Box 211, 1000 AE Amsterdam, The Netherlands
P.O. Box 882, Madison Square Station, New York, NY 10159, USA

Absorbent Polymer Technology

edited by **L. Brannon-Peppas,** *Eli Lilly Research Laboratories, Greenfield, IN, USA and* **R.S. Harland,** *KV Pharmaceutical Company, Saint Louis, MO, USA*

(Studies in Polymer Science, 8)

In recent years, there has been a veritable explosion of research and development in consumer-oriented fields that utilize polymeric materials which absorb large amounts of water. These fields encompass the preparation, characterization and commercialization of separation systems, pharmaceutical and personal care products such as infant diapers, feminine products, incontinence products and many other related areas. The polymeric materials utilized in these applications are known as absorbent or superabsorbent materials because of their ability to swell rapidly and to retain large volumes of water, urine and other biological fluids.

The aim of this book is to introduce the fundamentals of polymer structure and swelling as related to polymers used for these superabsorbent materials. In the field of absorbence, particular attention is given to crosslinked structures which swell to more than fifty times their initial weight in water or electrolytic solutions. The book also provides descriptions of novel applications of superabsorbent materials as well as a detailed analysis of water transport in crosslinked polymers. *Absorbent Polymer Technology* should be of interest to chemists, polymer scientists, chemical engineers, and industrial scientists working with swellable systems in personal care, pharmaceutical, agricultural, waste treatment and separation industries.

Contents. **Section I. Fundamentals of Absorbent Materials: Preparation, Structure, and Characterization.** 1. The evolution of absorbent materials *(J.R. Gross)*. 2. Preparation and structure of polyacrylates (F.L. Buchholz). 3. Preparation and characterization of crosslinked hydrophilic networks *(L. Brannon-Peppas)*. 4. The equilibrium swelling behavior of porous and non-porous hydrogels *(L. Brannon-Peppas and N.A. Peppas)*. 5. Characterization of ionic water-absorbent polymers: Determination of ionic content and effective crosslink density *(D.C. Harsh and S.H. Gehrke)*. 6. Swelling behavior of water-soluble cellulose derivatives *(E. Doelker)*. 7. Structure and swelling behavior of poly(ethylene glycol)/poly(methacrylic acid) complexes *(J. Klier and N.A. Peppas)*. 8. Transport in porous polymers (W.M. Saltzman). **Section II. Recent Experimental Studies.** 9. Molecular thermodynamics of aqueous polymers and gels *(H.H. Hooper, H.W. Blanch, and J.M. Prausnitz)*. 10. Dynamic and equilibrium swelling characteristics of hydrophilic copolymers with carboxylic functional groups *(A.R. Khare and N.A. Peppas)*. 11. Kinetics of swelling of absorbent polymers *(F.L. Buchholz)*. 12. Effect of superabsorber-pulp interactions on the performance of absorbent structures *(D.L. Visioli and K.R. Williams)*. 13. A microstructural analysis of polymer networks formed from graft copolymers in mixed aqueous solvents *(C.G. Varelas and C.A. Steiner)*. Subject Index.

1990 x + 278 pages
Price: US$ 120.00 / Dfl. 210.00
ISBN 0-444-88654-0

Elsevier Science Publishers
P.O. Box 211, 1000 AE Amsterdam, The Netherlands
P.O. Box 882, Madison Square Station, New York, NY 10159, USA

Future Opportunities in Catalytic and Separation Technology

edited by **M. Misono,** *Department of Synthetic Chemistry, Faculty of Engineering, The University of Tokyo, Tokyo, Japan,* **Y. Moro-oka,** *Research Laboratory for Resources Utilization, Tokyo Institute of Technology, Yokohama, Japan, and* **S. Kimura,** *Department of Chemical Engineering, Faculty of Engineering, The University of Tokyo, Tokyo, Japan*

(Studies in Surface Science and Catalysis, 54)

The production of useful materials and the removal of polluting substances are fundamental to chemical technology, and in this respect catalytic and separation processes play essential roles. In order to cope with increasing demands to find solutions for the shortage of natural resources and global environmental pollution, rapid and significant progress in the technology is required.

This book results from the successful seminar on Selective Reactions and Separation, held at Oiso, Japan, in February 1988. The seminar was organised by ASPRONC (the Association for the Progress of New Chemistry) as the fourth in a series of seminars on Frontier Technology. ASPRONC was inaugurated in 1986 and its membership comprises major companies in the chemical industry and various other sectors interested in chemistry. The aim of this seminar was to explore the frontiers of catalytic and separation technology and to discuss the requirements for its future development. The many interesting lectures and active discussions which resulted stimulated the editors to prepare this book. Each lecturer has written a chapter which represents a significantly revised and extended version of his original lecture.

The book will appeal to many readers and will undoubtedly help to make a positive contribution to the future development of chemical technology.

Contents: **I. Present and Future of Catalytic and Separation Technology.** Future opportunities in industrial catalysis *(J.F. Roth).* Design of practical solid catalysts at atomic/molecular levels *(M. Misono).* Characteristic dynamic behaviour of adsorbed species under reaction conditions *(K. Tamaru).* Recent advances in catalytic oxidations relevant to oxygenases *(N. Kitajima, Y. Moro-oka).* New trends in membrane separation technologies *(S. Kimura).* **II. New Aspects of Heterogeneous Catalysis.** Novel catalytic functions of zeolites in liquid-phase organic reactions *(Y. Izumi, M. Onaka).* Activation and functionalization of methane *(K. Otsuka).* Catalytic decomposition of nitrogen monoxide *(M. Iwamoto).* Effect of additives on the selectivity of metal catalysts *(K. Kunimori et al.).* Selectivity changes by alloying. Principles and application *(A.J. den Hartog, V. Ponec).* Recent advances and future developments in zeolite catalysis *(Y. Ono).* **III. Catalysis Combined with Laser, Electrochemical and Membrane Technology.** Application of lasers to control of chemical reactions - partial oxidation of alkanes in the gas phase *(H. Tominaga, Y. Oshima).* Electrocatalytic reactions with electron carriers *(S. Torii).* Recent development in membrane reactors *(D.R. Seok, S.T. Hwang).* Simultaneous operation of reaction and separation by a membrane reactor *(N. Itoh).* Functional membranes for separations based on reactions *(T. Uragami).* **IV. Asymmetric Synthesis and Separation.** New carbonylations by means of transition metal catalysts *(I. Ojima).* New chiral Rh(I) and Ru(II) complexes: highly efficient catalysts for homogeneous asymmetric hydrogenation *(H. Takaya et al.).* Isolation of isomers and optical resolution by a host-guest complexation method *(F. Toda).* Recent progress and industrial application of optical resolution by high-performance liquid chromatography *(K. Saigo).* **Author Index. Subject Index.**

1990 viii + 382 pages ISBN 0-444-88592-7
US$ 179.50 / Dfl. 350.00

ELSEVIER

P.O. Box 211, 1000 AE Amsterdam, The Netherlands
P.O. Box 882, Madison Square Station, New York, NY 10159, USA

Thermodynamics of Polymer Solutions

Phase Equilibria and Critical Phenomena

by **K. Kamide,** *Asahi Chemical Industry Co., Ltd., Osaka, Japan*

(Polymer Science Library, 9)

This is the first self-contained book on the thermodynamics and critical phenomena of polymer solutions, ranging from the rather elementary level to the advanced and up-to-date level. The books covers the rigorous theories of phase equilibrium, computer experiments based on these theories, as well as actual experiments, molecular fractionation and application to membrane and fiber production. An extensive list of references and literature data on the thermodynamic interaction ξ-parameter, critical point, fractionation and polymer blends is also provided. This book should prove invaluable for courses on polymer science, thermodynamics and polymer solutions at graduate, university and polytechnic level.

Contents. **1. Introduction. 2. Quasi-binary solutions of polydisperse polymers and a single solvent.** Gibbs' free energy of mixing ΔG. Chemical potentials $\Delta \mu_0$ and $\Delta \mu_{xi}$. Two-phase separation characteristics. Fractionation based on solubility differences. Spinodal curve and critical solution point. Cloud point curve. Flory temperature and Flory entropy parameter. Flory enthalpy parameter. Experimental determination of phase diagram on polymer solutions. **3. Quasi-ternary solution consisting of multicomponent polymer dissolved in binary solvent mixture.** Chemical potential. Two-phase separation characteristics. Spinodal curve and critical solution point. Flory solvent composition. Cosolvency. Fractionation based on solubility differences. **4. Quasi-binary solution consisting of multicomponent polymer 1 and multicomponent polymer 2 system.** Introduction. Theoretical background of the critical solution point and spinodal curve. Theoretical background of the cloud point curve. Effect of polymer characteristics on two-phase equilibrium of multicomponent polymer 1 and multicomponent polymer 2. Experimental determination of polymer-polymer interaction parameter $\xi_{1\,2}$. **5. Quasi-ternary solution consisting of multicomponent polymer 1, multicomponent polymer 2 and single solvent system.** Introduction. Spinodal curve and critical solution point. Effects of molecular weight distribution of polymers and three ξ parameters on the spinodal curve and critical solution point. **6. Application of phase equilibria: Formation of porous polymeric membrane by phase separation method.** Introduction. Nucleation and growth of particles. Growth of primary particles by amalgamation to give secondary particles. Formation of pores by contacting the secondary particles. Critical points of casting solution/nonsolvent system and pore shape of membranes cast from the solution. Experimental relations between the solvent-casting conditions and pore characteristics of membranes. Formation of multi-layered structure of membranes. Some of the performances of multi-layered membranes. **7. Concluding remarks. Glossary of symbols. Author index. Subject index**

1990 xiv + 652 pages

Price: US$ 220.50 / Dfl. 430.00

ISBN 0-444-88184-0

Elsevier Science Publishers

P.O. Box 211, 1000 AE Amsterdam, The Netherlands

P.O. Box 882, Madison Square Station, New York, NY 10159, USA

Computer Applications in Chemical Engineering

Proceedings of the European Symposium on Computer Applications in Chemical Engineering, ComChem '90, The Hague, The Netherlands, May 7-9, 1990 (21st Symposium of the Working Party on the Use of Computers in Chemical Engineering of the European Federation of the Chemical Engineering (418th Event))

edited by **H.Th. Bussemaker**, *IBM Nederland, Zoetermeer, The Netherlands and* **P.D. Iedema**, *DSM Research B.V., Geleen, The Netherlands*

(Process Technology Proceedings, 9)

This book presents the latest trends in computing, computer graphics and computerized design tools. It also gives a state-of-the-art overview of modelling, process integration and process design. All papers describe new computer algorithms and/or techniques for the whole range of computers from the PC to the supercomputer. Unit operations are well covered, as well as a number of topics in reactor engineering and control engineering.

Contents. **Session 1: Process modelling in revamp and design.** Process integration - a new challenge to modelling. A dynamic simulator for design and analysis of chemical processes. A second generation nonequilibrium model for computer simulation of multicomponent separation processes. Process simulation with undefined mixtures using structure-based model compounds. Process integration retrofit subject to pressure drop constraint. Numerical methods used in reactor design (design of distributor top with internals) Using process synthesis and process simulation together - a new process engineering environment. Topology traps in evolutionary strategies for heat exchanger network synthesis. Modelling dynamic behaviour of multiple-effect falling-film evaporators. The use of sensitivity analysis to validate laboratory developed models of chemical reaction systems. Computer simulation for alcoholic fermentation process based on a heterogeneous model. MERITS, a simulation tool for multiphase, chemical reactor engineering. **Session 2: Design and engineering graphics.** Graphical representation of multidimensional functions in process design and optimisation. Design of integrated total flowsheet: a combined approach. An expert system for the design, operation and diagnosis of solid-liquid separators. User interfaces for process plant design - the benefits of Windows based systems. The architecture of SEPEX a SEParation system EXpert. Computer-assisted selection of equipment for liquid-liquid extraction. An algorithm for generating process flow diagrams automatically. **Session 3: Process logistics and control.** Models, modelling and management. Rigorous dynamic modelling and control system synthesis for distillation processes: an integrated approach. Control system design for an exothermic batch chemical reactor. Adding intermediate storage to noncontinuous processes. Scheduling ethylene plant operations. Simulation and optimization of an ethylene production plant. A computer-aided decision support system for the optimal long-term planning in large-scale chemical and related process systems. Computer aided analysis and control of a distillation train. Optimal operation of ethylene plants. On-line conversion estimation as an example of model supported process control. **Session 4: Education and training.** Education and training. A course in interactive graphics for undergraduate chemical engineers. Object-oriented hypermedia as a teaching aid in chemical engineering education. A simulation based system for operator training. The application of an operator training system in education. High fidelity real time simulation and its application to olefins plant operator training. **Session 5: Trends in computing.** Trends in computing. Computer aided molecular design by group contribution method. Flexibility, reliability, and availability analysis of manufacturing processes: a unified approach. A parallel computing strategy for multicomponent separation calculations. Optimal synthesis of nonsharp separation sequences. A mathematical framework for representation of heuristic rules. Two-phase flow simulation with cellular automata. **Session 6: Information and data management in the chemical industry.** Managing the IT function. A database approach for the interactive control of technical processes. Use of realtime and relational databases for CIM implementation. The case for a new database structure for computer-aided process design tools. **Poster session.**

1990 xii + 386 pages
Price: US$ 151.25 / Dfl. 295.00
ISBN 0-444-88679-6

Elsevier Science Publishers
P.O. Box 211, 1000 AE, Amsterdam, The Netherlands
In the USA/Canada: P.O. Box 882, Madison Square Station, New York, NY 10159, USA

An Introduction to Rheology

H.A. Barnes, *Unilever Research, Port Sunlight Laboratory, Wirral,*
J.F. Hutton, *formerly of Shell Research Ltd., Ellesmere Port, and*
K. Walters, *University College of Wales, Aberystwyth, UK*

(Rheology Series, 3)

Rheology is, by common consent, a difficult subject and some of the theoretical components are often viewed as being of prohibitive complexity by scientists without a strong mathematical background. There are also the difficulties inherent in any multidisciplinary science like rheology for those with a specific training. Therefore, newcomers to the field are sometimes discouraged, and for them the existing texts on the subject are of limited assistance because of their depth of detail and highly mathematical nature.

This book introduces the subject of rheology in terms understandable to non-experts. It takes the reader *step by step* through the subject, and describes the application of rheological principles to many industrial products and processes. It provides a simple but authoritative guide which shows clearly how mathematics, physics and chemistry have contributed to the development of rheology. The generic features of all liquid-like materials are summarised, i.e. viscosity, linear viscoelasticity, normal stresses and extensional viscosity. Particular systems are discussed, i.e. polymeric liquids and suspensions. The final chapter gives an outline of the theoretical advances which have been made. Consistent notation and nomenclature have been used throughout the book, and the key textbooks and publications which will enable the reader to follow up particular topics are listed.

1989 x + 200 pages
Hardcover edition: US$ 92.00 / Dfl. 175.00
ISBN 0-444-87140-3
Paperback edition: US$ 60.50 / Dfl. 115.00
ISBN 0-444-87469-0
Students' pack (5 copies of paperback): Dfl. 475.00
(available only **outside** *the USA & Canada)*

"While there now exists a number of excellent but mathematically rigorous texts on Rheology and a few on application in specific industries, there has been up to now no overview text suitable for the newcomer to the field that provides a painless introduction and overview to the subject and at the same time leads the reader with appropriate references to the more detailed texts and literature references.

"Barnes and Hutton, with their years of industrial experience in application of Rheology, have combined with the academic maturity of Walters to create the first text for the beginner in Rheology - either for the student who has not had the appropriate formal training, for the industrial scientist, or for the industrial manager who needs sufficient information to be convinced that knowledge extending beyond a shear rate dependent viscosity may be necessary to solve his or her problem... Overall, the book will be a necessary part of your Rheology library, but most importantly it provides a well written and useful introduction to the subject and thus will be the first book for the newcomer to the subject."

David V. Boger, The University of Melbourne, Australia

Contents: 1. Introduction. 2. Viscosity. 3. Linear Viscoelasticity. 4. Normal Stresses. 5. Extensional Viscosity. 6. Rheology of Polymeric Liquids. 7. Rheology of Suspensions. 8. Theoretical Rheology. Glossary of Rheological Terms. References. Author Index. Subject Index.

ELSEVIER

P.O. Box 211, 1000 AE Amsterdam, The Netherlands.

P.O. Box 882, Madison Square Station, New York, NY 10159, USA.

SUBMISSION OF PAPERS

Papers should be submitted to the Editor: Dr. H.K. Lonsdale, 64550 Research Road, Bend, Oregon 97701, USA. Submission of a manuscript implies that it is not under consideration for publication elsewhere and further that, with the exception of review papers, original work not previously published is being presented.

Three copies of the *manuscript* should be submitted in double-spaced typing on pages of uniform size with a wide margin on the left. The top copy should bear the name and full postal address of the person to whom the proofs are to be sent. An abstract of 100–200 words is required as well as five relevant keywords.

The *language* of the Journal is English.

References should be numbered consecutively throughout the text and collected together in a reference list at the end of the paper. Journal names should be abbreviated. The abbreviated journal name should be followed by volume number, year (in parentheses), and page number. Titles should be supplied to all referenced papers and reports.

All *tables* and *illustrations* should be numbered consecutively and separately throughout the paper. *Line drawings* should be in a form suitable for reproduction, drawn in Indian ink on drawing paper. They should preferably all require the same degree of reduction, and should be submitted on paper of the same size as, or smaller than, the main text, to prevent damage in transit. *Photographs* should be submitted as clear black-and-white prints on glossy paper. Each illustration must be clearly numbered. *Legends* to the illustrations must be submitted in a separate list.

PROOFS AND REPRINTS

Authors will receive *proofs*, which they are requested to correct and return as soon as possible. No new material may be inserted in the text at the time of proofreading.

A total of 50 *reprints* of each paper will be supplied free of charge to the author(s). Additional copies can be ordered at prices shown on the reprint order form which accompanies the galley proofs.

MEMBRANE SCIENCE AND DESALINATION is a two-part publication made up of the journal **DESALINATION** and the **JOURNAL OF MEMBRANE SCIENCE**.
Papers dealing with water desalination and purification should continue to be submitted to **DESALINATION**.

© 1991, ELSEVIER SCIENCE PUBLISHERS B.V.

0376-7388/91/$03.50

All rights reserved. No part of this publication may be reproduced, stored in a retrieval system or transmitted in any form or by any means, electronic, mechanical, photocopying, recording or otherwise, without the prior written permission of the publisher, Elsevier Science Publishers B.V., P.O. Box 330, 1000 AH Amsterdam, The Netherlands.
Upon acceptance of an article by the journal, the author(s) will be asked to transfer copyright of the article to the publisher. The transfer will ensure the widest possible dissemination of information.
Submission of an article for publication entails the author(s) irrevocable and exclusive authorization of the publisher to collect any sums or considerations for copying or reproduction payable by third parties (as mentioned in article 17 paragraph 2 of the Dutch Copyright Act of 1912 and in the Royal Decree of June 20, 1974 (S. 351) pursuant to article 16b of the Dutch Copyright Act of 1912) and/or to act in or out of Court in connection therewith.
Special regulations for readers in the USA. – This journal has been registered with the Copyright Clearance Center, Inc. Consent is given for copying of articles for personal or internal use, or for the personal use of specific clients. This consent is given on the condition that the copier pay through the Center the per-copy fee for copying beyond that permitted by Sections 107 or 108 of the US Copyright Law. The per-copy fee is stated in the code-line at the bottom of the first page of each article. The appropriate fee, together with a copy of the first page of the article, should be forwarded to the Copyright Clearance Center, Inc., 27 Congress Street, Salem, MA 01970, USA. If no code-line appears, broad consent to copy has not been given and permission to copy must be obtained directly from the author(s). All articles published prior to 1980 may be copied for a per-copy fee of US $2.25, also payable through the Center. This consent does not extend to other kinds of copying, such as for general distribution, resale, advertising and promotion purposes, or for creating new collective works. Special written permission must be obtained from the publisher for such copying.
No responsibility is assumed by the Publisher for any injury and/or damage to persons or property as a matter of products liability, negligence or otherwise, or from any use or operation of any methods, products, instructions or ideas contained in the material herein.
Although all advertising material is expected to conform to ethical standards, inclusion in this publication does not constitute a guarantee or endorsement of the quality or value of such product or of the claims made of it by its manufacturer.

This issue is printed on acid-free paper.

PRINTED IN THE NETHERLANDS

VOL. 57, NO. 1 JOURNAL OF MEMBRANE SCIENCE APRIL 1, 1991

CONTENTS

The formation of microporous polyvinylidene difluoride membranes by phase separation
A. Bottino, G. Camera-Roda (Genova, Italy), G. Capannelli (Messina, Italy) and S. Munari (Genova, Italy) 1

Continuous membrane fermentor separator for ethanol fermentation
Chung-Won Cho and Sun-Tak Hwang (Cincinnati, OH, USA) 21

A stability model for the striping phenomenon in ultrafiltration
P.S. Larsen (Lyngby, Denmark) 43

Transport properties of anion exchange membranes in contact with hydrochloric acid solutions. Membranes for acid recovery by electrodialysis
M. Boudet-Dumy, A. Lindheimer and C. Gavach (Montpellier, France) 57

A two step mechanism of diffusion-controlled ethylene vinyl alcohol membrane formation
Tai-Horng Young and Leo-Wang Chen (Taipei, Taiwan) 69

Electrode responses to phenolic species through cellulosic membranes
Z. Koochaki, I. Christie and P. Vadgama (Salford, UK) 83

Formaldehyde production from methanol using a porous Vycor glass membrane reactor
Jin-Young Song and Sun-Tak Hwang (Cincinnati, OH, USA) 95

Meetings Calendar 115

SUBSCRIPTION INFORMATION

Subscription price for 1991 (Vols. 55–63): Dfl. 2925 plus Dfl. 270 (p.p.h.) = Dfl. 3195 (approx. US $1900). On a combined subscription to both *Journal of Membrane Science* and *Desalination* a discount of 10% applies. All back volumes are available. Our p.p.h. (postage, package and handling) charge includes surface delivery of all issues, except to subscribers in the USA, Canada, Australia, New Zealand, P.R. China, India, Israel, South Africa, Malaysia, Thailand, Singapore, South Korea, Taiwan, Pakistan, Hong Kong, Brazil, Argentina and Mexico, who receive all issues by air delivery (S.A.L. — Surface Air Lifted) at no extra cost. For Japan, air delivery requires 50% additional charge; for all other countries airmail and S.A.L. charges are available upon request. Subscription orders should be sent to: Elsevier Science Publishers B.V., Journals Department, P.O. Box 211, 1000 AE Amsterdam, The Netherlands. Tel: (020) 5803642; fax: (020) 5803598; telex 18582. A specimen copy will be sent on request. Claims for issues not received should be made within three months of publication of the issue. If not, they cannot be honoured free of charge. Customers in the USA and Canada wishing information on this and other Elsevier journals, please contact Journal Information Center, Elsevier Science Publishing Company, Inc., 655 Avenue of the Americas, New York, NY 10010. Tel: (212) 633-3750; fax: (212) 633-3764. For advertising rates apply to the publishers.